UNIVERSITÀ DEGLI STUDI DI PADOVA

UNIVERSITA' DEGLI STUDI DI PADOVA

Dipartimento di Ingegneria Industriale DII

Corso di Laurea Magistrale in Ingegneria dell'Energia Elettrica

INNOVATIVE SOLUTIONS FOR GRIDS WITH HIGH PENETRATION OF LOW-INERTIA VARIABLE RENEWABLE GENERATION

Relatore: Prof. Ing. Fabio Bignucolo

Laureando: Riccardo Stecca 1128735

Anno Accademico 2017/2018

RINGRAZIAMENTI

Innanzitutto un ringraziamento a mia madre e mio padre per avermi permesso di arrivare fino a questo traguardo, e a mia sorella per darmi sempre un consiglio quando serve. Poi a Cervi, Pavan e Vian per l'aiuto datomi in questi mesi in laboratorio ed in tutto il mio percorso universitario. Agli "amici di merda" per tutti i momenti trascorsi assieme in questi ultimi anni. Agli amici di una vita, in particolare Francesco, Massimiliano e Sandrone, sui quali so di poter sempre contare. Ai miei ex-coinquilini per i due anni di vita padovana passati insieme. Alla squadra del Biadene per tutti gli sforzi di gruppo e le serate in compagnia. Ai ragazzi di "Strength Farm" per farmi allenare al meglio tutto l'anno. Infine, ultimo ma non meno importante, un grazie al Prof. Fabio Bignucolo, a Massimiliano Coppo e Martino Pettinà per aver reso possibile questo lavoro di tesi.

ABSTRACT

In this master's thesis, the frequency stability analysis in a grid with high penetration of variable energy generation has been studied. The main focus of the study has been the introduction of possible solutions to overcome the problem of the reduction of inertia, which force the need for converters capable of generating synthetic inertia. In order to develop different control systems, DIgSILENT PowerFactory has been used as a simulation environment. The alternative technology analysed are SEBIR (Swing Equation Based Inertial Response) and VSM (Virtual Synchronous Machine): the former is the easiest way to produce synthetic inertia, the latter is the more prospect. SEBIR is a control system that generates a power response proportional to the frequency variation (ROCOF) while VSM is a technology that allows the convert to act as a synchronous generator. Both models have been implemented in DIgSILENT Powerfactory starting by various solutions present in literature. In order to have a more detailed analysis a complete parameterization of the VSM has been done in MATLAB Simulink. Results show that VSM, as a synchronous generator, is able to counteract the ROCOF variation in the first milliseconds while SEBIR responds with a delay, therefore VSM has a greater impact on the ROCOF and Frequency Nadir. However, VSM entails worse frequency oscillations.

RIEPILOGO

Oggigiorno, a seguito di un necessario aumento della penetrazione di fonti rinnovabili, i maggiori TSO (Transmission System Operator) devono fronteggiare numerosi problemi legati alla diminuzione di inerzia e di riserva primaria in rete. Questo fenomeno, infatti, comporta una maggiore instabilità di frequenza che andrà man mano a peggiorare nei prossimi anni. Risulta, quindi, di fondamentale importanza andare a trovare delle soluzioni alternative in grado di sostituire la generazione sincrona tradizionale. In questo lavoro di tesi, è stata analizzata la stabilità di frequenza in una rete con elevata penetrazione di generazione rinnovabile variabile, come i parchi fotovoltaici e gli impianti eolici. L'obiettivo principale di questo studio è stato l'introduzione di possibili soluzioni, ovvero convertitori statici in grado di generare inerzia sintetica, per aumentare l'inerzia della rete. Per sviluppare diversi sistemi di controllo, DIgSILENT PowerFactory è stato utilizzato come ambiente di simulazione. Le tecnologie alternative implementate sono SEBIR (Swing Equation Based Inertial Response) e VSM (Virtual Synchronous Machine): il primo è il modo più semplice per produrre inerzia sintetica, mentre il secondo è il più prospettico. SEBIR è un sistema di controllo che genera una risposta di potenza proporzionale alla variazione di frequenza (ROCOF), ovvero calcola una potenza di riferimento che viene usata dal convertitore DQCI per produrre una corrente. VSM è una tecnologia che consente al convertitore di agire come un generatore sincrono, e di conseguenza il convertitore si comporta come un generatore di tensione. Entrambi i modelli sono stati implementati in DIgSILENT Powerfactory a partire da varie soluzioni presenti in letteratura. Essendo VSM un sistema complesso che emula un generatore sincrono, i parametri di questo controllore sono stati parametrizzati in modo tale da avere una risposta in potenza similare a quella di un generatore sincrono: per fare questo è stato costruito in MATLAB Simulink un modello semplificato di VSM. I risultati mostrano che VSM, come un generatore sincrono, è in grado di contrastare il ROCOF sin dai primi millisecondi mentre SEBIR risponde con un ritardo, pertanto VSM ha un impatto maggiore sul ROCOF e sul Frequency Nadir. Tuttavia, VSM comporta oscillazioni di frequenza peggiori all'aumentare della sua taglia.

CONTENTS

LIST OF FIGURES

LIST OF TABLES

INTRODUCTION

Nowadays the Renewable Energy Sources (RES) are becoming one of the central topics of energy supply and energy politics in developed and emerging countries. Encouraged by subsidies, in Europe, the capacity of solar and wind energy installed is increasing. As a consequence, the inertia of the grid, ie the synchronous generation directly connected to the grid, is decreasing so new solutions to improve the frequency stability are necessary. A promising method is the Synthetic Inertia (SI), which can be divided in two category: SEBIR (Swing Equation Based Inertial Response) and VSM (Virtual Synchronous Machine). While the former has already been widely analyzed, because it is easy to implement in existing VSCs (Voltage Source Converters), the latter is a technology in its initial stages. These technologies could be used in ESSs (Energy Storage Systems) in order to allow a higher penetration of RES.

GOALS AND STRUCTURE OF THIS THESIS

In this master's thesis, the frequency stability of a system with high penetration of Variable Renewable Generation (VRG) has been studied. Particularly the frequency response of the grid with different levels of SEBIR/VSM rated power has been tested. Mainly, in this study the following questions have been pursued:

- Is a grid with high penetration of variable renewable generation more stable with the introduction of SEBIR/VSM?
- How much SEBIR and VSM could improve the frequency stability?
- Which kind of problems could SEBIR and VSM introduce in the grid?

Therefore, this master's thesis report is structured as follow:

1. in Chapter 1 a brief introduction on the concepts related to the frequency stability is presented;
2. in Chapter 2 the problems related to the increase of the penetration of VRG, and therefore the impact of the reduced inertia of the grid, are explained;
3. in Chapter 3 the alternative technology solutions to improve the frequency stability are presented;
4. in Chapter 4 the control systems, implemented in DIgSILENT Powerfactory, are illustrated;
5. in Chapter 5 the case study is discussed;
6. in Chapter 6 the simulation results are analyzed;

1. STABILITY AND DYNAMICS OF THE POWER SYSTEM

1.1 POWER SYSTEM STABILITY

As stated in [1], the power system stability is the ability of an electric power system in a given initial operating condition, to return to a state of operating equilibrium after being subjected to a physical disturbance, with most system variables bounded so that practically the entire system does not change. This definition can also be applied to an electric power system interconnected, so that can be seen as a whole system. It is important to note that this definition implies that the stability of a power system depends on both the initial conditions and the nature of the disturbance. Electric power systems are objects of a high number of disturbances, which may be of low relevance, such as changes in loads that occur continuously, and so the system must easily respond to these variations, or of high importance, such as loss of a high-power plant or the interruption of a line. Furthermore, the disturbances can be short or long lasting and local, which is associated with a small portion of the system, usually a single generator, or global, which is linked to a large group of generators. The problem of the stability of power systems is essentially unique, however, it may be useful to classify the stability of the electrical system in different categories as can be seen in Figure 1.1.

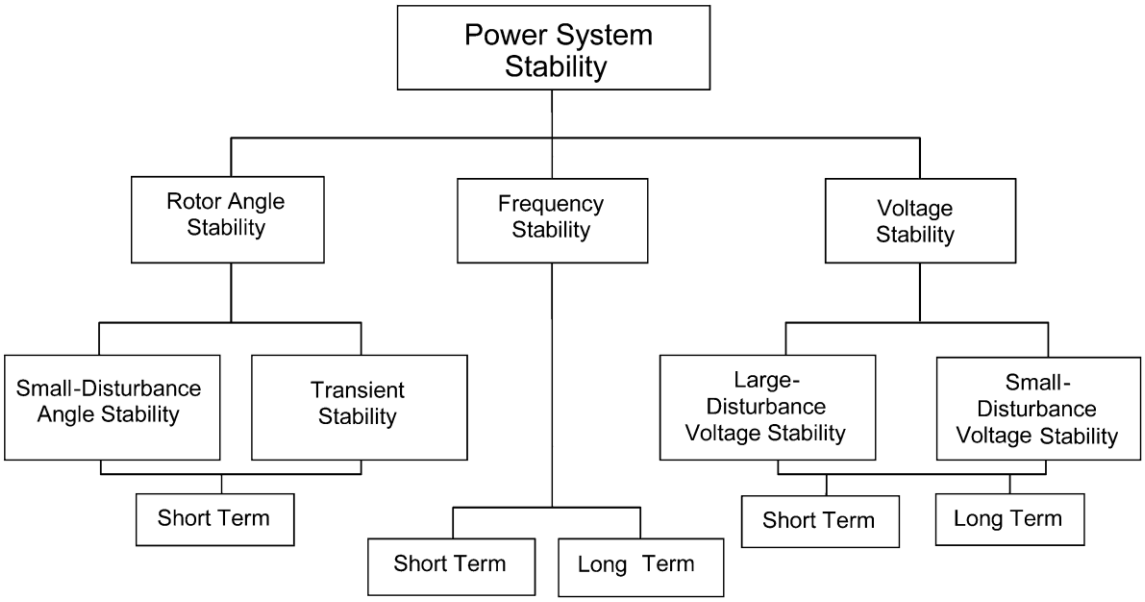

Figure 1.1: Classification of power system stability.

1.1.1 Rotor angle stability

The stability of the rotor angle refers to the capacity of a synchronous machine connected to an electric power system to remain in synchronism after being subjected to a disturbance; it depends on the ability to maintain or restore the balance between the electromagnetic torque and the mechanical torque of each machine. As a result, when the generator is in balance, its speed is constant because the torques are balanced. However, following one perturbation the electromagnetic torque varies and therefore it is possible to have

variation of the angle of the rotor and the rotor speed. In any case, the stability of the machine depends on the capacity of the machine to absorb or release kinetic energy, or if there is enough stabilizing torque sufficient. These torques can be resolved into two components:

1. Synchronizing torque component, in phase with rotor angle deviation;
2. Damping torque component, in phase with the speed deviation.

Therefore, the rotor stability depends on the presence of sufficient components of the torque; a lack of synchronizing torque leads to aperiodic or non-oscillatory instability, while the lack of damping torque results in periodic or oscillatory instability. Depending on the nature of the disturbance the stability of the rotor angle can be categorized as:

- Small-disturbances (or small-signals) rotor angle stability refers to the ability of the system to remain in synchronism under small perturbations. These small perturbations could lead to aperiodic or periodic oscillations, however, nowadays, small-signal instability has been eliminated thanks to the introduction of Active Voltage Regulators (AVR) in the generator. Small perturbations can be local or global. In any case, the duration of these is 10-20 seconds and therefore are short-lived. Such imbalances are considered so small that the problem linked to this type of stability can be linearized;
- Large-disturbances in rotor angle stability (or transient stability) is concerned to the ability of the system to maintain synchronism when subjected to a severe disturbance, such as a short circuit in a line. Usually this type of instability involves aperiodic oscillations due to insufficient synchronizing torque. The duration of this phenomenon is 3-5 seconds but can be extended to 10-20 seconds for extensive systems. It should be noted that, due to wide rotor angle excursions, in this case the problem can not be considered linear.

1.1.2 Voltage stability

Voltage stability is the ability of the power system to maintain a constant voltage at each node in the system, after being subjected to a disturbance; it is therefore the ability to maintain/restore the balance between load demand and supply of power from the electrical system. This type of problem may last a few seconds (short duration), due to variations in load controlled by power electronics, or a few minutes (long duration) due to maneuvers on elements of the electrical system such as OLTC (On Load Tap Changer) or current limiters of the generators. In addition, the voltage stability can also be divided according to the severity of the disturbance: large perturbations, due to the loss of generation or short circuits and small perturbations, due to load variations.

1.1.3 Frequency stability

Frequency stability refers to the ability of the electrical system to maintain a constant frequency following a perturbation resulting in a generation and load unbalance; it is therefore the ability to re-establish and maintain the balance between generation and load, with the minimum loss of load desired (Load Shedding) or uncontrolled. Generally, the problem of frequency stability is linked to inadequate response of the equipment (inertia of the network), low power reserve (primary reserve) and insufficient control and coordination of the protection systems. Nowadays the electric power systems are connected to each other to create a single large interconnected system, consequently severe disturbances, which entail wide frequency excursions, are linked to the division of the system into islands, following a loss of a line. As a consequence,

stability is obtained if each island is able to reach an operating point of equilibrium with the minimum loss of load. During frequency excursions, the time of intervention of the various systems varies from fractions of a second, corresponding to the inertial response of the generators, under-frequency load shedding and generator controls and protections, up to a few minutes, as the response of the prime motor of the generators or load voltage regulators. As a result, frequency stability can be seen as a short or long-lasting phenomenon. An example of short-term frequency instability is the formation of an under-generated island with poor generation and insufficient load shedding, consequently the frequency decays rapidly causing a blackout of the island in a few seconds. On the other hand, a more complex situation is when the instability is caused by overspeed controls of the steam turbine or the boiler/reactor protections, which are long-term phenomena with a time ranging from tens of seconds to several minutes.

1.2 FREQUENCY DYNAMICS ON THE ELECTRIC POWER SYSTEM

After a disturbance in the electric power system, the frequency changes likely Figure 1.2.

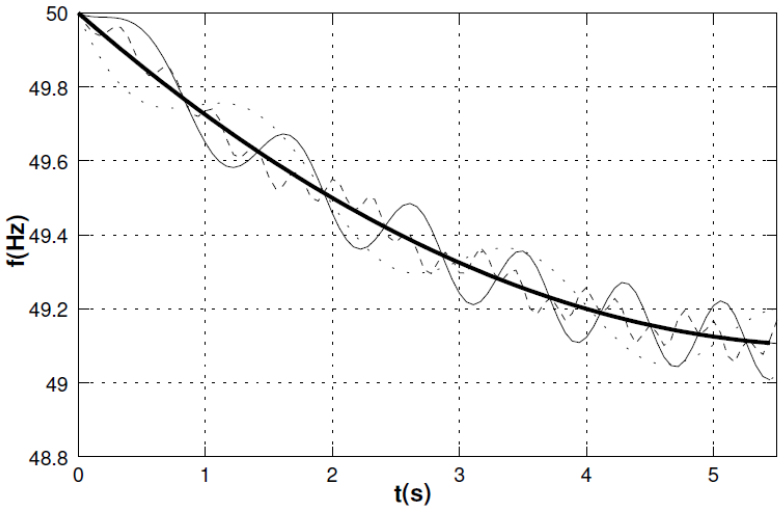

Figure 1.2: Frequency dynamic following a disturbance.

On the other hand, in the normal operation conditions the frequency has very small variations compared to an average frequency of the system, which can be defined by starting from the inertia center (COI) of the system. In the analysis of the dynamics of a large-scale power system are used the equations of Swing [2] [3] for a rotating electric machine, namely:

$$\frac{Jd\omega_i}{dt} = (T_{m_i} - T_{e_i}) \tag{1.1}$$

where J_i is the moment of inertia of the rotating masses, ω_i it is the angular velocity of the rotor and T_{mi} and T_{ei} are respectively the mechanical and electrical torque.

1.2.1 Dynamics of the generators

To describe the dynamics of a single generator, as previously mentioned, the Swing Equations are used. First of all, it is convenient to introduce the inertia constant H_i of a single generator, which represents the time in which the machine can supply energy thanks to its kinetic energy alone. Therefore, it is the relationship between the kinetic energy of the machine and its nominal power:

$$H_i = \frac{\frac{J_i}{p_i^2}\omega_0^2}{2S_{b_i}} = \frac{\frac{J_i}{p_i^2}(2\pi f_0)^2}{2S_{b_i}} \tag{1.2}$$

where S_{bi} is the nominal power of the *i-th* generator, ω_0 is the angular electrical frequency of the rotor, p_i the number of poles of the machine and f_0 the nominal frequency. It can be observed that the inertia constant depends precisely on the moment of inertia and on the nominal power of the machine. It is measured in seconds and takes typical values of 2-10 seconds for high power plants.

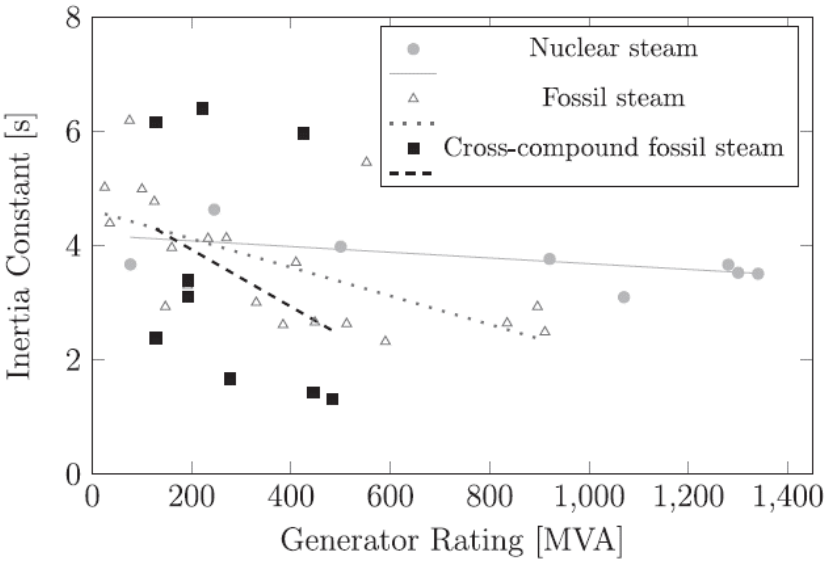

Figure 1.3: Inertia constant as a function of generator rating power.

In general, as can be seen in Figure 1.3, for systems with the same technology, the inertia constant is inversely proportional to the rated power of the generator. Consequently, by introducing the inertia constant into (1.1) and by bringing the torque in *pu*, for a single generator *i* will have:

$$\frac{d\omega_i}{dt} = \frac{\omega_o}{2H_i}(T_{m[pu]_i} - T_{e[pu]_i}) \tag{1.3}$$

In which *m* and *e* indicate respectively the mechanical (turbine) and electrical quantities, ω_i is the absolute value of the angular velocity of the generator rotor *i*. The initial condition for (1.3), ie the angular velocity before the disturbance, can defined as $\omega_0 = \omega_i\ (t_0)$. Deviation from the latter parameter is of fundamental importance:

$$\Delta\omega_i = \omega_i - \omega_0 \tag{1.4}$$

By deriving the (1.4) with respect to the time it is obtained $\frac{d\Delta\omega_i}{dt} = \frac{d\omega_i}{dt}$, consequently it is possible to replace the absolute values in (1.3) with the relative values. Moreover, by using the relation $P_{[pu]} = T_{[pu]}\frac{\omega}{\omega_0}$, the (1.3) can be rewrite as:

$$\frac{d\Delta\omega_i}{dt} = \frac{\omega_o^2}{2H_i\omega_i}(P_{m[pu]_i} - P_{e[pu]_i}) \tag{1.5}$$

The power can be expressed in the SI units (*MW* instead of *pu*) by multiplying with the basic power S_b, which represents the power of the single generator *i*. In addition, it is possible to reorder the (1.5) in order to have the same measurement unit on both sides of the Swing Equation:

$$\left(\frac{2H_iS_{b_i}}{\omega_o}\right)\frac{d\Delta\omega_i}{dt} = \frac{\omega_o}{\omega_i}(P_{m_i} - P_{e_i}) \tag{1.6}$$

Considering now a meshed system having *n* generators, it is possible to assume that all the units are connected to the same bus, which represents the center of inertia of the system. Furthermore, by further simplifying the system it is possible to condense all the generators into a single unit.

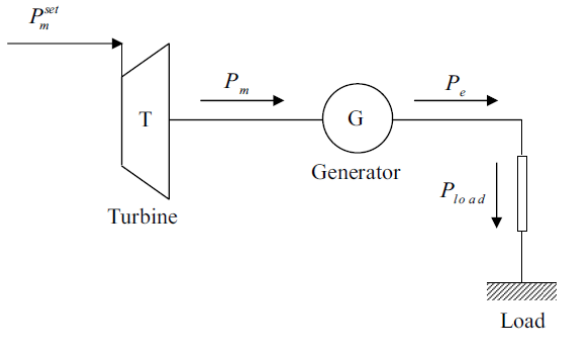

Figure 1.4: Simplified representation of the electric power system.

Consequently, the 1.6 for *n* generators results:

$$\sum_{1=1}^{n}\left(\left(\frac{2H_iS_{b_i}}{\omega_o}\right)\frac{d\Delta\omega_i}{dt}\right) = \sum_{1=1}^{n}\frac{\omega_o}{\omega_i}(P_{m_i} - P_{e_i}) \tag{1.7}$$

in which the following quantities are defined:

$$S_b = \sum_{1=1}^{n} S_{b_i} \; Total\ power$$

$$H = \frac{\sum_{1=1}^{n} H_i S_{b_i}}{\sum_{1=1}^{n} S_{b_i}} \; Total\ inertia$$

$$\omega = \frac{\sum_{i=1}^{n} H_i \omega_i}{\sum_{i=1}^{n} \omega_i} \; Center\ of\ inertia\ (COI) \tag{1.8}$$

$$P_m = \sum_{1=1}^{n} P_{m_i} \; Total\ mechanical\ power$$

Consequently, the frequency dynamics of the system can be defined by the following non-linear differential equation:

$$\frac{d\Delta\omega}{dt} = \frac{\omega_o^2}{2H_i S_b \omega}(P_m - P_e) \tag{1.9}$$

Note that also for the angular velocity in the center of inertia it is valid:

$$\Delta\omega = \omega - \omega_0 \tag{1.10}$$

However, to get a linear approximation of the problem we can assume that $\omega \approx \omega_0$ for the right side of (1.9) because the realistic variations of the electrical system are very small. This leads to writing:

$$\frac{d\Delta\omega}{dt} = \frac{\omega_o}{2H_i S_b}(P_m - P_e) \tag{1.11}$$

Finally, it is possible to express the equation in terms of frequency, being that $\omega = 2\pi f$, as it is more convenient to use; thus the ROCOF (Rate of Change of Frequency) is obtained:

$$\frac{df}{dt} = \frac{f_o}{2H_i S_b}(P_m - P_e) \tag{1.12}$$

1.2.2 System model for the analysis of frequency dynamics

To obtain a simple and usable model for the analysis of the frequency variation after an imbalance between the mechanical and electrical power it is necessary to make simplifying assumptions; as a result, we are going to define:

$$P_m = \sum_{1=1}^{n} P_{m_i} = P_{m_0} + \Delta P_m \tag{1.13}$$

in which P_{m0} is the mechanical power produced by the steady-state generators while ΔP_m is the deviation from this value. This generated power is used by the loads and dispersed in the transmission losses, therefore:

$$P_e = \sum_{1=1}^{n} P_{e_i} = P_{load} + P_{loss} \tag{1.14}$$

Which, similarly to mechanical power, can be written as:

$$P_e = P_{e_0} + \Delta P_{load} + \Delta P_{loss} \quad \text{con} \quad P_{e_0} = P_{load_0} + P_{loss_0} \tag{1.15}$$

As a consequence that the system before the disturbance is balanced:

$$P_{m_0} = P_{e_0} = P_{load_0} + P_{loss_0} \tag{1.16}$$

Furthermore, it is possible to assume that the transmission losses are the same before and after the disturbance, ie $\Delta P_{loss} = 0$, if both the disturbance and the oscillations in the transmission system are not too large. Starting from these approximations (1.11) can be written as:

$$\frac{d\Delta\omega}{dt} = \frac{\omega_o}{2H_i S_b}(\Delta P_m - \Delta P_{load}) \tag{1.17}$$

or, equivalently, with respect to the frequency:

$$\frac{df}{dt} = \frac{f}{2H_i S_b}(\Delta P_m - \Delta P_{load}) \tag{1.18}$$

1.2.3 Frequency dependency of the loads

The loads present in the electric network can be dependent or independent by the frequency; in real power electric systems, most of the loads have a frequency dependence, in fact they have a reactive component that depends directly on the frequency. Furthermore, the presence of large motors connected directly to the network involves a further contribution as kinetic energy can be stored in the rotating masses. This behavior of electrical loads has a stabilizing effect on the system as can be seen from the following section. A model of a generic load present on the network can be described by:

$$P_{load}(f) - P_{load}(f_0) = \Delta P_{load}(f) = K_{load}\Delta f + g\left(\frac{df}{dt}\right) \tag{1.19}$$

where:

- $P_{load}(f_0)$ is the load power for frequency nominal value;
- K_{load} is a coefficient that indicates the dependence of loads on frequency;
- $g\left(\frac{df}{dt}\right)$ is a function that models the rotating masses.

The coefficient that indicates the frequency-dependence depends on the load power variation with respect to the frequency variation, ie:

$$\frac{\partial P_{load}}{\partial f} = K_{load}\Delta f = \frac{1}{D_{load}}\Delta f \tag{1.20}$$

According to the current estimates D_{load} is between 0-2%. The function that describes the rotating masses can be obtained starting from the definition of kinetic energy:

$$E_{kin_{(f)}} = \frac{1}{2}J(2\pi f)^2 \tag{1.21}$$

It can be observed how a variation of frequency involves a variation of kinetic energy, or in other words if the frequency drops the motor will tend to release energy in the network, while if the frequency increases the motor absorbs energy from the network. The variation in kinetic energy is equal to the power consumed by the P_M engine, ie:

$$P_M = \frac{dE_{kin}}{dt} \quad \text{o in alternativa} \quad \Delta P_M = \frac{d\Delta E_{kin}}{dt} \tag{1.22}$$

The energy variation can be approximated as:

$$\begin{aligned} E_{kin}(f_0+\Delta f) &= 2\pi^2 J(f_0+\Delta f)^2 = \\ &= 2\pi^2 J(f_0)^2 + 2\pi^2 J f_0 \Delta f + 2\pi^2 J(\Delta f)^2 = \\ &= E_{kin_{(0)}} + \frac{2E_{kin_{(0)}}}{f_0}\Delta f + \frac{E_{kin_{(0)}}}{f_0^2}\Delta f^2 \end{aligned} \tag{1.23}$$

The values of $E_{kin(0)}$ and D_{load} are highly correlated to the structure and type of load and may vary over time, consequently it is difficult to have precise real time data on these two parameters.

1.2.4 Inertial response of the electric grid

First of all, it is fundamental to give a definition of inertia: it is the resistance given by a physical object to a change in its state of movement, both in verse and speed. Consequently, for a traditional power system, moving objects are rotating machines (synchronous generators, motors, etc.) connected directly to the electrical network. The resistance provided by the rotating machines is expressed through the moment of inertia, which is one intrinsic characteristic of the object. In other word, [4] inertia is the parameter that represents the capability of rotating machines (including loads, when applicable) to store and inject their kinetic energy to the system. The level of inertia influences the frequency gradient (ROCOF) and transient frequency values during a system incident. The transient value of the system frequency is important, because

an increase of transient deviation of frequency caused by an inertia decrease can raise the risk of reaching values which are dangerous for the system stability (generators trip, load shedding intervention, etc.). It is important to note, as will be explained later in detail, that the rotating machines connected through power electronic converters are decoupled from the electrical network and therefore do not contribute to the inertial response. As already seen in eq. (1.2), the kinetic energy stored in a single generator is usually expressed by the inertia constant H_i. Since the synchronous generators are directly connected to the network, their mechanical angular velocity is strictly connected to an electrical parameter, that is the electrical angular frequency ω_0:

$$\omega_m = \omega_0 / p \tag{1.24}$$

As a consequence, the inertial response of the generator, following a significant imbalance between generation and load, due to a disturbance in the network, is determined, as previously seen, from the Swing Equation, which describes the inertial response of a synchronous generator as the variation of the rotor frequency of the rotation, following a power imbalance:

$$\frac{dE_{kin}}{dt} = J(2\pi)^2 f \frac{df}{dt} = \frac{2HS_b}{f}\frac{df}{dt} = (P_m - P_e) \tag{1.25}$$

Where P_m is the mechanical power supplied by the generator while P_e is the required electrical power. Observing that the frequency excursions are usually small deviations around the reference value, it is possible to replace f with f_0. To model the power system response, it is possible to reformulate the classic Swing Equation for a network with n generators, j loads and l connection lines by considering the following equations:

$$\begin{aligned}
S_b &= \sum_{1=1}^{n} S_{b_i} \; Total\ power \\
f &= \frac{\sum_{i}^{n} H_i S_{b_i} f_i}{\sum_{i}^{n} H_i S_{b_i}} COI \\
H &= \frac{\sum_{1=1}^{n} H_i S_{b_i}}{\sum_{1=1}^{n} S_{b_i}} Total\ inertia \\
P_m &= \sum_{1=1}^{n} P_{m_i} \; Total\ mechanical\ power \\
P_{load} &= \sum_{1=1}^{j} P_{load_i} Total\ load\ power \\
P_{loss} &= \sum_{1=1}^{l} P_{loss_i} \; Total\ loss\ power
\end{aligned} \tag{1.26}$$

Where S_b the total power of the n generators, f is the frequency of the inertia center of the network, H is the total inertia constant of the n generators, P_m the total mechanical power of the generators, P_{load} the total power consumed by the loads and P_{loss} the total losses in the transmission lines. Moreover it is necessary to consider the self-stabilizing property of the electric power systems, as previously analyzed, due to the presence of frequency-dependent loads, which leads to insert a term D_{load} is the equation. The Aggregate Swing Equations (ASE) are thus obtained:

$$\frac{df}{dt} = \frac{f_0}{2HS_b}\left(P_m - P_{load} - P_{loss}\right) - \frac{f_0}{2HS_b D_{load}} \tag{1.27}$$

The model of the ASE, as mentioned, is valid for a highly meshed network in which it is possible to assume that all the units are connected at the same point, represented by the center of inertia of the system. Moreover, since the frequency variations are normally relatively small, it is possible to hypothesize the Swing Equations as linear. Therefore, the system variations between before and after the disturbance can be considered:

$$\frac{d\Delta f}{dt} = \frac{f_0}{2HS_b}\left(\Delta P_m - \Delta P_{load} - \frac{\Delta f_0}{D_{load}}\right) \tag{1.28}$$

Furthermore the losses before and after the disturbance can be assumed equal and consequently $\Delta P_{loss} = 0$. Finally by replacing $\Delta P_m - \Delta P_{load} = \Delta P$, where ΔP is the power imbalance in the network, the Swing Equation for the inertial response of the grid are obtained:

$$\frac{d\Delta f}{dt} = \frac{f_0}{2HS_b}\left(\Delta P - \frac{\Delta f}{D_{load}}\right) \tag{1.29}$$

The inertial response of the machines immediately after a disturbance will be distributed over the entire network. Synchronous generators will have to absorb or deliver kinetic energy based on the frequency deviation, however each generator will undergo a different variation of the load angle and speed, based on its inertia and the electrical distance from the disturbance. Furthermore, synchronous generators with a minor inertia will suffer greater rotor oscillations than those with higher inertia: these oscillations will have to be damped by mains losses, rotor damping windings and other systems such as Power Stabilizer Systems (PSS).

1.2.5 Control systems for frequency stability

The frequency control system has the task of keeping the frequency constant around a predetermined value (50 Hz in EU) and to bring it back to this value after a disturbance. The automatic control system consists of two main parts, primary and secondary control. Tertiary control, on the other hand, is activated manually and aims to restore primary and secondary control reserves following a disturbance, consequently this type of control is based on economic optimizations (ancillary services) similar to the dispatching of the electricity production. The basic control structures just described are shown in Figure 1.5.

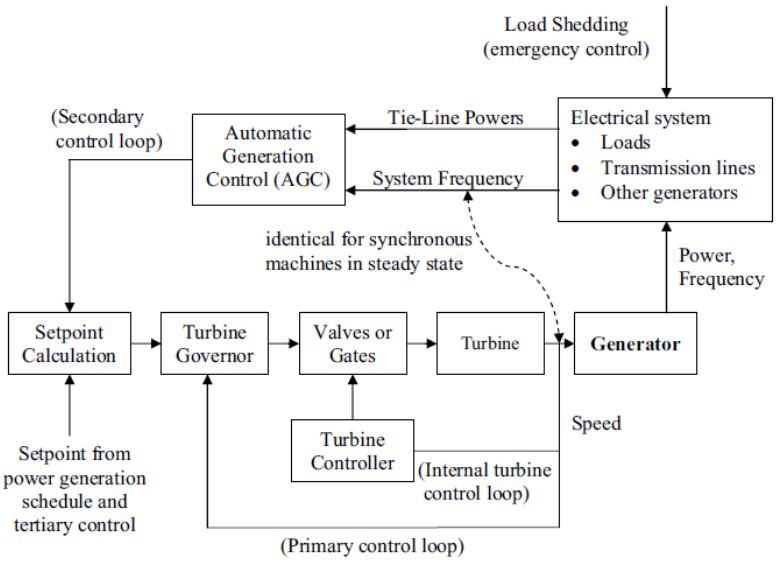

Figure 1.5: Model of the frequency control system.

Figure 1.6 instead shows the time intervals in which these different control circuits are active after a disturbance. Note that primary and secondary control are continuously active, even in normal network operation, to compensate the small fluctuations. In contrast, the use of tertiary reserves occurs less often. Consequently, in order to guarantee the possibility of frequency control, in traditional power plants there is a power reserve used for primary and secondary control. An additional form of protection of the system, which operates in a period far below one second, is the reduction of load (under-frequency load shedding); since the activation of this scheme implies the loss of load in whole regions, it must be activated only if absolutely necessary to save the system. In the ENTSO-E Continental Europe system, the first stage is activated at a frequency of 49 Hz, resulting in the loss of about 15% of the total load. Further stages occur at 48.7 Hz and 48.4 Hz with an additional loss of 10-15% load each. Finally at 47.5 Hz the generators are disconnected from the network with a consequent blackout.

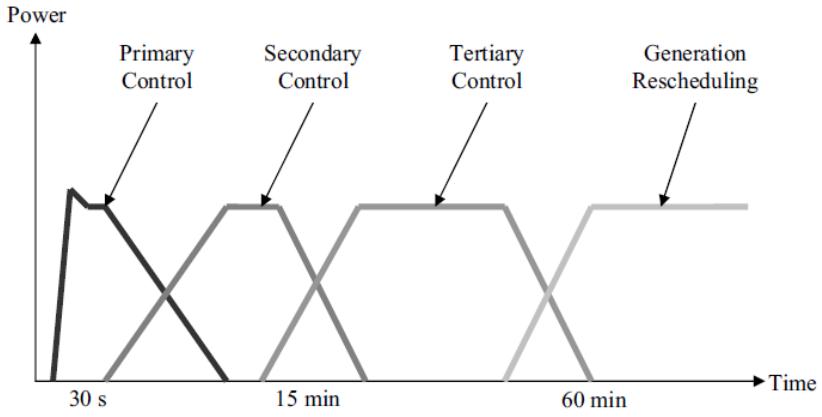

Figure 1.6: Time of intervention of the various frequency control systems.

The first two types of control are now analyzed in more detail:

1. The primary control, also called the Frequency Containment Process (FCP), refers to actions that take place locally, ie at the production plant itself, and are based on pre-established power and frequency values. The actual values of the latter can be measured locally and deviations from the set values lead to a signal that influences the control systems of the generator and the turbine, of a power plant that makes the primary control, so that the desired active power is delivered at the output. In practice, any generator equipped with a speed regulator will act as soon as the frequency deviation exceeds a certain dead band, and it increase/decrease the working point of the prime mover, with an action proportional to the speed deviation. In primary frequency control, the priority is to return the frequency to acceptable values as quickly as possible, in fact it must react with a maximum delay of 5 seconds and be fully activated within 30 seconds. The primary control provides output power proportional to the frequency deviation to stabilize the system but does not return it to the frequency f_0. As a consequence, an unavoidable error of control system remains on the frequency, because the control law is purely proportional. The action carried out should therefore be included in the Swing Equations, thus obtaining:

$$\frac{d\Delta f}{dt} = \frac{f_0}{2HS_b}\left(\Delta P - \frac{\Delta f}{D_{load}} - \frac{\Delta f}{S_{prim}}\right) \tag{1.30}$$

It should be noted that the control activity is shared by all the generators with power greater than 10 MW [5], which are obliged to participate in the primary frequency control regardless of the location of the disturbance, however the generation from variable renewable sources is, in most of the cases, exempt from having to supply power for primary control. The primary reserve for FCP is ±1.5% of the nominal power P_n: o limitation of amplitude and gradient to the provision of the primary reserve is permitted; the methods of delivery of the primary regulation contribution must comply with the following requirements:

- Within 15 seconds from the start of the frequency change, at least half of the request must be delivered.
- Within 30 seconds from the start of the frequency change, the entire request must be issued. [5]

Each of these generators will have its own lowering constant Ri (Droop Costant) [6], which determines the relationship between power and frequency of the generating unit and it is set in the speed regulator by a gain K_i. It can be expressed according to:

$$R_i = \frac{1}{K_i} = \frac{\Delta f}{\Delta P_i}100\% \tag{1.31}$$

where, as mentioned, R_i represents the sinking constant and K_i is the gain of the controller of the *i-th* synchronous generator while Δf is the deviation of the system frequency and ΔP_i is the active power of the synchronous generator which contributes to the primary control during a disturbance. For example, with a 5% lowering constant (in a 50 Hz system), a frequency deviation of 2.5 Hz results in a variation in power output from the generator of 1 pu.
The equation 1.35 can be rewrite as:

$$\Delta P_e = -\frac{\Delta f}{50} \cdot \frac{P_{eff}}{\sigma_P} \cdot 100 \tag{1.32}$$

where ΔP_e is a portion of the available primary reserve of the synchronous generator, proportional to the frequency variation Δf and the efficient power P_{eff} , and dependent on the permanent statism degree σ_p.

For the Italian Transmission System Operator (TSO), according to [7], speed regulators must be calibrated as follows:

- For all hydroelectric units: the statism degree must be set equal to 4% and the intentional deadband must not exceed ± 10 mHz.
- For all thermoelectric units: the statism degree must be set equal to 5%. The intentional deadband must not exceed ± 10 mHz for le single cycle steam units and ± 20 mHz, for turbo gas units and combined cycles steam units.

2. In secondary frequency control, also called Frequency Recovery Process (FRP), the power values of the generators are set to compensate the remaining frequency error, after the primary control has acted, by increasing/decreasing the working point of the prime mover to reduce the frequency variation to zero. In addition to this, another unwanted effect must be compensated by the secondary control: the active power imbalances and the primary control actions cause changes in power flows on power lines, ie power exchanges not based on the planned transfers. The secondary control ensures, with a special mechanism, that this effect is removed in a short period of time.

2. THE IMPACT OF INERTIA IN THE ELECTRIC GRID

In most of the accidents that occur in the power grid, ie the loss of a power plant, the term ΔP_m - ΔP_{load} of the equation (1.28) is negative and consequently there is a decrease in the network frequency, with a ROCOF that is greater for more serious network disturbance. On the other hand, it is also possible that the frequency increases above the reference value, for example when, in interconnected systems, an area with a high level of generation splits and remains in island. In both cases, the inertial response and the network control systems must ensure that the frequency remains at acceptable values, even during the disturbance, and returns to its predetermined value in the shortest time possible. In fact, keeping the network frequency within an acceptable range is necessary to ensure stable and secure operations in the electrical system. The inertia of the network is, therefore, of fundamental importance as it influences the frequency variation over time (ROCOF) and the minimum/maximum value (Frequency Nadir) during a disturbance: a greater number of synchronous generators connected to the network entails a greater inertia constant, consequently, following an accident, there will be lower ROCOF and Frequency Nadir.

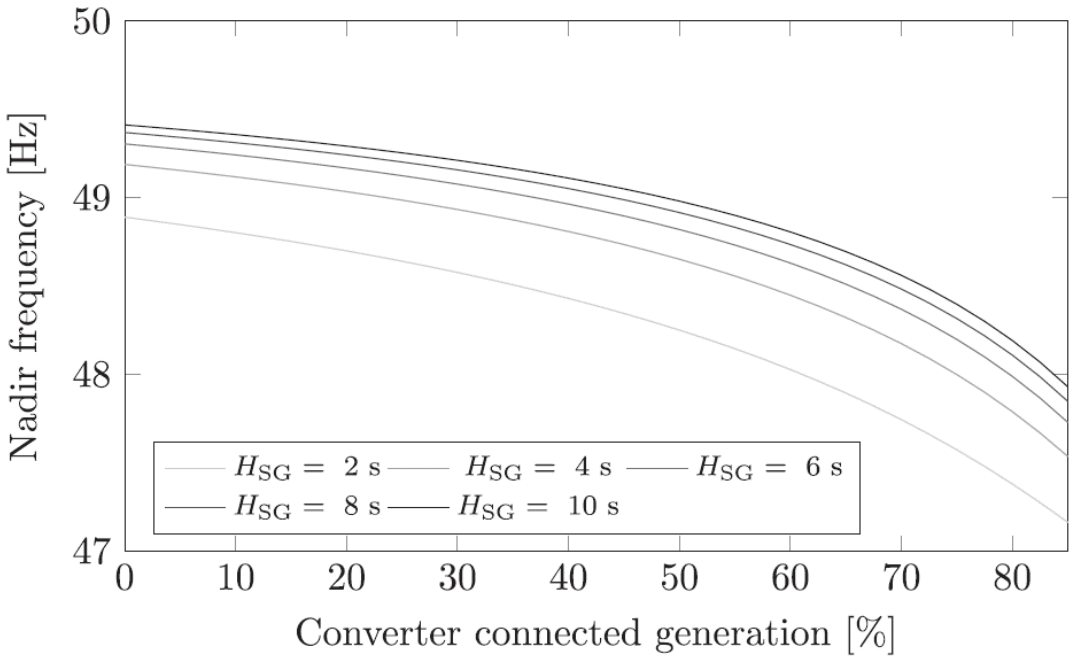

Figure 2.1: Frequency Nadir according to the levels of converter connected generator.

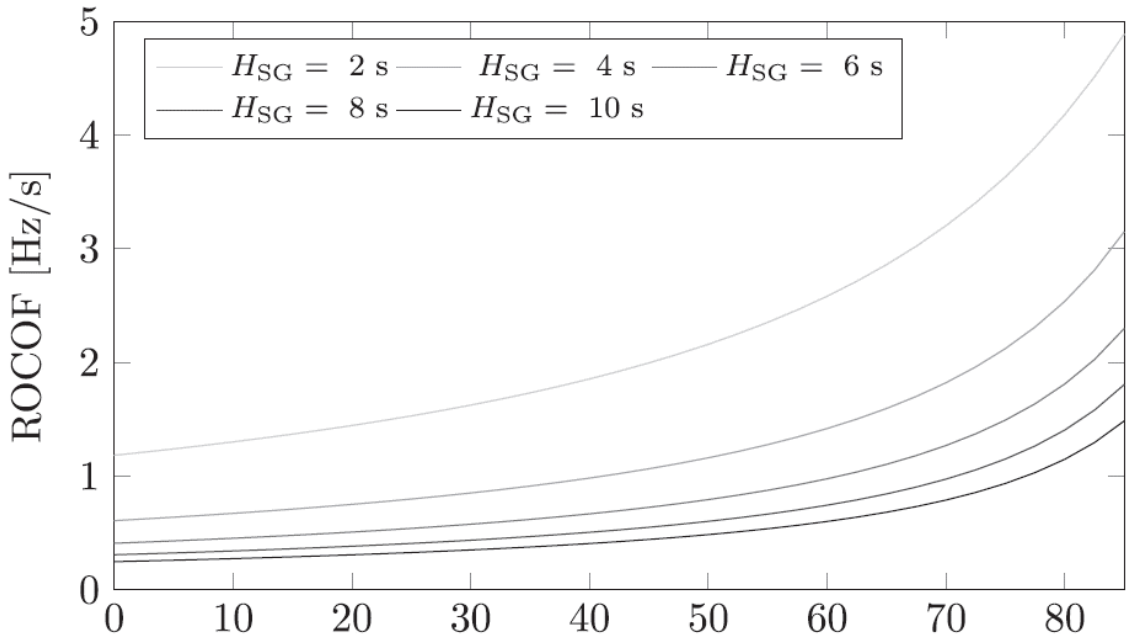

Figure 2.2: ROCOF in function of the levels of converter connected generator.

In fact, as can be seen in Figure 2.1 and Figure 2.2 with the increase of generators connected to the network through static power converters, there is a decrease of the synchronous generators connected to the network, which implies that the Frequency Nadir and the ROCOF get worse. Moreover it can be observed that a greater inertia allows to have a greater generation decoupled from the network. The stability of the system is therefore strictly connected to the value of the inertia of the network, which must therefore be monitored. Consequently, reducing the amount of synchronous generators connected to the network entails a reduction in the inertia of the network which influences the stability of the frequency of the power system, since the system's ability to maintain a constant frequency after a significant imbalance between generation and load is closely linked to the inertia of the network. In fact, if the balance between the power produced and required is not re-established, there are wide oscillations of the frequency that can lead to the interruption of generation plants and/or loss of loads connected to the network. As analyzed in Chapter 1, the behavior of the network following a power imbalance can be described as Figure 2.3, in which is possible to observe:

- the inertial response that occurs immediately following a power imbalance, in which the synchronous generators release or absorb kinetic energy to counter the frequency deviation;
- the primary control that, with an action proportional to the deviation of frequency, leads to a stable frequency;
- the secondary control, which acts after the primary control to bring the frequency at its nominal value.

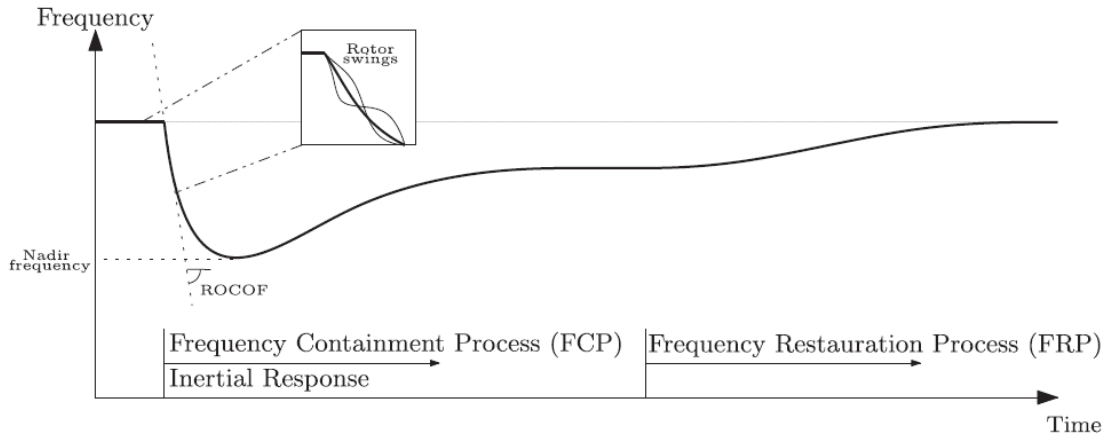

Figure 2.3: Classification of frequency control mechanism.

As previously said, immediately after an imbalance between power generation and demand, the system begins to deviate from its reference value with a ROCOF that is inversely proportional to the total system inertia; such deviations, if possible, are stabilized by the available primary control reserve. In the European continental system [4], these reserves are designed in such a way that the frequency of the system remains between 49.8 Hz and 50.2 Hz, both for ordinary (single incident) and extraordinary accidents (multiple accidents but with a common cause), which usually involve frequency gradients of 5-10 mHz/s. Instead, in the case of incidents outside the limits (multiple accidents without a common cause), if the primary reserve becomes exhausted or if the imbalance exceeds the reference value of 3 GW, the system enters the state of alert. Subsequently, if the global security of the system is at risk and/or load shedding has been activated, the system results in an emergency state. Finally, if the frequency exceeds the limits of 47.5 Hz or 51.5 Hz, a blackout cannot be avoided. In recent years, the European system has experienced ROCOF disturbances between 100 mHz/s and 1 Hz/s, however, based on the recording of the frequency dynamics of the system, in case of unbalance greater than 20% with ROCOF greater than 1 Hz/s the European continental system could present unpredictable events. In [4] ENTSO-E states that, by analysing all of the latest serious events within the Continental European System, the ranges of 500 mHz/s up to 1 Hz/s correspond to a system imbalance ratio of 20%. With the current power plant capabilities and system protection devices this is the maximum range that can be operated successfully. However, market simulations for the future ask for a capability to handle a frequency gradient of 2 Hz/s and an imbalance ratio of 40%. Therefore, future improvements with respect to generation performance and load shedding are required.

2.1 THE IMPACT OF RENEWABLE ENERGY SOURCES IN THE ELECTRICITY GRID

Traditionally, electric power systems are based on the hypothesis that electric energy is produced with constancy and it is easily controllable, due to the fact that it is produced by thermal or hydroelectric plants, and is generated by synchronous generators directly connected to the network. This implies an almost constant and high inertia constant, thanks to the kinetic energy stored in the rotating machines. Moreover, traditional systems are able to supply power for primary and secondary frequency control, both in normal operation and in case of extraordinary events. However, to cope with climate change, and therefore reduce CO_2 emissions, and to have a secure response to the problems of fossil fuel supply, a large number of

countries, especially in Europe, the percentage of plants based on Renewable Energy Sources (RES) connected to their electricity system is increasing. [8] As a result of this, shown in Figure 2.4, the number of hours per year, in which the generation of RES most contributes to the total generation, is increasing.

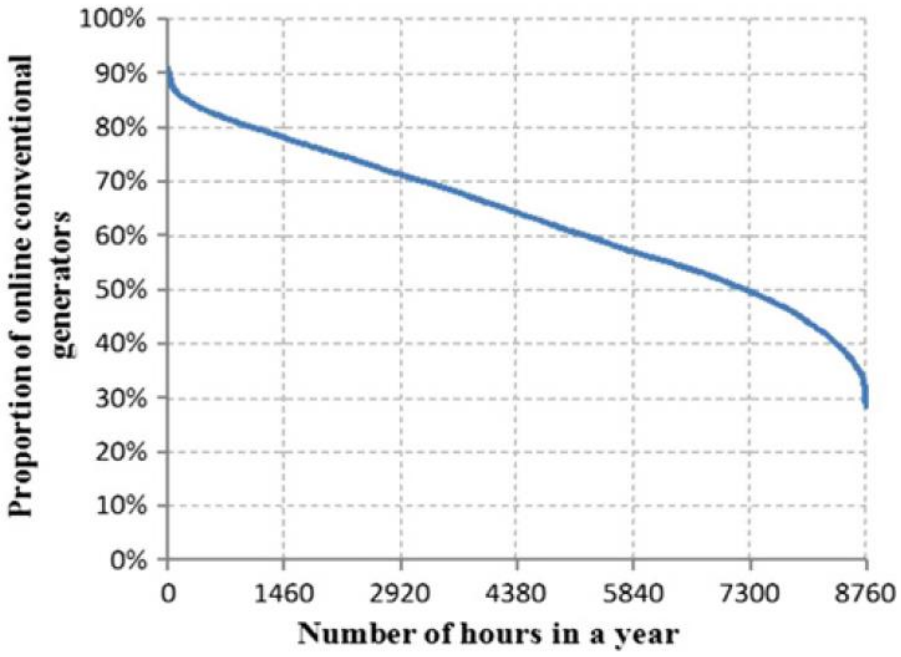

Figure 2.4: Duration curve of the proportion of online conventional generators in the European grid.

This change in the generation park is increasingly leading to an increase in non-synchronous generation, connected to the grid by power converters, and therefore a reducing of the synchronous generation and also the system inertia. The impact of a reduced system inertia must be analyzed to see the effects on the stability of the operations that occur in the electrical system. In the report [4], ENTSO-E asserts that, as long as the system remains interconnected, a low system inertia is not considered critical for the reference incident for the regulation, ie the loss of 3000 MW of generation. However the European interconnected system in recent years, is rapidly changing the structure and geographical distribution of the synchronous generation, which implies a decrease in the inertia and increase of the temporal and zonal variability of the inertia, and it is increasing the capacity of its transmission lines, which leads to a greater transfer of the power between different parts of the system. As a result, following a system split, more than 40% imbalances may occur with ROCOF of 2 Hz/s or more.

2.1.1 The consequences on the frequency stability

Although this phenomenon is necessary to decarbonise electricity production, from the point of view of frequency stability it represents a huge problem. In fact, plants that use variable renewable sources, such as wind and photovoltaic ones, present several points of disadvantage: [8] [9] [10]

- The intermittent nature of such systems implies that the percentage of synchronous generators connected to the network varies over time consequently the inertia of the network can no longer be assumed to be almost constant as in traditional power systems;

- The inertia of the network is more and more heterogeneous due to a greater presence of Variable Renewable Generation (VRG), so some areas of the network are more stable than others. Consequently, after the loss of a transmission line, there could be major problems in the areas with lower inertia;
- Most of these plants are connected to the grid by static power converters, consequently they are decoupled from the grid and cannot contribute to the total inertia of the system. It should be noted that even modern traditional low-power systems can be connected to the grid through an inverter and therefore they also do not provide inertia. A possible solution to this problem is represented by synthetic inertia (also known as virtual inertia), which is the capacity of the conversion system to simulate the inertial response of a synchronous generator, and fast frequency response, which is a primary frequency control that acts in few seconds;
- Plants based on variable RES do not contribute to the power reserve required to control the frequency, as they feed the entire power produced into the grid. This leads to a more severe frequency nadir and higher oscillations. To overcome this, it has been proposed to make these plants work in a sub-optimal point in order to create a power reserve.

These consequences have led to major network management problems:

- The programming of load shedding in networks with high penetration of Distributed Generation (DG) is increasingly more complex because load shedding schemes are coordinated by TSO while DGs are mostly installed in the distribution network. However, the TSO has a poor and limited view of distributed generation, as it is based on historical data and not on the instantaneous state of the system. As a consequence, the UFLS (Under Frequency Load Shedding) schemes, in which predetermined feeders (power lines) are disconnected, must be adapted otherwise the loads could be disconnected from the network as well as the DGs. The consequences of this are different:
    - The total loss of load is the sum of the load seen by the TSO and the load masked by the distributed generation so the resulting load disconnected from the network can be greater than expected.
    - The possible disconnection of DG can cause greater power imbalances that can lead to wider frequency oscillations, which can cause vibrations that damage the synchronous generators, further load shedding, or even to the black-out.

  It is therefore essential that the various TSOs have a clear view in real times of the power produced by the DGs, in order to have load shedding schemes that adapt to the daily/seasonal variation of production from distributed generation. The creation of a UFLS plan, and therefore the choice of the feeders to be interrupted, in case of imbalance on the network, and the activation levels of UFLS protections, must consider the following aspects: [7]
    a. The type of scheme must be chosen in such a way as to reestablish the balance between generation and demand of the loads, and therefore must provide a certain number of steps based on their activation frequency and the amount of load to be disconnected;
    b. The priority level of the various feeders must be categorized according to the type of loads connected to them, in general the lowest priority is given to residential areas and the highest priority to hospitals, communication facilities, etc;
    c. A balanced geographical distribution is necessary to distribute the feeders to be disconnected in a homogeneous manner in order to minimize variations in the power flows;
    d. Distributed generation is an aspect that is catching on due to the increase of the penetration of RES. Feeders connected to renewable energy plants must have a high priority because a disconnection of these feeders leads to a further loss of power. In this regard, the

example proposed in [11] and shown in Figure 2.5 may be interesting. It can be seen how the power measured at the feeder (red curve) varies: due to the presence of a large number of photovoltaic plants connected to the feeder, of which the generation is represented by the green curve, the demand for loads (blue curve) is sometimes counterbalanced or even exceeded. As a result, the TSO will not see the load really connected and this could lead to the problems previously analyzed.

According to the ENTSO-E technical guide [12], the first activation step of the UFLS protections must be 49 Hz, in order to have a range of 1 Hz (between 50 Hz and 49 Hz) where the control primary try to compensate for the power imbalance, the maximum number of steps should be ten and the last one must activate at 48 Hz. Below 48 Hz there is a margin of about 0.5 Hz in which the generators can still operate then it is necessary disconnect them from the network with consequent blackout.

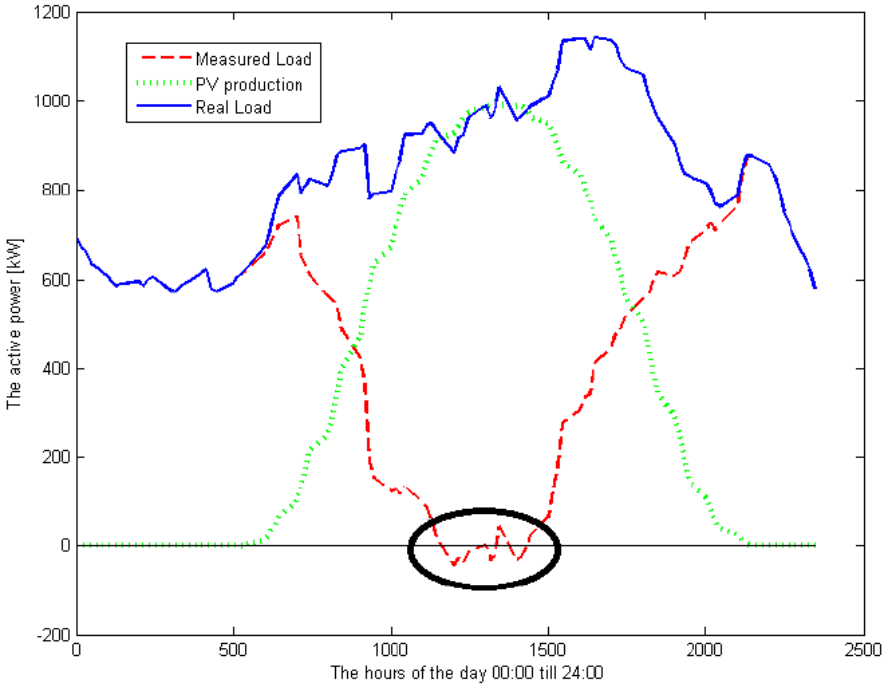

Figure 2.5: Measurement in a mixed feeder.

- The management of ROCOF-based protections in RES high-penetration networks can be difficult and complex because, due to a lower inertia value of the network than that for which they are designed, there is a higher ROCOF value which can lead to untimely tripping of the protections in the first instants of a disturbance. The ROCOF measurement is the most widely used technique by anti-islanding protections [13], consequently the increase in DG penetration in the network is going to undermine the stability and reliability of these protections. The island mode, or also known as Loss of Main (LoM), occurs when one or more distributed generators continue to power a part of the network that has been electrically isolated from the main network.

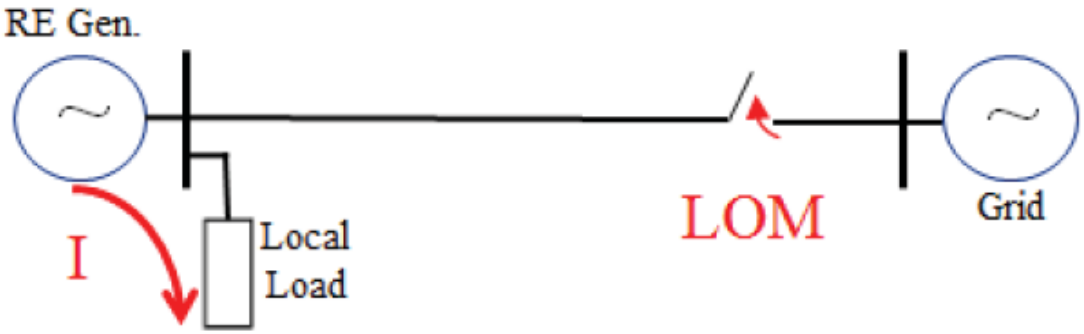

Figure 2.6: Loss of Main (LoM).

This phenomenon, if uncontrolled, is strictly prohibited as it can lead to power quality and safety problems:

- If the network presents an automatic reclosing scheme of the circuit-breakers, there could be close of the circuit in a counter-phase; this phenomenon can cause damage to the rotating machines and to the network as it can lead to short circuits and mechanical torques to the generator shaft.
- The RES generator could operate in island mode without the appropriate ground connections, with consequent security risks.
- The quality of the energy supplied in the island area cannot be guaranteed by the TSO, with consequent load problems.

As a result, the identification of islanding is fundamental but is also difficult and complex because it is necessary to balance two aspects: on the one hand the ability to identify an undesired island situation, on the other the need to avoid unwanted activation of anti-islanding protections. The protections against the LoM therefore must minimize these two types of errors, however it is difficult to find a method that is reliable without increasing the risk of malfunctions and at the same time eliminate the non-detection zone. In general, there are three techniques for identifying islanding: [13] [14]

1. Passive methods: ROCOF, VSS (Voltage Vector Shift), Rate of Change of Power, Change of VAR; The protections based on passive methods measure a certain system parameter and they activate if a certain threshold is exceeded.
2. Active methods: AFD (Active frequency Drift) and impedance measurement. They are based on introducing a small disturbance into the system, which is amplified in case of islanding.
3. Communication-based methods: they are the most efficient but are still too expensive and complex.

The passive methods, and in particular the one based on the ROCOF, as previously mentioned, are the most used for distributed generators, as they can be used for any type of DG, however, recently, active methods have been introduced for DGs connected to the grid via inverters, because they present a Non-Detection Zone (NDZ) smaller than the passive ones. To analyze the performances of an anti-islanding protection, the performance curves are used: in these curves the power imbalance (ΔP) and the intervention time (t) are correlated. These are created starting from a dynamic simulation, where the frequency is monitored: an islanding situation is created and the time between the passage over the threshold frequency and the protection intervention is measured. This is repeat for different power imbalances and so more points are obtained and the curve is created by interpolation. Obviously it can be observed that the time necessary to reach the threshold frequency is inversely proportional to the power imbalance. Furthermore, it is possible to find the NDZ, ie those values of ΔP for which the threshold frequency is not exceeded and those for which the imbalance of power implies an islanding condition that is not detected in a timely manner. in [14] a simulation of a system with different DGs was made to see the impact of DG on the performances of the anti-islanding protections: it was observed that the factor of greatest impact

on the intervention time is the inertia of the system in fact, as it grows, the intervention time increases. This phenomenon can be explained by the fact that greater inertia results in a better system response. As a consequence, the increase in distributed generation has a negative effect on the NDZ of the protections, as these fail to intervene in an effective time.

2.1.2 The critical penetration of variable renewable generation

Another aspect of fundamental importance is linked to the demand of energy itself: as a result of the economic crisis, energy demand has fallen, but the percentage of generation from RES is increasing, so, as a consequence, there is a greater drop in traditional systems connected to the network and therefore lower inertia. In other words, a decrease in energy demand leads to a decrease in inertia. In this regard it is of fundamental importance to define a parameter that allows identification the maximum penetration of VRG, as wind and photovoltaic plants:

$$\tau_{VRG}(t) = \frac{P_{VRG}(t)}{D(t)} \tag{2.1}$$

where the numerator is the total power produced by VRG at the time t while the denominator is the total demand of the system at the instant t. This parameter is necessary to define the maximum instantaneous penetration of RES plants that the system can withstand without having to resort to UFLS (Under Frequency Load Shedding) after the reference accident defined by the ENTSO-E (the loss of 3000 MW of generation). Consequently, succeeding in correctly estimating the generation mix for a given energy demand is a current problem: the dispatch of energy generation is therefore no longer seen only as an economic and operational problem (power flows in the lines) but also as a frequency stability problem, which must be tackled with dynamic studies in real time. As an example, for the European Interconnected System (EIS) it is necessary that each country estimates, starting from historical, technical and meteorological data, the power generated from hydroelectric, conventional heating plants and VRG and the capacity of interconnection. Moreover, thanks again to historical and meteorological data, it is necessary to define the production costs and the energy demand and price. The study [10] has produced, for the continental European area (ECSA European Continental Synchronous Area), a vast number of scenarios in which:

- The τ_{VRG} varies between 10 and 71% of the total demand, consequently this value has an enormous impact on the amount of synchronous generation connected to the network;
- The annual penetration of VRG varies between 33 and 38%;
- The inertia of the ECSA varies between 1.1 and 3.5 MWs/MVA as can be seen from the

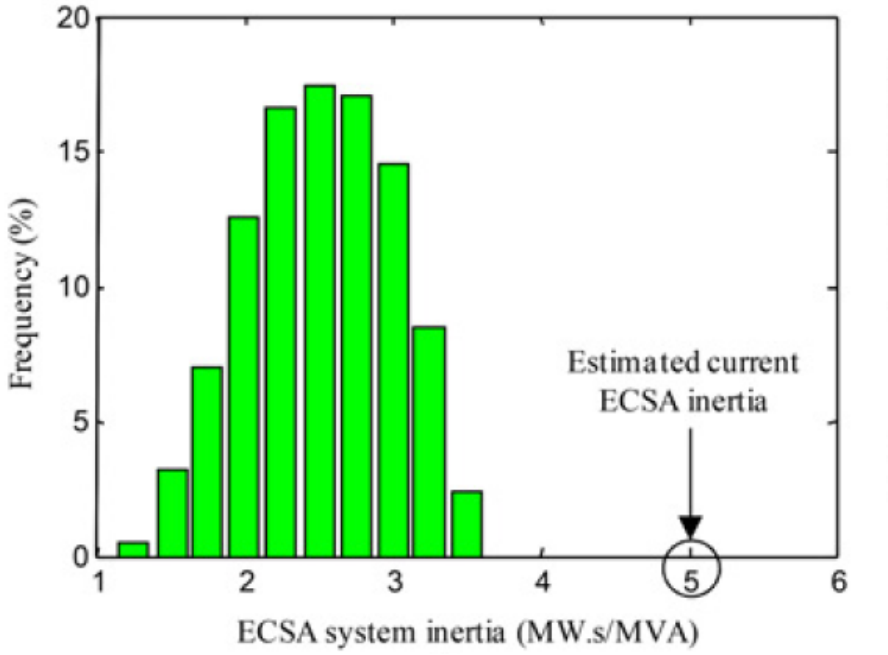

Figure 2.7: Histogram of the probability of hourly inertia value in ECSA.

It should be noted that the value estimated by ENTSO-E is about 5 MWs/MVA, much higher than the one expected by these scenarios.

Furthermore, it has been concluded that there is an almost linear relationship between system inertia and the penetration of VRG, which can be represented by the following equation:

$$H_{ESCA}(t) = H_0(1-\tau_{VRG}(t)) \tag{2.2}$$

where $H_{ESCA(t)}$ is the inertia in the time instant *t*, while H_0 is the basic inertia, ie for τ_{VRG} null, which is 3.85 MWs/MVA in a system with an annual penetration between 33 and 38%. Consequently, even in periods of low penetration of VRG, system inertia is lower than 5 MW/MVA, which is the current reference value defined by ENTSO-E. This point out the need to define a critical level of penetration of VRG ($\tau_{VRG}^{critical}$) for the reference incident: in fact, with the increase of τ_{VRG}, the inertia of the network decreases and therefore the robustness of the system is mined because both the ROCOF and the frequency nadir increase. As a consequence, the $\tau_{VRG}^{critical}$ is defined as the penetration level of VRG for which the frequency does not fall below the level at which the UFLS is triggered, ie the 49 Hz for the EIS. To analyze the impact of the reduction of inertia (caused by the increase in penetration of VRG) on the ROCOF and on the frequency nadir it is necessary to analyze the dynamic behavior of the frequency in the first minute after the reference accident defined by the ENTSO-E, ie the loss of 3 GW of generation corresponding to the loss of two large nuclear generators. However, it should be noted that the frequency behavior depends not only on the inertia of the network but also on:

- the value f_0 of the frequency preceding the accident,
- the value of the imbalance ΔP,
- the loads self-regulation constant D_{load},

- the primary control of the frequency σ_{prim} and
- the time T_{prim} necessary for the intervention of the primary reserve

as can be seen in Table 2.1:

Parameters behavior	$H \downarrow$	$f_0 \downarrow$	$\Delta P \downarrow$	$D_{load} \downarrow$	$\sigma_{prim} \downarrow$	$T_{prim} \downarrow$
Frequency behavior		*ROCOF* $\uparrow$			*Frequency Nadir* $\uparrow$	

Table 2.1: Dependency of frequency dynamics from different parameters

By analyzing the critical penetration of VRG into the network, the following conclusions can be reached for the different parameters:

- As the generation loss increases (at parity of demand), the $\tau_{VRG}^{critical}$ drops because it is needed a greater synchronous generation to have a better inertial response and a higher reserve of control;
- The initial frequency value f_0 has a huge impact on the maximum penetration of RES plants. In fact, for a fixed energy demand, it has been observed that a reduction of 0.1 Hz leads to a 10% drop in $\tau_{VRG}^{critical}$. As a result, studies based on an initial frequency of 50 Hz for EIS are too optimistic;
- As previously seen, the self-regulation effect of the loads leads to an improvement in the stability of the network and, therefore, allows a greater penetration of VRG. However, it should be noted that the trend for the future is to have more and more loads connected to the network via power electronics and therefore this effect is supposed to be lower;
- Finally, it can be noted that $\tau_{VRG}^{critical}$ also depends on the energy demand. In fact, as already mentioned above, the penetration of VRG can be greater as the energy demand increases, thanks to a greater presence of regulating loads and synchronous generation.

In conclusion, it has been seen that $\tau_{VRG}^{critical}$ depends on several factors, such as the configuration of the system, the level and type of loads, the type of generation and the type of control of the converters therefore it is important to understand the effects of these factors in order to be able to have the maximum instant penetration of plants based on renewable sources.

3. POSSIBLE SOLUTIONS TO IMPROVE FREQUENCY STABILITY IN LOW INERTIA GRIDS

It has been stated in the previous chapters that most of the electricity grids, and in particular the European one, are undergoing a process of transformation from a centralized synchronous generation to a distributed one, based on renewable sources. This phenomenon, although necessary to improve the environmental conditions of our planet, in the future could lead to problems of stability in the network, in particular a low and variable system inertia and a reduction in the reserve for primary control. Therefore, it is necessary to:

- Limit the ROCOF of the system: after a major disturbance in the network it is essential that the ROCOF does not exceed certain levels otherwise there could be unwanted activations of ROCOF anti-islanding protections, resulting in disconnection of loads and/or distributed generation. For this aspect it is necessary to have a contribution within 100 ms, since the maximum ROCOF occurs in the first moments after the disturbance in the network, ie during the inertial response of the system. The possible solutions for this problem are represented by the Synchronous Compensators (SC) and the synthetic inertia.
- Limit the Frequency Nadir of the system: limit how low/high the frequency drops/increases after an accident in the network is necessary for not having load shedding and loss of generation. Since the frequency nadir is reached in a time frame of a few seconds to overcome it, it is possible to use to a fast primary reserve (FPFC Fast Primary Frequency Control).

3.1 METHODS FOR SUPPORTING FREQUENCY STABILITY

It is important to define the concept of "synthetic inertia" (also known in literature as "virtual inertia") and to distinguish it from the "fast frequency reserve". In [15] Synthetic Inertia (SI) is defined as the controlled contribution of electrical torque from a converter, of a photovoltaic/wind park, a storage system or even an HVDC, that is proportional to the ROCOF at the terminals of the unit. The torque response should be proportional to ROCOF to deliver an inertial response therefore the converters providing synthetic inertial response should react proportionally to ROCOF. Other units can, however, be controlled to support the system by reacting to frequency deviation. Fast Frequency Reserve (FFR) is the controlled contribution of electrical torque from a unit that acts rapidly on a frequency measure. It can react proportionally to the deviation or inject power according to a pre-determined schedule. In others words fast frequency response is the controlled contribution of electrical torque from a unit, which responds quickly to changes in frequency in order to counteract the effect of reduced inertial response. As previously stated, SI means the facility provided by a power park module or HVDC system to replace the effect of inertia of a synchronous power-generating module. [16] As of today, the synthetic inertia (SI) response is known as SEBIR (Swing Equation Based Inertial Response). [17] The most common existing control strategy applied to converters is Direct Quadrature Current Injection (DQCI) with Phase Locked Loop (PLL) type controls. These converters have an inner control strategy based on current control, and therefore rather shows a current source behaviour in the fundamental frequency (although confusingly they are commonly called Voltage Source Converter). Due to ROCOF measurement delays, a True Inertial (TI) response may be complicated to deliver. In facts in [18] [19] is identified the shortcomings of this control strategy for high penetration even if the virtual inertia described as SEBIR is added. Therefore this approach to inertia may have limited value, as the need for inertia contribution is itself closely linked to high penetration. A possible solution to this problem is represented by virtual synchronous machine (VSM), which was firstly introduced in [20] and is also used in [21] [22] [23] [24] [25]. VSM mimics the behaviour of a real synchronous machine (SM) by controlling a converter. Thus, any VSM implementation contains more or less explicitly a mathematical model of a SM. The specific model of the SM and its parameters is largely an arbitrary design choice as

proved by the many different solutions discussed in literature. However, the emulation of the inertial characteristic and damping of the electromechanical oscillations are common features for every VSM implementation. Additional aspects as the transient and sub-transient dynamics can be included or neglected, depending on the desired degree of complexity and accuracy in reproducing the SM dynamics. Furthermore, the parameters selected for VSM implementations are not constrained by the physical design of any real SM. Therefore, the VSM parameters can be selected to replicate the behaviour of a particular SM design or can be specified during the control system design to achieve a desired behaviour. Moreover, these parameters could be controlled in real time. In [26] is presented a classification of the types of inertia emulation and the control schemed introduced in the converters.

3.1.1 Synthetic Inertia

As previously seen in "The impact of inertia in the electric grid", with ever higher penetration of converters, for TSOs, there are various significant areas of concerns, most notably: [22] [27]

- Increased Rate of Change of Frequency (ROCOF);
- Loss of synchronising torque/power and reference voltage;
- Possibility of high frequency instability and controller interaction;
- Inadequacies of RMS models and the associated difficulties with modelling the electricity system;
- Reduced and possibly delayed fault in feed and associated challenges in transmission system protection performance;
- Possibility of voltage instability during or post fault e.g. collapse, blocking or over voltage post fault;
- Potential for sub-synchronous oscillations and interaction with conventional machines;
- Potentially increased sensitivity to load imbalance and harmonics.

Consequently, TSOs need to create control strategy to counteract these problems. Synthetic inertia is defined as the service provided by a power plant or by an HVDC system to replace the inertia effect of a synchronous generator. [28] Through the power converters, which connect the plant with variable renewable sources to the network, it is possible to imitate a synchronous generator with control mechanisms that supply active power proportionally to the frequency variation or converters that simulate the behavior of a SM. In literature the approach to emulate inertia are essentially two, the SEBIR control and the VSM: [16] [20] [22] [23] [24] [29]

1. *SEBIR* is a control scheme in which the response of the converter is provided by, initially, measuring the frequency with a PLL, then estimating the ROCOF and computing the active power output through the Swing Equation. This is the easiest method for "generating" synthetic inertia for manufactures: in facts the majority of the grid-connected converters are controlled in I_d-I_q references (DQCI), so the active (P) and reactive (Q) power set-point can be easily modify. Therefore, in an existing DQCI converter can be implemented an active power adjustment based on a measure of the ROCOF and a chosen per-unit synthetic inertia H_{si}, based on the well-known Swing Equation. [17] However this technique needs a time to complete the ROCOF measurement and close the control loop so this is not a TI response. On the other hands a TI response can be obtained with a VSM.

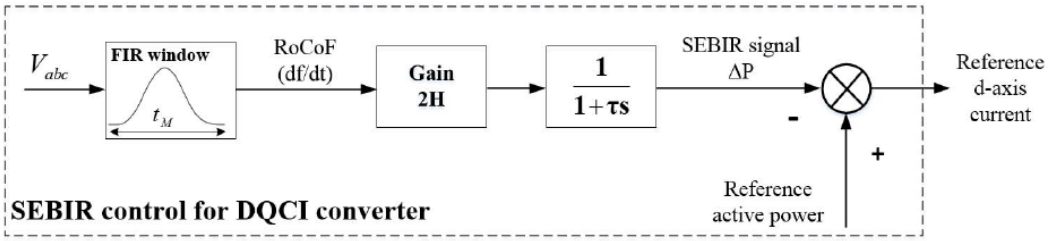

Figure 3.1: Model of the SEBIR control.

2. *VSM* is a complex control method which combines advanced inverter technology and electromechanical synchronous machine model. While the SEBIR method provides a power response proportional to ROCOF, inside machines and converters which closely emulate synchronous machines the analysis is reversed and a "virtual rotor" frequency is obtained. [16] In recent years several control techniques have been developed for the so-called VSM, which are able to emulate the behaviour of the synchronous generator, in such a way that the response of the inverter is practically equal to the one of a real synchronous generator. The main objective of the techniques of control is to simulate the dynamics of a synchronous generator, using different models or specific characteristics of them and, in some cases, to add further properties to improve the inertial response. In any case the models present in literature can be divided in three categories: [30]

    a. Mechanical Model: the goal of this system is to generate a virtual electromotive force (EMF) at the output of the inverter, checking the magnitude of the voltage *E* and the phase θ using:

$$f = -f_0 \int \frac{\Delta P_{[pu]}}{2H} \tag{3.1}$$

As can be seen from Figure 3.2, the phase is obtained from *Pref*, which is the active reference power value for the converter, and ω_0 is the value of the nominal angular frequency of the network.

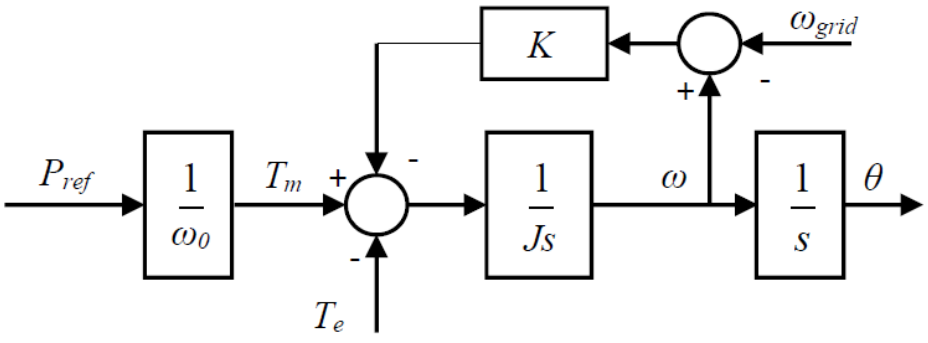

Figure 3.2: Mechanical model.

In Figure 3.3, on the other hand, two types of control of the EMF amplitude are illustrated: one uses reactive power while the other uses the output voltage.

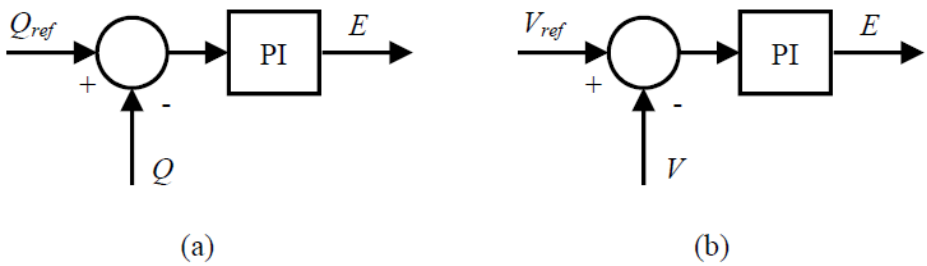

Figure 3.3: EMF amplitude calculation: a) reactive power control loop, b) voltage control loop.

Finally, in Figure 3.4 it is shown: (a) the equivalent circuit of a synchronous generator, where L is the network inductance while L_s and R_s represent the impedance of the generator and V_s is amplitude and phase at the generator terminals and (b) the equivalent circuit of the inverter connected to the grid is controlled with the mechanical model of the VSM, in which the active power transferred to the grid can be calculated according to:

$$P = \frac{EV}{L\omega_0} sin\delta \tag{3.2}$$

where the load angle, δ is the difference between VSM phase (θ) and grid voltage phase (θ_0):

$$\delta = \theta - \theta_0 = \int \omega - \omega_0 \tag{3.3}$$

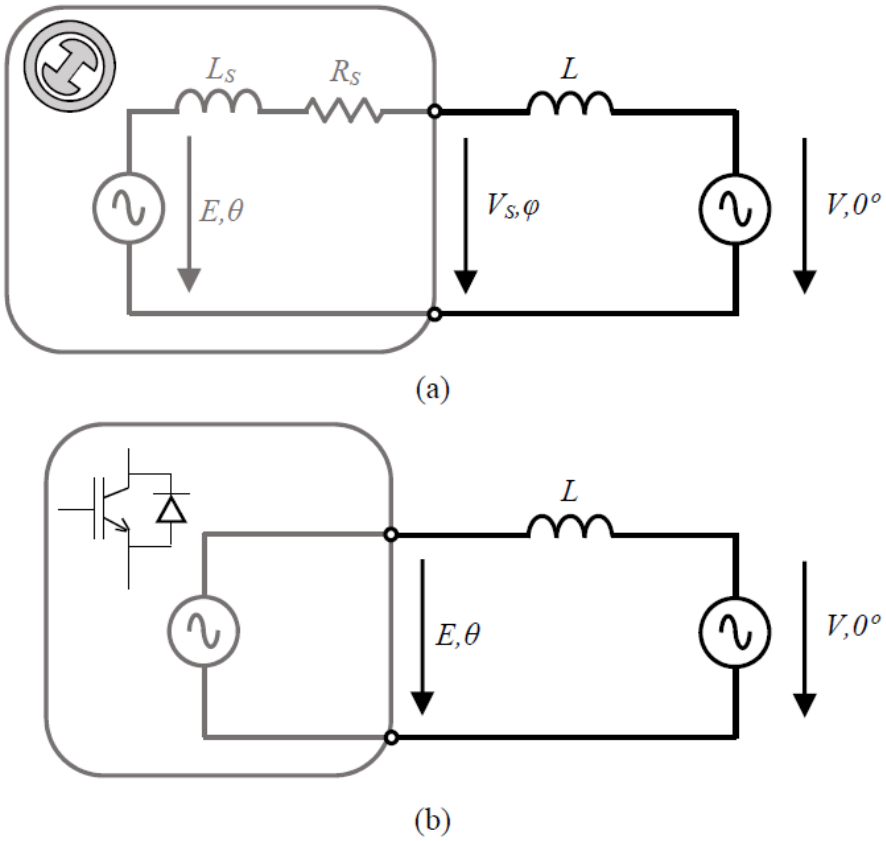

Figure 3.4: Equivalent circuit of: a) Synchronous generator, b) VSM mechanical model.

The mechanical model has both positive and negative aspects: it is a simple technique to improve frequency stability and to implement further control thanks to the damping coefficient, however the electrical characteristics of the generator, such as dependence on the frequency of the inductance, are not simulated and some problems remain, as power quality, the behavior against harmonics and imbalances, and the contribution to the currents of short circuit during an accident. In fact, non-desirable behaviors of synchronous generator are emulated, such as loss of synchronism during voltage sags: in this situation the active power output is almost zero as a consequence the virtual speed increases, as there is an imbalance between the reference power and the real power. When the voltage is re-established, according to the parameters of the VSM and the duration of the voltage sag, the system can lose control of the EMF phase with consequent uncontrolled power oscillations that require disconnection of the inverter from the grid.

b. Complete Model: to solve the problems of the mechanical model, in some VSM were implemented both the mechanical and electrical characteristics of a generator, therefore the flow lines and the effect of the damping circuits are emulated by the converter. As a consequence, the reactance of the converter has a frequency dependence, ie when the frequency increases the inductance decreases. This implies that the inverter's response to non-linear and unbalanced currents and voltages is better, while maintaining all the benefits of the mechanical model. However, as in the previous model, there is the same

response to voltage fluctuations and the inverter must be able to supply high currents during a short circuit, similar to a synchronous generator. Moreover, from a technical and economic point of view, the complete model could be an excessively complex control system with problems related to the measures and delay times.

c. Simplified Model: to avoid the complexity of the previous model, it has been proposed to use a simplified electric model, with the same characteristics of the mechanical model. Moreover, in this model of the synchronous generator there is an impedance *RL* that simulates the reactance of the generator. In practice, once the virtual EMF is calculated, a virtual impedance (L_s and R_s) is created and it is used to calculate the voltage at the VSM terminals:

$$v_{VSM} = e - i_{VSM} R_s - L_s \frac{di_{VSM}}{dt} \tag{3.4}$$

Consequently, as can also be seen in Figure 3.5, the converter is not used to generate the EMF as in the mechanical model and in the complete one, but produces the v_{VSG} voltage or, as in most cases, the i_{VSG} current. The simplified model thus allows to avoid the problems of the complete model, such as current variations due to small outputs of the filter inductance. Moreover, thanks to a closed control and a higher inductance value, the stability and robustness of the control system is higher. However, the dependence of the inductance from the frequency is lost but, to avoid this problem, different inductances can be used for different frequency ranges.

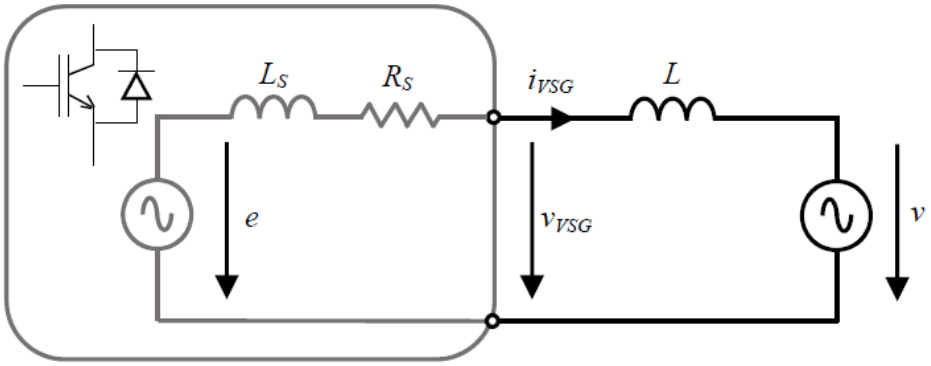

Figure 3.5: Equivalent circuit of the simplified model.

3.1.1.1 The converter behaviour to mimics inertia

Previously, several alternatives for synthetic inertia have been discussed. These models need to be interfaced with the power electronic converter through additional controllers which should receive reference signals from the control system and translate them into gate signals for the converter. These signals define if the converter is seen from the grid as a current source or a voltage source. However, it is important to note that all actual converters are called Voltage Sourced Converter (VSC): for major details refers to

Appendix . The control schemes proposed in literature can be divided into three main groups based on the nature of the output reference from the SM model. [26]

1. *Current Source SEBIR*: various types and implementations of SEBIR control have been proposed to enable NSG to support system frequency recovery in response to disturbances however, the principles of these control techniques are common, and are invariably based on the Swing Equation. The SEBIR technique, uses conventional PLL synchronised (rotating reference frame) with the grid so it is based on DQCI control. This mean that the converter performs as a current source that control the id current reference on the base of the active power output set by the SEBIR control. [13] The advantage of this scheme is that is relatively simple to be implemented by the manufacturers in existing VSC. On the other hands the disadvantages are that the control will rely on grid synchronization by a PLL and the presence of an external grid with a rotating inertia. Therefore, for this converter there are problems related to the delays caused by the time of measurement and the presence of filters, that makes the response significantly different to TI, and they need a voltage reference, which is accomplished by real SG and VSM voltage source. Moreover, operation in very weak grids can be dubious, and the control system will not have any inherent capability for black-start or islanded operation. [16] [18] [26] Figure 3.6 shows the typical configuration of a SEBIR control system, which can be described by the following equation:

$$\Delta P_{pu} = -R(s)F(s)M(s)\left(\frac{2H}{f_0}\frac{df}{dt}\right) \tag{3.5}$$

   where *M(s)* represents the measurement and filtering of *df/dt*, *F(s)* is the post-filtering applied to *df/dt* and *R(s)* describes the actual response of the converter. As previously said, a first problem arises from the fact that the measurement methods of the ROCOF involve delays and have problems of effectiveness and accuracy, while a second problem is the delay introduced by the "mechanical" response of the converter. As a consequence, this response is significantly different from the real inertial response of a synchronous generator. The synthetic inertia provided by a VSC-DQCI is therefore effective in improving the frequency nadir, however the phase of this response may be different from the one of a synchronous machine, ie *ΔP* in advance of 90° with respect to the frequency (*ΔP* responds to *df/dt*). As a consequence, if the delay is too high, the synthetic inertia is not able to mitigate the ROCOF during a disturbance. Moreover, if the delay leads to a 180° phase response (compared to the one of a synchronous generator) the power supplied by the synthetic inertia is in counter-phase with the rotor oscillations and favors the rotor oscillations, thus worsening the stability of the network.

2. *Current Source VSM*: in such schemes, the full order or reduced order model of a SM generates a current reference i_{ref}. This allows a quite natural implementation of high order electrical models for the SM since the measured voltage at the converter interface to the grid can feed a simulation model calculating the currents that would result from a real SM. This approach was applied by the VISMA concept, which was the first proposal of a VSM implementation, where the voltages at the point of common coupling with the grid are measured to calculate the phase currents of the VISMA in real time. These currents are then used as reference currents for the inverter, and hence, the inverter behaves as a current source connected to the grid. If the current tracking error is small, then the inverter behaves like a synchronous machine, justifying the term VISMA. If the current tracking error is large, then the inverter behaviour changes. [20] [24] The current controller can be realized by hysteresis controllers on phase currents, by PI-controllers or by any other conventional current controller in the stationary or synchronous reference frames. In principle, the current regulators can be easily tuned while saturations and limitations can be embedded directly on the i_{ref}. This control schemes as the advantages that does not require a PLL for ROCOF estimation and the maximum current feed by the inverter can be easily control. However, it needs a measurement of the voltage on the point of common coupling (PCC) [20] [24] [25], which can lead to instability.

3. *Voltage Source VSM*: the last approach is to configure a VSM model to provide a voltage reference output. In [16] [18] [19] the problem of limitation on the penetration of Current Source converters is presented: due to the fact that nowadays grid-connected converters (even so-called voltage-sourced converters, using forced-commutation devices) are controlled by software to operate as current sources that are grid following. Physically, this means that converters provide a current that is shifted according to the correct phase angle with respect to the grid voltage to provide the desired active and reactive power. Practically, it means that these converters require "appropriate support" to provide the grid with a stiff voltage, which is presently accomplished by synchronous machines. Eliminating all synchronous machines would mean that no frequency reference would be available to the grid; therefore, grid-following converters would not be viable. Hence, it is essential for some converters to control the voltage. These converters, called grid-forming converters, have controls that ensure the grid's voltage waveform is stable even at a very short time scale. This type of control enables the system to operate at a stable voltage even if loads connect/disconnect from the grid. [18] This converter behaviour is widely presented in [19] [21] [22] [23] [24] [29]. It takes the same VSC hardware, but completely changing the lower-level control software, the converter can be reprogrammed to operate as a true voltage source. The goal of the converter can be to achieve *P* and *Q* set-points, or to achieve frequency and voltage (*F&V*) set-points, or a *P&V* pair, or an *F&Q* pair. In this mode, the controller synthesises only balanced, positive-sequence sinusoidal voltages at the switching bridge. This is done by controlling the magnitude and angle of the "rotor" voltage compared to the magnitude and angle of the voltage, which exists at the point-of-common-coupling (PCC) with the grid. Between the bridge and the PCC is the filter inductor, and this can be thought of as an exact analogy of *X'* in a synchronous machine. *P* and *Q* flow in or out of the machine, based on the relative magnitudes and angles of the voltages at the bridge and at the PCC. The controller software which determines the rotor voltage, must have a bandwidth of less than 50Hz, and often it is significantly less, for example <5 Hz. This ensures that the synthesised voltage set contains only a slowly changing, balanced, positive-sequence, sinusoidal set of components. Since a converter controlled in this way behaves as a balanced positive-sequence sinusoidal voltage, behind a filter impedance *X'*, it has many of the same beneficial properties of a Synchronous Machine (SM).

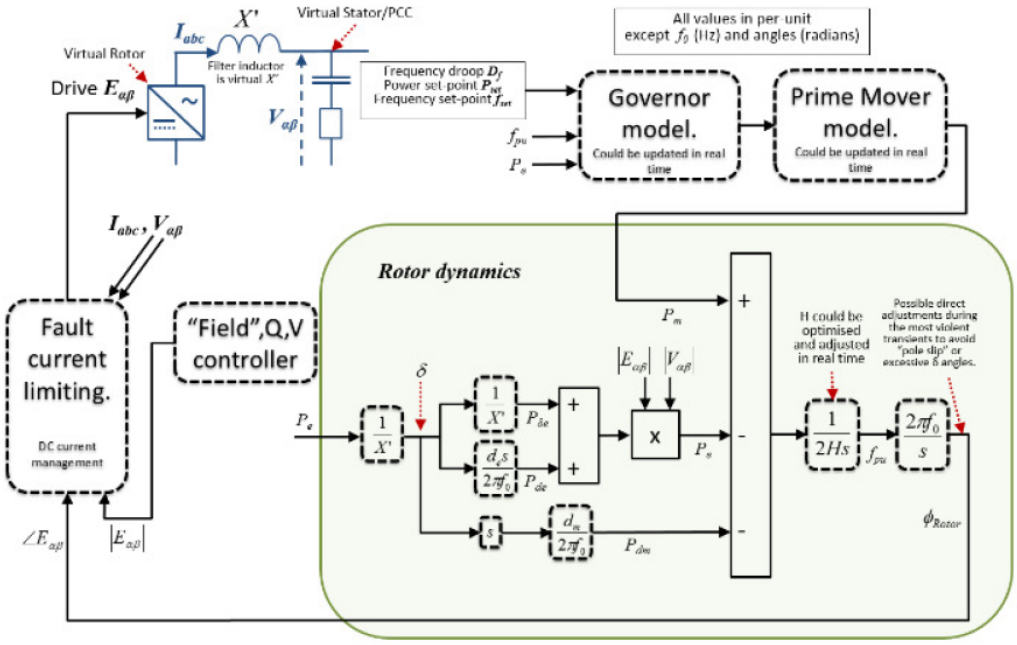

Figure 3.6: Model of the VSM.

3.1.1.2 The maximum penetration of DQCI converters

A further problem arises from the fact that the DQCI controllers are normally designed to be connected to a strong AC system and operate under the assumption that a balanced and symmetrical voltage source, ie a high presence of aggregate synchronous generators, is present in the network, but as the penetration of the systems interfaced with a DQCI converter increases, the actual network impedance between synchronous and non-synchronous generation increases, with a consequent possible instability of the DQCI converters. This phenomenon is caused by the aggregate transient reactance (X_{0d}), which becomes so large that, when a disturbance occurs, there may be large-band voltage disturbances at the connection point. [16] [18] [19] It is therefore essential to understand the effect of the increase of DQCI converters with SEBIR on the maximum renewable penetration in the network. In [29] a simplified network, shown in Figure 3.7, has been studied and critical penetration has been analysed: it has only a synchronous generator, a DQCI converter, with PMU measuring system, a main load and a load step (note that the VSM0H has been used for others analysis).

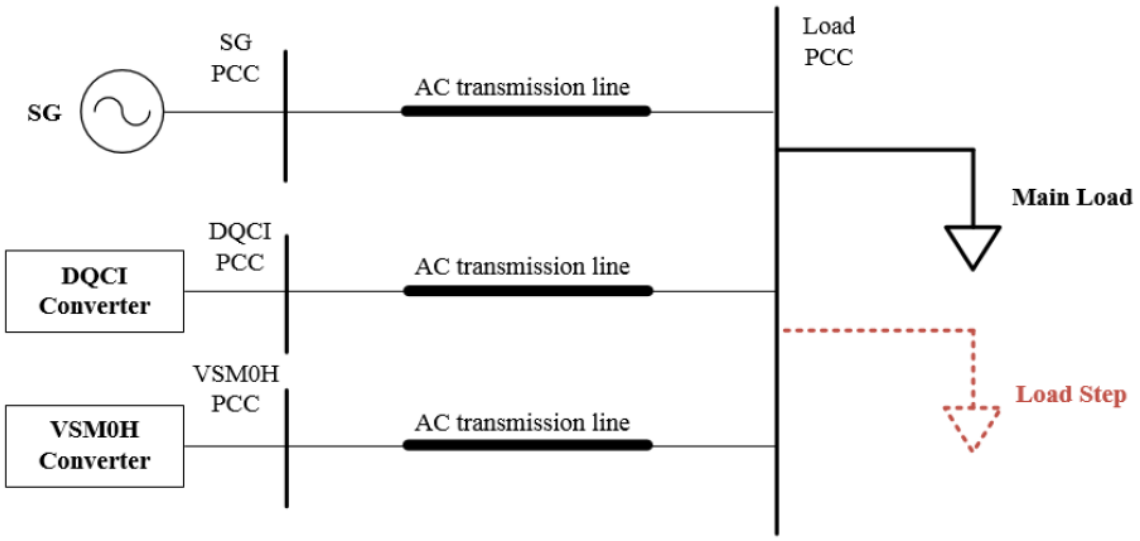

Figure 3.7: Simplified configuration of an electric system.

In [27] the results obtained, from this experiment, can be seen.

Virtual Inertia Constant [s]	*Maximum Penetration [%]*	
	PMU type P	*PMU type M*
H = 3	52.3	63.0
H = 4	47.5	59.4
H = 5	43.8	53.6

Table 3.1: Maximum penetration of DQCI-SEBIR converters in function of the virtual inertia and the measuring system.

It can be observed that:

- Depending on the different measurement accuracy class, there are different levels of maximum penetration and, as expected, it is higher for the DQCI with a better measurement system.
- When the synthetic inertia introduced into the network changes, the maximum penetration varies. However, it has been observed that higher virtual inertia levels result in a lower maximum penetration.

3.1.1.3 The VSM0H

As previously stated in "The maximum penetration of DQCI converters", typically for penetration levels below 50% the remaining traditional synchronous plants provide the appropriate response to power imbalances, it mitigate voltage instability and allow normal system operation and modelling. However, it has been anticipated that at some point between 50 and 80% [27] one or more of these effects will adversely affect operation and/or modelling. Therefore, to reach a renewable penetration close to 100% it is necessary to introduce a VSCs that behaves as controlled voltage source, producing a balanced three-phase voltage set behind an inductive filter impedance X_0, with the control bandwidths set to <5 Hz. This provides the plug-and-play functionality required to:

- Allow the system to be modelled at an aggregated and system level;

- Allows the converters to mitigate voltage power quality (e.g. unbalance or inter-harmonics) in a stable manner, in proportion to the converter ratings and per-unit filter impedance magnitudes;
- Allows converters to operate at extremely low fault levels – indeed to the fully islanded case including black-start scenarios;
- Allows converters to supply unbalanced and harmonic currents to unbalanced and non-linear loads, when loads require this;
- Provides the highest probability of network stability with 100% converter penetrations.

Nowadays, in literature [22] [23] [29] [27], there are two possible solutions, that use the VSCs operating by voltage generator: the VSM and the VSM0H. The VSM has already been presented, while the VSM0H will be discussed below. The VSM0H, also known as "inertia-less" VSM, as already mentioned, goes to control the converter in order that this behaves like a balanced voltage source, of direct sequence and only at the fundamental frequency. Moreover, it is able to filter unbalanced tensions and possible harmonics and interarmonics, thus mitigating tension quality problems at the point of common coupling. [27] However, the VSM0H controller represents a virtual synchronous machine but with zero inertia. Figure 3.8 shows the block diagram of the VSM0H control system: a balanced three-phase voltage, whose amplitude and frequency is controlled by two parallel cycles that respond to active and reactive power measurements, is generated but there is nothing, in the VSM0H control system, that tries to introduce a form of synthetic inertia, in fact the converter does not change its output power as soon as the frequency starts to drop, however as soon as the frequency deviation reaches significant values there is a dramatic increase in output power. Moreover, since the dynamic behaviour of the rotor is not introduced into the control system, the rotor damping oscillations are not emulated. As a result, this control strategy does not directly mitigate ROCOF, however, if there is sufficient power on the DC side, the VSM0H can greatly improve the frequency nadir. In [27], a percentage of 5% and 10% of VSM0H has been introduced in the network in Figure 3.7: in both case it was found that the maximum penetration is almost 100%, consequently the introduction into the network of a certain percentage of VSM0H allows to use DQCI converters and, at the same time, to have a stable system with only renewable sources.

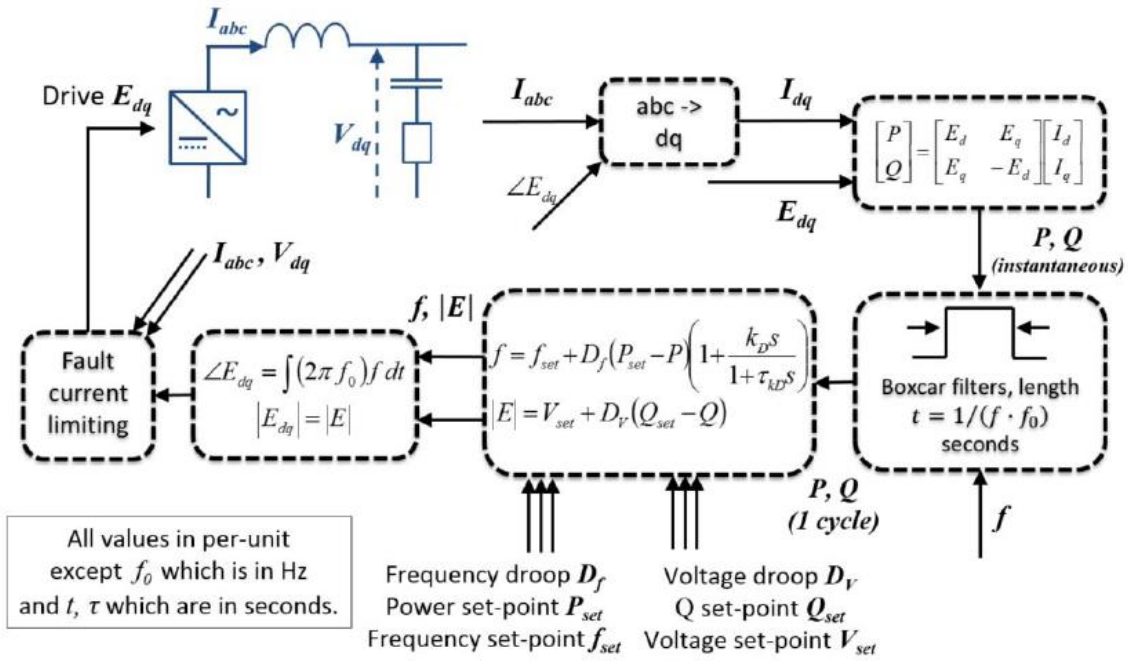

Figure 3.8: Model of VSM0H.

3.1.2 Fast Primary Reserve

A very interesting option for low inertia networks, and consequent wide frequency oscillations, is represented by the fast primary response, which can be obtained from wind or photovoltaic systems and storage systems. This control system will therefore influence the response of the system in the first seconds following a disturbance. As seen in (1.29) the response of the primary control system is greater for higher the frequency variation. However, due to the presence of a delay in the primary control, the answer can be seen as:

$$\delta_{prim}(t) = -\frac{1}{S_{prim}} \Delta f (t - T_{prim}) \tag{3.6}$$

Furthermore, limitations in the speed of power output increase must be added. Consequently, the primary control is much more complex than a system proportional to the frequency variation. However, by reducing the delay T_{prim}, it is possible to have a fast primary reserve. [9]

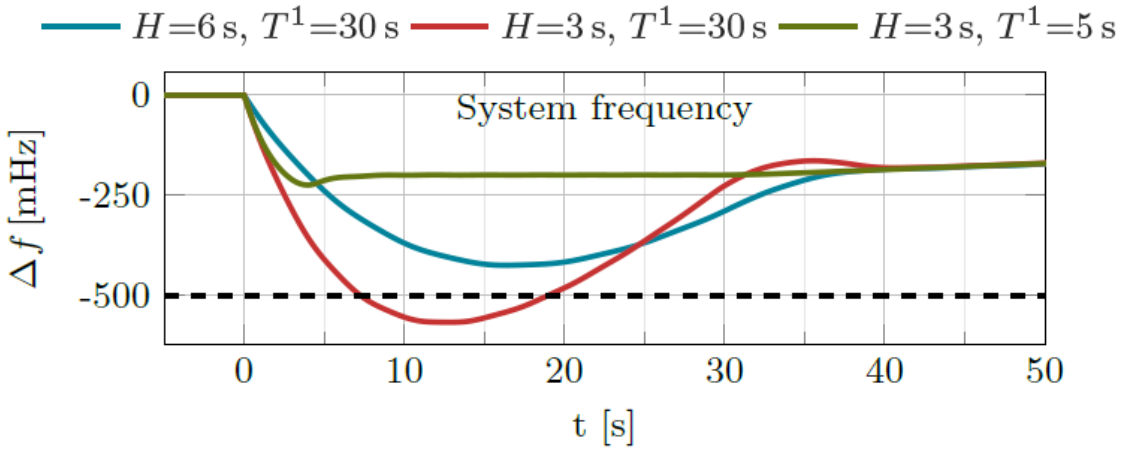

Figure 3.9: Dynamic response of the Continental European area power system to faults.

In Figure 3.9 can be observed that an improvement of the response time of the primary control, lead to an enormous improvement of the frequency nadir following a disturbance. In fact, the green curve represents the situation of a low inertia network but with renewable plants used to have produce a fast reserve: although there is not an improvement of the ROCOF, compared to the red curve, ie the curve with the same inertia but normal reserve, the frequency nadir improves dramatically and it is better than that of a network with high inertia but a normal control reserve (blue curve). Moreover, the time in which the frequency nadir is reached is lower, but this could lead to instability problems.

3.1.3 Comparison between synthetic inertia and fast frequency reserve

Table 3.2 sums up the concepts previously exposed:

	Synthetic Inertia	***True Inertia***	***Frequency Droop***
SEBIR	Yes	No	No
VSM	Yes	Yes	Yes
Fast Primary Reserve	No	No	Yes

Table 3.2: Comparison between VSM, SEBIR and Fast Frequency Reserve.

It can be noted that the VSM is the only control system that is able to provide a synthetic inertia comparable with the inertia of a SM, because VSM mimics the true inertial response of a SM. Moreover, VSM has a frequency droop that generate a primary reserve. On the other hands SEBIR is a simple and effective control system but presents a synthetic inertia that is not a true inertial response due to the delay in the ROCOF measurements, and it does not provide a primary reserve. Finally, Fast Primary Response is a method to create a more effective primary reserve, but it does not influence the inertial response of the system.

	ROCOF	***Frequency Nadir***
SEBIR	Minimal	Medium
VSM	High	Medium
Fast Primary Reserve	Zero	High

Table 3.3: Effect of SEBIR, VSM and Fast Primary Reserve on ROCOF and Frequency Nadir.

Table 3.3 presents the possible effect of SEBIR, VSM and Fast Primary Reserve on ROCOF and Frequency Nadir, on a scale that goes from zero to high effect: SEBIR has a minimal influence on ROCOF due to the

delay in the ROCOF measurements and a medium effect on Frequency Nadir, while VSM is the best solution to limit the ROCOF, due to its true inertial response. On the other hands, even if Fast Primary Reserve does not give improvements in the ROCOF, it has the most beneficial effect on Frequency Nadir.

3.2 THE SUPPORT ON THE FREQUENCY STABILITY BY VRG

Although variable renewable energy systems cannot contribute to inertia without the use of special control systems, the wind farms have kinetic energy stored in the blades while the photovoltaic parks, even if they do not have rotating parts, have a small energy stored in the capacitors: these forms of energy can therefore be used to support frequency stability. Moreover, both can be coupled with Energy Storage Systems (ESS) to store energy during peak hours. In fact, in order to provide inertia to the network, fast energy reserves, such as batteries or supercapacitors, can be used to generate synthetic inertia. The ESS stores the excess energy produced and release it after a generation loss. It is therefore necessary a control system that coordinates the ESS and the VRG to optimize the power output. A further solution, known as deloading technique, is represented by the possibility of reducing the power output from the plant to work in a sub-optimal point, in order to create a power reserve suitable for the frequency control. However, it should be noted that this method is economically very disadvantageous.

3.2.1 Frequency support from wind farms

In a wind turbine the blades, the gearbox and the generator contribute to the inertia of the wind farm, which settles on values of 2-5 s, depending on the type and size of the turbine and if the gearbox is installed or not. It therefore has values comparable with those of a traditional system, however there are several problems to consider:

- The stored kinetic energy varies with the speed of the turbine and therefore depends on the wind. As a consequence, it results variable over the time. In other words, the wind turbine inertia constant, which is defined by its nominal speed, varies in the wind turbine operating speed range, as can be seen in Figure 3.10. At the minimum rotor speed, the stored kinetic energy is lowered by about 60% compared to the nominal conditions. Furthermore, it has been observed that in half of the operating time of the wind turbine, the stored kinetic energy is less than 50% of the maximum possible energy.
- Nowadays wind farms are connected to the grid via a power converter, which involves decoupling from the grid. Consequently, in this case there is no contribution to inertia by wind generators.
- If the power converter is used to have synthetic inertia from the wind generator, there will no longer be a direct relationship between the rotor speed and the ROCOF, consequently it is not possible to add the inertia of a traditional generator with that one of a wind plant. However, this can also be an advantage as the energy released can be controlled independently of the ROCOF.

Wind energy is, to date, one of the most used renewable energy sources in the world. There are two main categories of wind turbines: [31]

1. Fixed-speed turbines: they have an induction generator that can be connected directly to the network and is therefore able to provide inertia, even if variable and lower than a traditional system;
2. Variable speed turbines: they can use two types of generators, those with permanent magnets (PMSG Permanent Magnet Synchronous Generator) or DFIG (Doubly Fed Induction Generator),

but in both cases, the connection to the grid is via a power converter and so they are decoupled from the network. However, this allows to operate with a wide range of wind speed values therefore this type is the most used. The PMSG is fully decoupled from the grid; this is because the stator of this type of generator is connected to the power electronic converter in order to inject the power into the grid. The DFIG is similar to the PMSG, except for the fact that this generator is connected to the grid via a rotor circuit.

The power produced by a wind turbine depends on the amount of wind that impacts the blades; this can be seen from equation (3.7), which expresses the mechanical power generated by a wind turbine: [32]

$$P_{mech} = \frac{1}{2}\rho A_R c_p(\lambda, \beta) v_w^3 \tag{3.7}$$

where ρ is the density of the air, A_R is the area of the rotor, c_p is the coefficient of power and v_w is the speed of the wind. It can be observed that the power coefficient is the only variable that does not depend on the external environment or on fixed geometric conditions. This coefficient is a function of the tip speed ratio λ, which is defined as the ratio between the velocity $u = \omega_R \cdot R_R$ and the one of the wind v_w, and the inclination of the blade β (blade pitch angle).

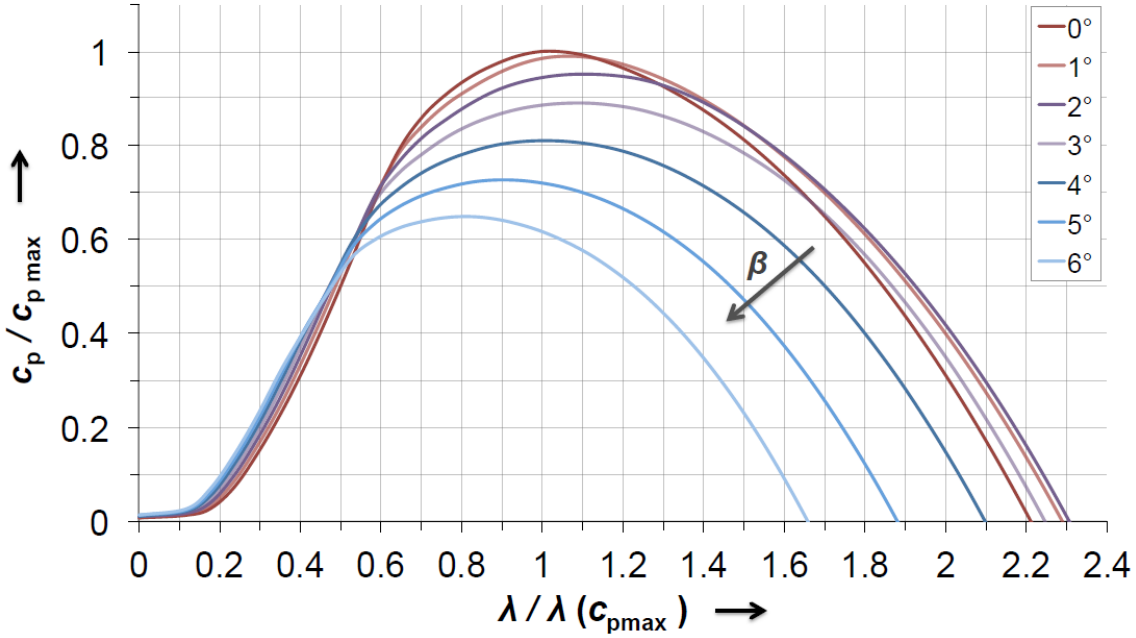

Figure 3.10: Power coefficient versus tip-speed ratio for different.

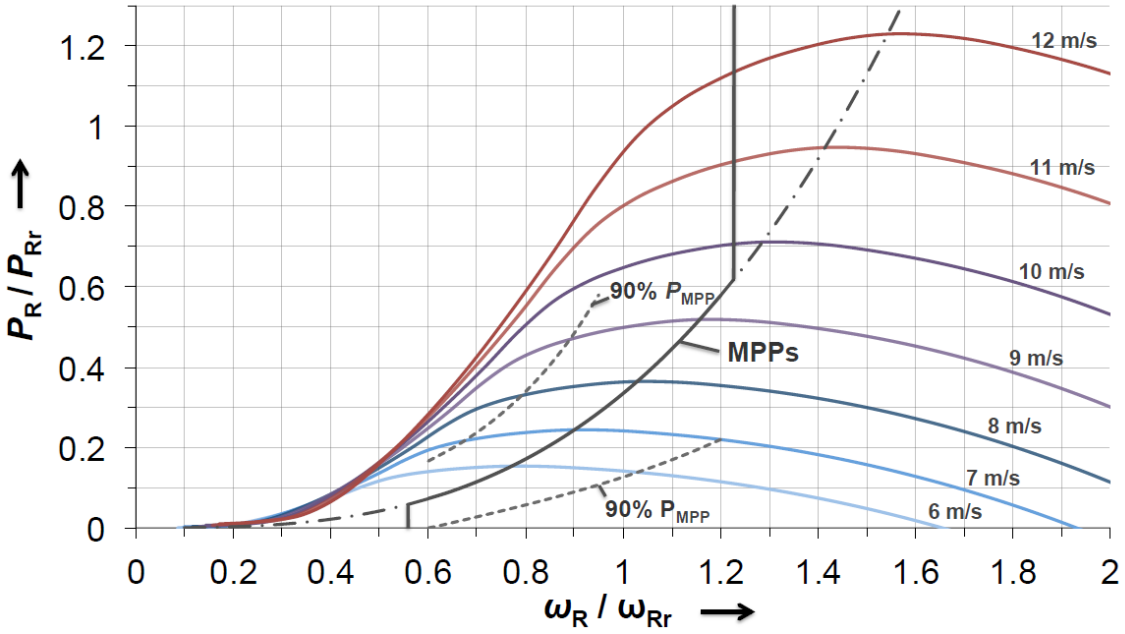

Figure 3.11: Power versus rotor speed and power reserve curve through speed control.

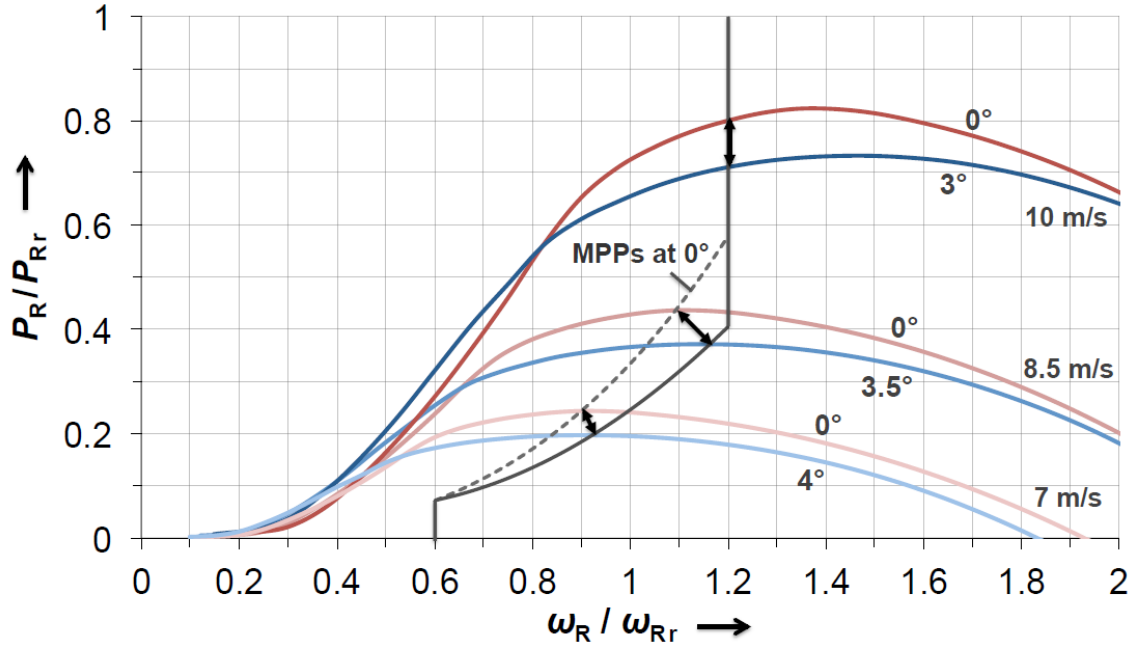

Figure 3.12: Power versus rotor speed and power reserve curve through pitch control.

Figure 3.10 shows the power coefficient as a function of λ for different values of β. Figure 3.11, instead, shows the power generated for different wind speed values, according to equation (3.7), while Figure 3.12 shows the power generated for different pitch angles. The turbine's speed controller changes the generator torque to follow the Maximum Power Point (MPP), as the wind speed increases, until the maximum rotor

speed is reached. From this point, the control of the inclination of the blades is activated to maintain this speed even if the speed of the wind increases, in order to avoid damage to the mechanical components of the wind turbine. Observe that it is possible to create a power reserve by making the turbine operate at a different point from the MPP. In several studies, various techniques have been studied to provide inertia response and support to power control from wind power plants, without or with the use of ESS. These techniques will be analyzed below:

3.2.1.1 Wind power plants without ESS:

Variable-speed wind turbines do not have the ability to release the energy stored into their rotating parts, so control techniques, that provide an inertial response, have been created:

- Inertia Emulation: through a specific control implemented in the converter, it is possible to release the kinetic energy, with an inertia constant in the range of 2-6 s. In general, this technique can be obtained through two types of inertial response, one with a single cycle (one loop) and the other with two cycles (two loops). In the first, a control cycle based on the ROCOF is used to release the stored kinetic energy in the rotating parts, while the second uses two control cycles, one based on the ROCOF and the other on the variation of frequency, which allows to overcome some problems of the single cycle. The Inertia Emulation control system is implemented into the turbine speed control system and then operates by changing the turbine speed.

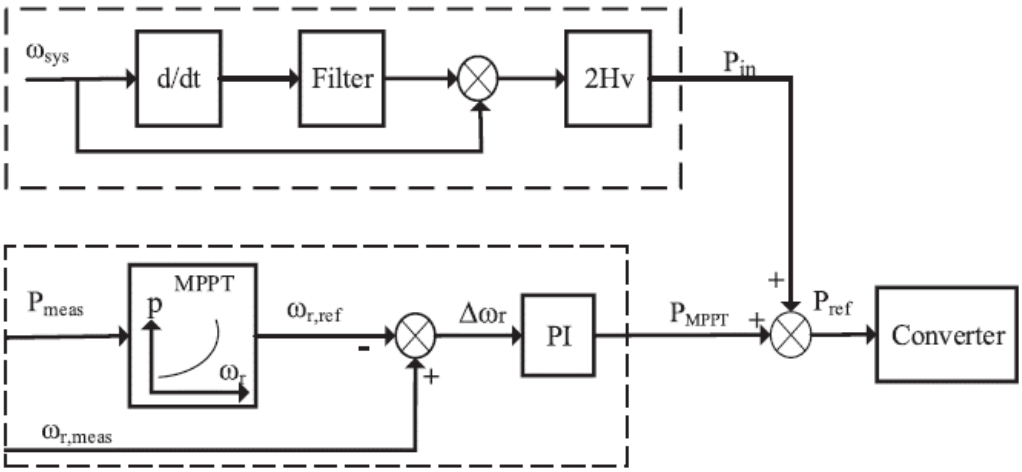

Figure 3.13: Inertia emulation for variable speed wind turbines.

Figure 3.13 shows a diagram of the cycle based on the ROCOF: during a disturbance, a certain amount of power, determined according to the ROCOF and the value of the virtual inertia, is added to the power found with the MPPT. The virtual inertia is inversely proportional to the system frequency so the torque transferred to the converter decreases as the frequency decreases, in order to prevent the rotor speed from falling too fast. The cycle based on the ROCOF therefore provides a decelerating torque proportional to the ROCOF, as long as the frequency is not restored. However, when the system has been restored to optimal conditions, the turbine will have a low speed and therefore the control of the MPP will reduce the power supplied to the network to speed up the turbine, with consequent loss of the support to the frequency stability. To overcome this problem a second cycle has been added which provides an additional torque, which is proportional to the

frequency deviation and therefore remains until the system returns to nominal frequency values. This system allows to delay the re-acceleration of the turbine as much as possible.

- Fast Power Reserve: this is another type of frequency control system that provides a constant power, in addition to the nominal power, for a certain time. Usually 10% more than the nominal active power is used, for 10 s. [31] This short-term constant power is released thanks to the kinetic energy stored in the rotating parts of the turbine. This fast power reserve can be obtained by controlling the working point of the rotor speed. The energy that is obtained from the fast reserve will therefore be:

$$P_{FPR}(t) = \frac{1}{2} J \omega_{r_o}^2 - \frac{1}{2} J \omega_{r_{(t)}}^2 \tag{3.8}$$

where P_{FPR} is the constant power, ω_{r_o} is the initial velocity, ie before the disturbance, and $\omega_{r_{(t)}}$ is the rotation speed at the end of the fast response. As a consequence, once the constant power and the initial speed have been defined, it is possible to obtain the speed that will be needed:

$$\omega_{r_{(t)}} = \sqrt{\omega_{r_o}^2 - 2\frac{P_{FPR}}{J}t} \tag{3.9}$$

The fast primary reserve system is activated when the frequency deviation exceeds a certain predefined threshold and generates a signal that bypasses the MPPT.

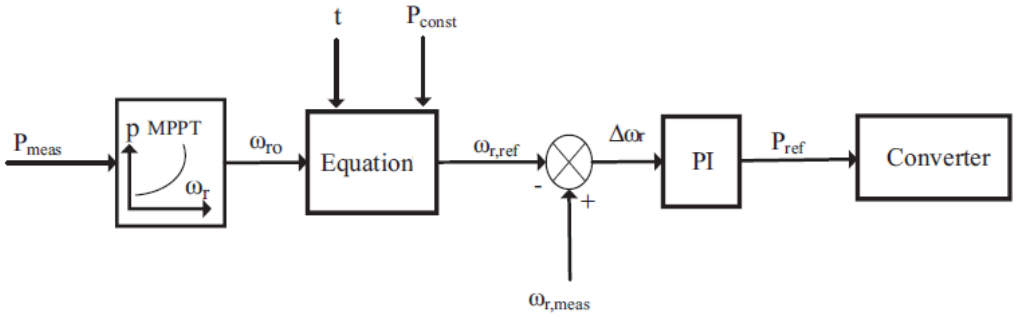

Figure 3.14: Fast power reserve controller for a wind turbine.

This system remains active as long as there is kinetic energy, then the speed regulator will return to act on the speed to restore the MPP. This phenomenon of speed restoration involves an under-production phase, in which a part of the power is not supplied to the network in order to bring the rotor back to the speed that guarantees the MPP. To avoid an instantaneous drop in power from the overproduction to the underproduction phase, a transition must be followed, as shown in Figure 3.15:

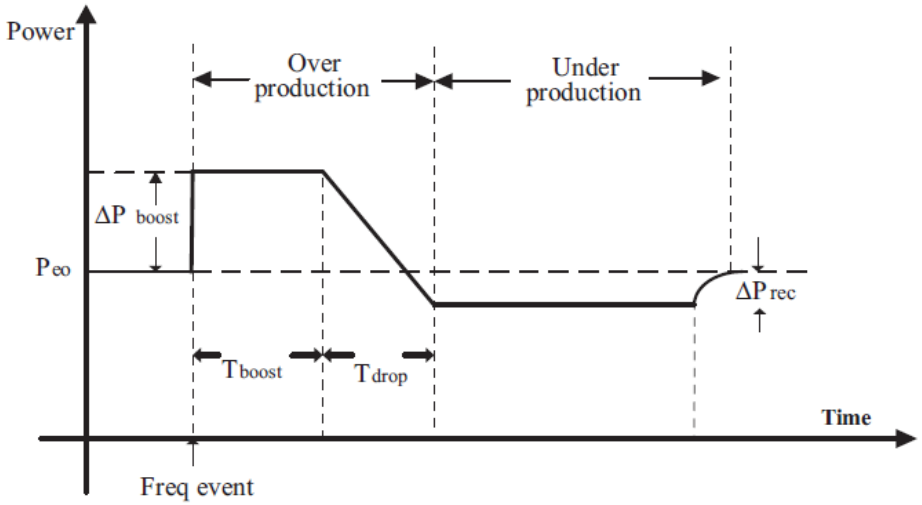

Figure 3.15: Power characteristics for fast power reserve control.

- Droop control: it regulates the output power of the wind turbine proportionally to the frequency variation, in this way it allows to improve the frequency nadir and the recovery process of the nominal frequency following a disturbance. The active power is adjusted according to a linear relationship given by:

$$\Delta P = P_1 - P_0 = -\frac{f_{meas} - f_{nom}}{R} \tag{3.10}$$

where R is the lowering constant, f_{meas} is the measured frequency, P_1 is the new value of power output while f_{nom} and P_0 are the initial working points.

- Deloading Tecnique: from a purely economic point of view, the wind turbines are built to work in the MPP and as a result do not have an available power reserve that allows them to participate in the frequency regulation. However, as already mentioned, it is possible to create a reserve of power by working in a different point from the MPP. From eq. (3.7), it can be noted how the power depends on the peak speed ratio λ and from the angle of inclination of the blades β, as a consequence, through the speed and/or angle regulator, it is possible to create a power reserve.
  - Deloading via speed control: the regulator acts on the rotor speed to operate at a different point from the MPP and in this way a power reserve is created. [32] From Figure 3.11 it can be observed that, due to the fact that the curve is convex, theoretically there are two points in which it is possible to create the desired power reserve, however only the point of over-speed can be taken into consideration, as the one of under-speed requires energy to accelerate when power reserve is required. Note that due to the limitations of maximum rotor speed, the available primary reserve decreases with the increase of the wind speed, consequently the control range of the speed regulator is limited to values close to the rated power.
  - Deloading via pitch angle control: by tilting the blades in relation to the wind direction, it is possible to create a power reserve. Following a request for this reserve, the inclination angle is reduced and therefore the output power is increased. This control system is

applicable throughout the operating range of the wind turbine. Figure 3.12 shows the primary reserve obtained through pitch control graphically.

In most cases, the two deloading techniques will be used together: the speed control is used until the maximum rotor speed is reached, then the blade inclination control comes into play.

3.2.1.2 Wind power plants with ESS

The variable nature of the energy production from wind power plants has led to considering the introduction of ESS to make the support from wind farms more reliable. Usually, therefore, the previously analyzed techniques are used in combination with a storage system, which allows to solve the problems related to frequency oscillations and frequency drop. In fact, the ESS allows to supply power during the re-acceleration phase of the turbine, in order to avoid the frequency drop, due to the lower power supplied to the network in this phase, and it acts as a backup system to absorb/supply power during the power unbalancing phases.

3.2.2 Frequency support from photovoltaic parks

The power produced by a photovoltaic plant can be controlled from the DC voltage of its modules, according to the following relation:

$$P = U_{DC} I_{SC} \left(1 - e^{K \frac{U_{DC} - U_{OC}}{U_{MPP} - U_{OC}}} \right) \tag{3.11}$$

where U_{DC} is the DC voltage, I_{SC} is the short-circuit current, K is the form factor, ie a constant factor that depends on the slope of the characteristic of a photovoltaic system shown in the figure, U_{OC} is the no-load voltage and U_{MPP} is the voltage in the MPP.

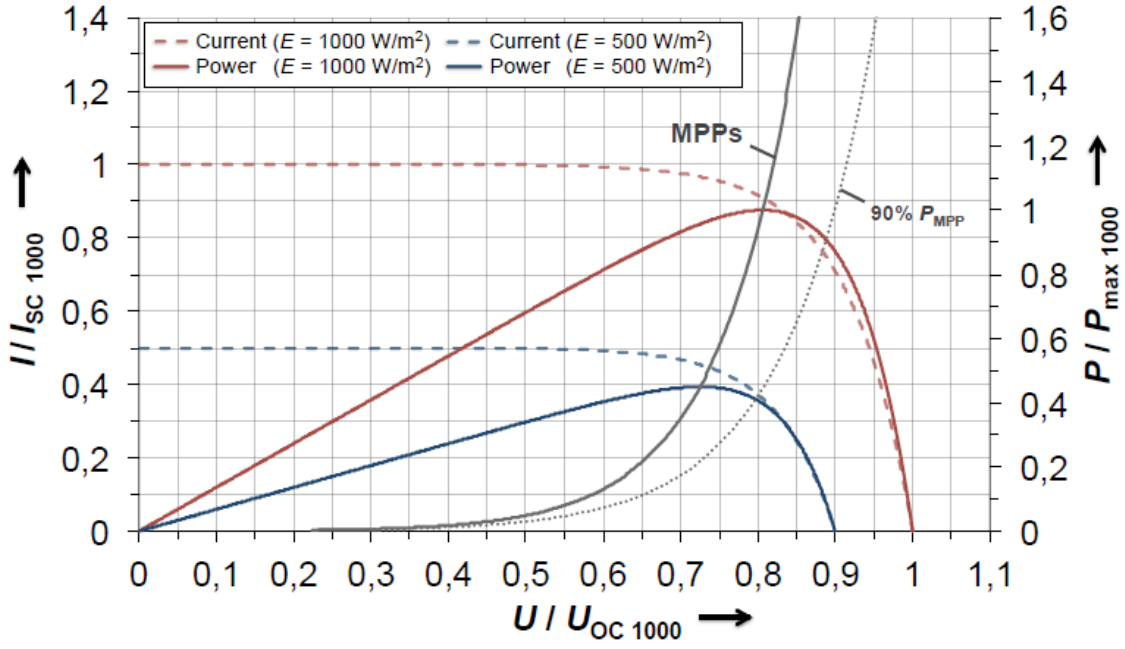

Figure 3.16: Current and power characteristic of a photovoltaic module.

Conventionally the DC voltage is set at the MPP, in order to convert all the solar radiation into electrical energy. However, as already mentioned, it is possible to create an energy reserve by working at a higher voltage point. It should be noted that, when the deloading technique is used, the photovoltaic plant generates an output current that is lower and so there are less electrical losses. As is known in photovoltaic systems there are no rotating masses, therefore, except for a very small amount of energy in the capacitors, there is no stored energy but it is possible to add ESS, which allow to introduce a control system able to provide both an inertial response and a fast primary reserve. For this purpose, batteries or supercapacitors are used, as they act as fast-acting storage units, ie they are able to inject/absorb power in times ranging from hundreds of milliseconds to a few seconds. [33] The Distributed Energy Storage System (DESS) thus allow an inertial response and primary control, even from photovoltaic systems. In [33] some characteristics, that the DESSs should have, are presented:

- Intervention time: the reserve must activate within 1 s in areas where the ROCOF can be higher than 1 Hz/s;
- Duration: they must be able to supply power until the primary control is activated.
- Deactivation: DESSs must be deactivated progressively in order to avoid a sudden imbalance in the system. A ramp of 10 seconds from full power to zero seems to be the optimal one.

3.3 ADDITIONAL SYSTEMS FOR FREQUENCY STABILITY

3.3.1 Synchronous condenser

Synchronous Compensators (SC) are one of the traditional solutions to various network stability problems: they play a fundamental role in reactive power compensation and voltage stability from more than fifty years, but they can also be used for frequency stability. In fact, in recent studies [34], it has been ascertained that SCs can also be used to support network inertia and, moreover, a compensator power control system has been created, which, through the modulation of reactive power, assists the generator regulator and allows to improve the primary response. Since the synchronous compensators are a rotating machine, they present stored kinetic energy in their rotating masses therefore inertia is one of their own characteristic. In other words, SCs can be used to absorb/release kinetic energy to promote frequency stability during a disturbance. However, it is important to note that the synchronous compensator is a rotating machine without the prime mover and therefore can provide a lower inertia, with typical values of 1 -1.25 s. [35] In addition, SCs cannot be controlled quickly and therefore cannot compensate for rapid load changes. Finally, a further disadvantage of the synchronous compensators is the high demand for a form of cooling.

3.3.2 STATCOM

In recent years, there have been numerous advances in the field of power electronics that have led to new FACTS devices (Flexible AC Transmission Systems). These include the STATCOM (Static Compensator), which is a static synchronous compensator based on VSC (Voltage Source Converter) technology. STATCOM is already widely used in the transmission network to provide dynamic and static voltage regulation and to improve power flows, through reactive power control. The STATCOM in fact, thanks to a capacitor connected in shunt on the DC-link, have the ability to exchange reactive power with the network, by keeping the output voltage in phase with the one of the network and acting on the amplitude of the fundamental voltage output. SVC PLUS is the technology of STATCOM, based on MMC (Modular Multilevel Converter), currently more used, due to its superior characteristics. [36]

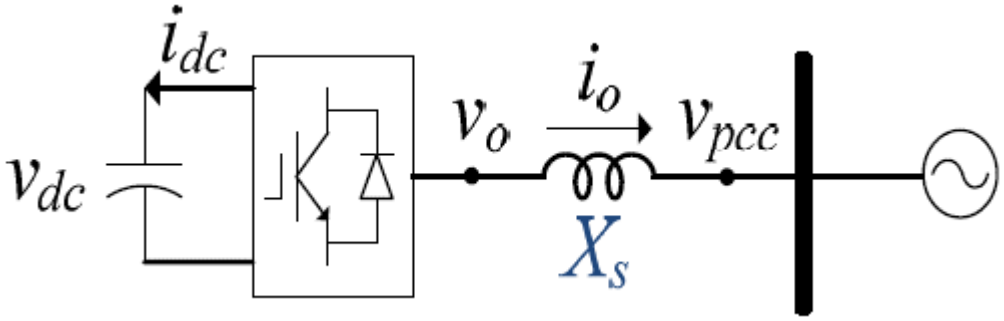

Figure 3.17: Single line diagram of the cascaded multilevel inverter based STATCOM.

In [35] the contribution to inertia by a STATCOM has been analyzed, by using the energy stored in the capacitor with a specific control technique. In fact, by varying the angle between the output voltage to the STATCOM and the grid voltage it is possible to transfer power to the network, however, given the low power density of the capacitors, it is possible to provide support only in the first moments inertial response. In any case, STATCOM is competitive with synchronous compensators, since the inertial response of SCs, while being natural and automatic, is limited by frequency variation while STATCOM, because it is device based on voltage control, can provide a higher inertia, even if for a much lower time, since its inertia constant does not depend on the frequency. Recently, in numerous studies such as [36] [37] [38], it has been proposed to equip the STATCOM with a frequency control system and a storage system in order to provide support for frequency stability, even if it does not have moving mechanical parts, thanks to the energy stored in the ESS. Frequency regulation using STATCOM can be achieved with four different techniques:

1. Control system based on the frequency deviation:

$$\Delta P_{STATCOM} = -K_{STATCOM}\Delta f \tag{3.12}$$

2. Control system based on the ROCOF:

$$\Delta P_{STATCOM} = -K_{STATCOM}\frac{d\Delta f}{dt} \tag{3.13}$$

3. Combination of the previous control system:

$$\Delta P_{STATCOM} = -K_{STATCOM_1}\Delta f - K_{STATCOM_2}\frac{d\Delta f}{dt} \tag{3.14}$$

4. Control system based on power measurement.

In any case, as previously mentioned, a storage system is necessary to provide the necessary active power: in most cases lithium-ion (Li-Ion) batteries are used, as they have a high energy density, however in [36] the use of supercapacitors in combination with SVC PLUS is proposed. Their characteristics, such as modularity and increased power density, and the fact that they are becoming a mature and proven technology, make them a beneficial alternative to BESSs, both technically and economically. In fact, for applications ranging from a few milliseconds to a few seconds (like the inertial response), they have lower investment costs and need less space. Furthermore, the main objective of STATCOMs equipped with ESS

is to support the inertial response following a serious disturbance in the network, so the higher power density of the supercapacitors is another advantage. However, it should be noted that the lower energy density compared to the batteries allows a short duration response and therefore does not allow to provide support to the primary control, which is instead possible with the BESS. In [36] the frequency response of the English transmission system, after the loss of a 1000 MW generation group, has been studied, with and without SVC PLUS (500 MVA), with supercapacitors and third-type control system, in order to analyze the impact on the network.

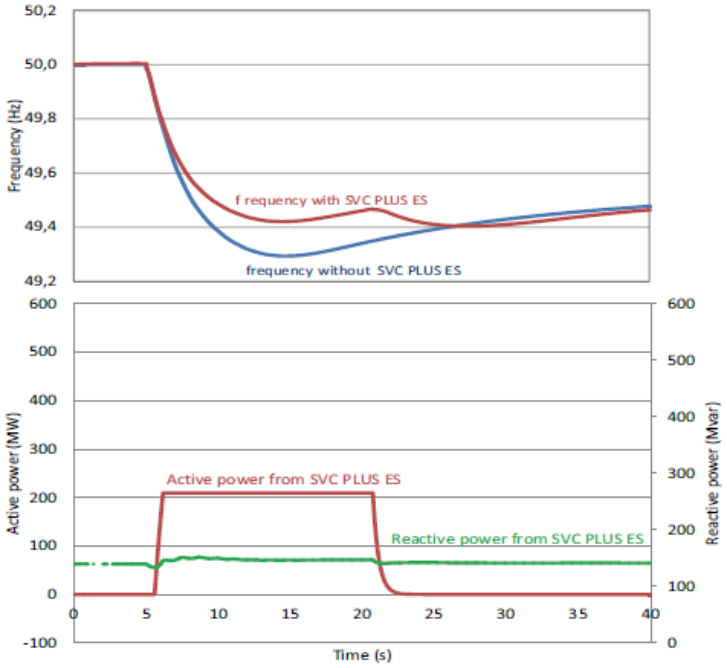

Figure 3.18: Frequency with and without SVC PLUS ES and its power output.

In Figure 3.18: Frequency with and without SVC PLUS ES and its power output. Figure 3.18 can be seen that when the frequency exceeds a certain threshold (49.9 Hz in this case) the STATCOM is activated. The answer inertial is much better, however, the fact of using SVC PLUS at full power means that the supercapacitors are quickly discharged resulting in a second lowering of frequency. To overcome this problem, the active power output from the STATCOM was limited to 40%. In Figure 3.19 can be seen that the results are much better.

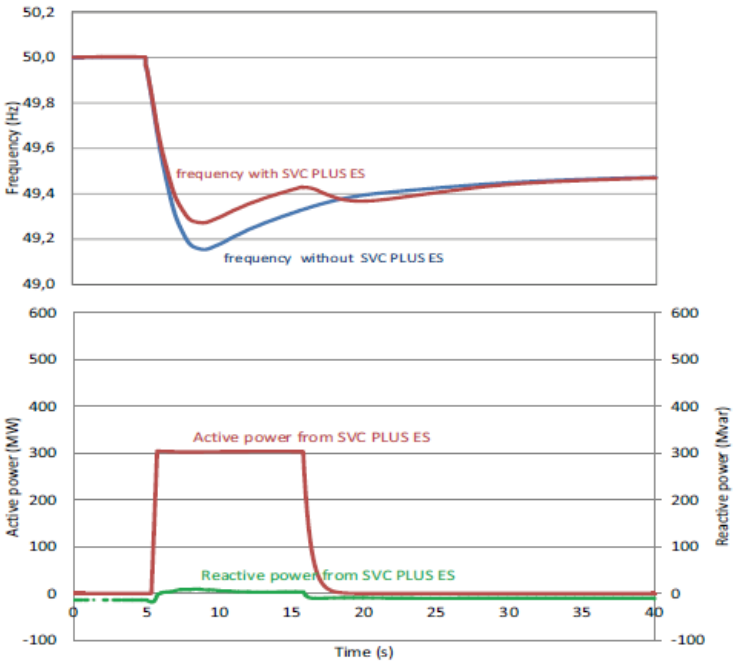

Figure 3.19: Frequency with and without SVC PLUS ES in the same grid with reduced inertia.

3.3.3 VSC-HVDC

High Voltage Direct Current (HVDC) systems are an effective solution for transmitting energy over long distances and for connecting power systems with different frequencies (de-synchronized). The most recent generation of HVDC uses Voltage Source Converter (VSC), which allows to control active and reactive power, voltage and frequency, independently on both sides. In fact, the VSC-HVDC have a more sophisticated control system of the CSC-HVDC (Current Source Converter HVDC) that allows to: feed passive networks, continuous control of tension and frequency, black-starting and rapid inversion of the power flow. On the other hand, as the CSC-HVDCs are a more mature technology, they have higher power levels and lower losses. [39] The VSC-HVDC system employs a simple and robust PI controller structure that includes: an internal and external current control cycle, active power control in the sending end converter, a DC voltage control in the receiving end converter and a control of the reactive power on both sides, which allows to maintain the AC voltage at the desired level. [40] Moreover, recently, several studies, to implement a frequency control system in VSC-HVDC, have been done. In [39] [40], the possible control strategies to obtain synthetic inertia and primary frequency control of the VSC-HVDC have been presented. First of all, it is necessary to briefly describe the behavior of a VSC-HVDC: it can be considered as a synchronous machine, quickly controllable, connected to an AC system through an AC filter. The output voltage of the Voltage Source Converter is a function of the modulation index M and the phase ϕ with respect to the grid voltage:

$$V_{VSC} = \frac{1}{2}(MV_{DC}sin(\omega t + \phi)) \tag{3.15}$$

The control system of the VSC-HVDC is based on the DQCI, previously discussed, and therefore allows to control P and Q set-point by adjusting I_d and I_q to obtain the required values of V_{VSC} and ϕ:

$$P = \frac{V_{VSC} V_{rete} sin(\phi)}{X} \tag{3.16}$$

$$Q = \frac{V_{VSC}^2 - V_{VSC} V_{rete} cos(\phi)}{X} \tag{3.17}$$

The control system presents external and internal cycles, as can be seen in Figure 3.20: there is an external cycle that measures V_{AC} and Q and calculate $I_{d_{ref}}$, which acts as a reference for the internal cycle that defines the required I_d, then there is a further external cycle which measures V_{DC} and P and calculate $I_{q_{ref}}$, which acts as a reference for the internal cycle that defines the required I_q. Therefore, this control systems can be used to support frequency stability with HVDCs.

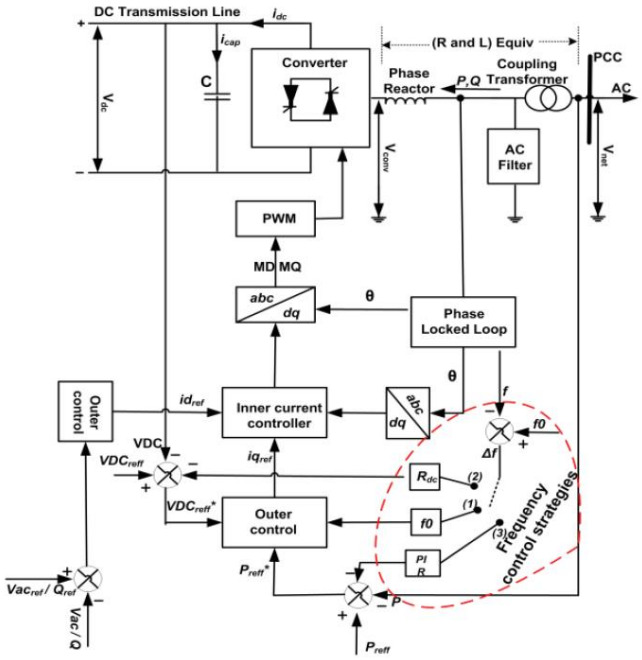

Figure 3.20: Block diagram of VSC-HVDC with frequency control strategies.

The methods present in the literature can be divided into:

- Synthetic inertia without ESS: a first technique for obtaining frequency support from VSC-HVDC is to use the energy stored in the DC capacitors of the HVDC system. Eq. (3.18) illustrates the relationship between the DC voltage and this energy:

$$E_{DC} = \frac{1}{2}(C_{DC} V_{DC})^2 \tag{3.18}$$

  This strategy for obtaining synthetic inertia uses a derivative controller that generate a signal proportional to the *ROCOF*, according to a term *H* which represents the virtual inertia, which changes the DC voltage or the active power. Two approaches to this type of control are possible: the first is the continuous one, which adapts to the frequency variations of the network but requires

a more complex filtering system, while the second one is the one-shot, which is based on the ROCOF initial and therefore is easier to implement but does not continuously adapt to frequency of the network. Moreover, it is important to observe that the energy stored in the DC capacitors of the HVDC system can also be utilized for fast primary reserve. However, the energy stored in DC capacitors is very limited therefore this method can be used only for a limited time.

- Synthetic inertia with ESS: in short, it uses a fast storage system and a control system, based on SEBIR or VSM, to generate inertia and, eventually, a primary reserve. This method has already been presented.

4. MODEL OF SEBIR AND VSM

In this chapter the SEBIR and VSM, modelled in DIgSILENT Powerfactory, are presented. DIgSILENT (acronym of DIgitalSImuLation of Electrical NeTworks) Powerfactory is a software for simulation and study of electrical networks, through which it is possible to insert graphic elements, representing the network elements, through the GUI (Grafical User Interface). The use of a single database equipped with all the components that can compose an electrical system (such as generators, lines, transformers, controllers, batteries, static converters, etc.) allows the software to perform all the simulation, such as the calculation of power flows, short circuits, coordination protections, dynamic simulations, etc., in a single work environment. In this thesis the response of a network model, after a frequency variation, determined (for analysis purposes) by a load insertion, has been studied. The transients in electrical power systems can be of short duration (electromagnetic transient), medium duration (electromechanical transient) and long duration. The simulations available on DIgSILENT Powerfactory are:

- Symmetrical Steady-State RMS, which considers only the fundamental components of tensions and currents. They are used for medium and long-term transients;
- Three-Phase RMS, in the case of asymmetry conditions, for example non-symmetrical failures;
- Three-Phase EMT, for the study of electromagnetic transients, ie of short duration, representing voltages and currents with their instantaneous values.

More information about the software can be found in [41].

4.1 SEBIR

In this section, the model and the frame of the SEBIR control system are introduced.

4.1.1 SEBIR frame

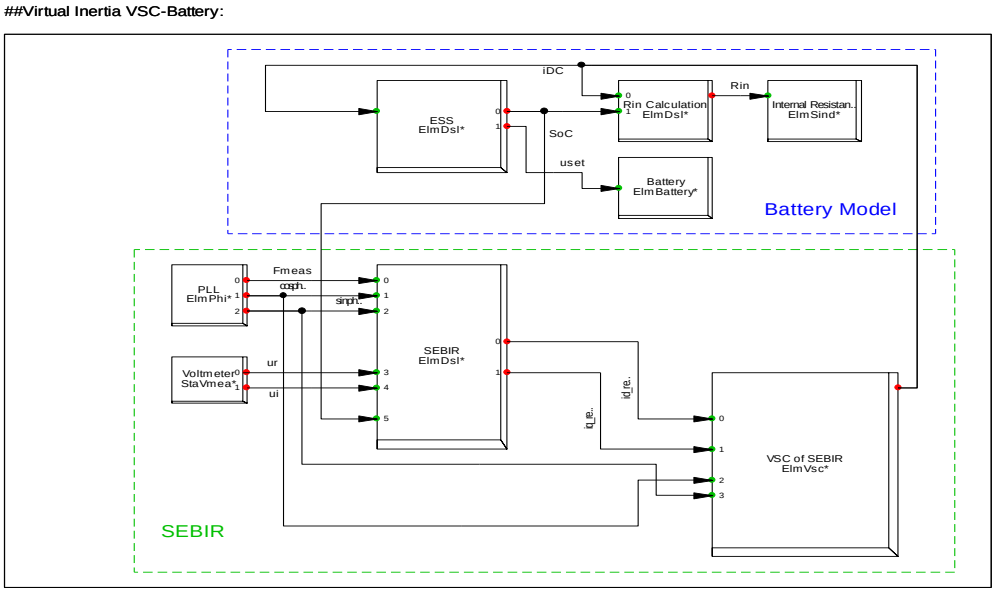

Figure 4.1: SEBIR frame in DIgSILENT Powerfactory.

Figure 1.1 shows the frame of the SEBIR, in which:

- PLL and voltmeter: these elements are necessary for measuring the frequency and tension at the PCC of the VSC. Moreover the PLL measures the $cos\varphi$ and $sin\varphi$ at PCC, which are used as a reference for the DQCI control system of the VSC;
- SEBIR: it is the SEBIR control system, which will be presented in 4.1.2;
- VSC of SEBIR: this is the real converter, which is controlled as a DQCI-VSC. As a consequence the VSC is used in "Integrated Current Controller" mode: the integration time constants parameters of the built-in current controller are set to $K_d = K_q = 0{,}75$ and $T_d = T_q = 0.05$, in order to have a step response within a second. I_d - I_q are defined in the SEBIR control while $cos\varphi_{ref}$ and $sin\varphi_{ref}$ are measured by the PLL;
- ESS, Rin calculation, Battery and Internal Resistance: these elements define the battery storage system, and will be explained in 5.1.3.

4.1.2 SEBIR model

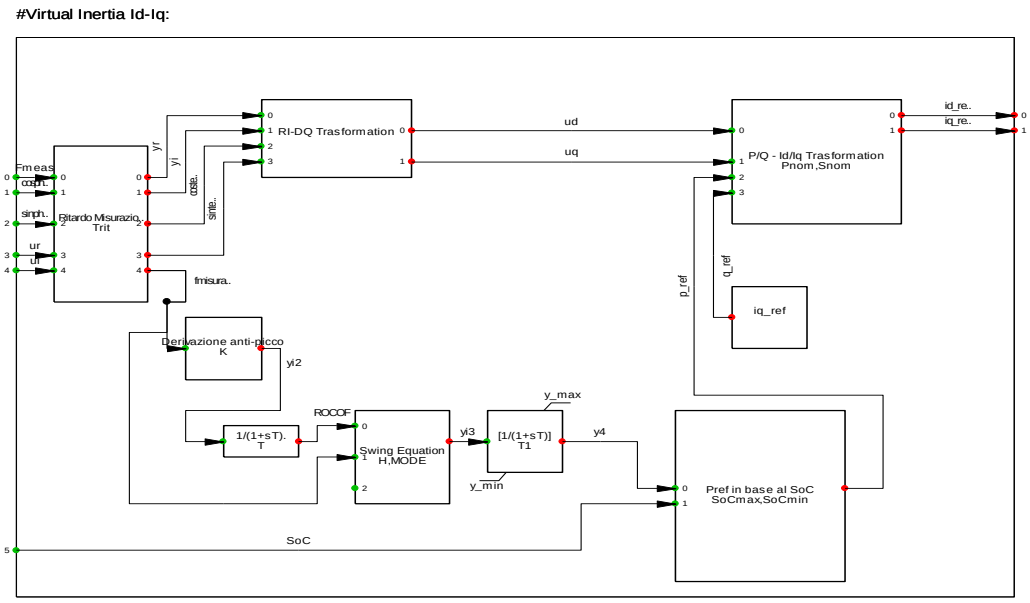

Figure 4.2: SEBIR model in DIgSILENT Powerfactory.

SEBIR model in Figure 4.2 introduces the SEBIR method illustrated in 3.1.1. The input frequency passes a derivative block in order to obtain the ROCOF, which is used to calculate the active power reference through the Swing Equation. Moreover, a State Of Charge (SOC) control strategy is introduced to stop the power supply if the SOC is too low. *PQ* - I_dI_q Transformation are applied to define $I_{d_{ref}} - I_{q_{ref}}$. Finally, note that various Low Pass Filter (LPF) are used, therefore the response presents delays.

4.2 VSM

In this section, the model and the frame of the VSM system are presented.

4.2.1 VSM frame

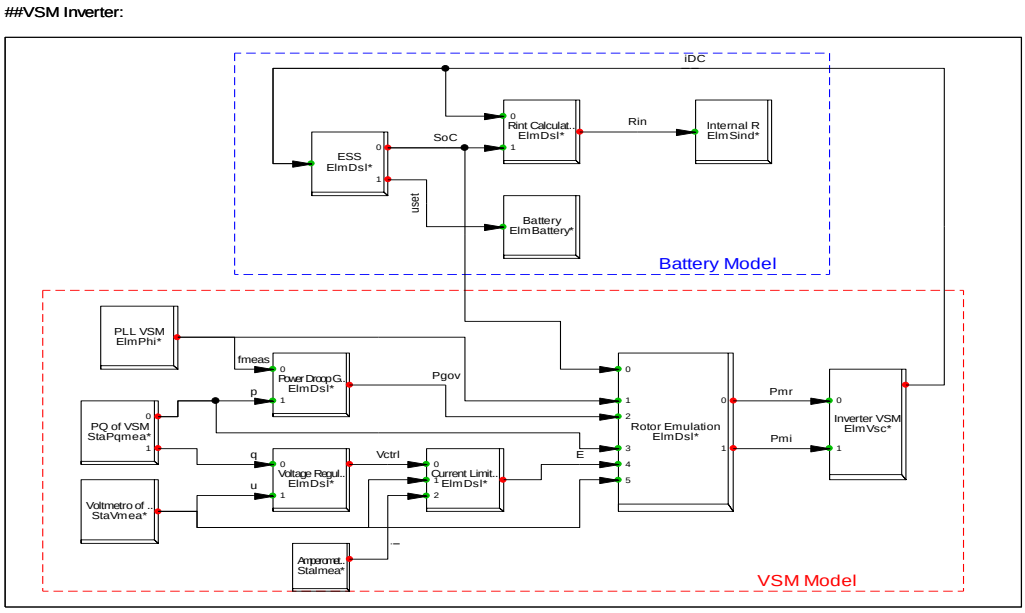

Figure 4.3: VSM frame in DIgSILENT Powerfactory.

Figure 4.3 shows the frame of the VSM, in which:

- PLL, voltmeter, amperometer and wattmeter: these elements are necessary for measuring the frequency and tension at the PCC of the VSC and the power exchanged by the VSM. Moreover the amperometer measures the output current from the VSC, because it must be limited;
- Power Droop Governor, Voltage Regulator, Rotor Emulation and Current Limiter: these models will be explained in 4.2.2.
- Inverter VSM: this is the real VSC, which is controlled with P_{mr} and P_{mi} control. Both P_{mr} and P_{mi} are determined through the VSM control system in order to generate U_{AC}, which is calculate according to the following equations:

$$\begin{aligned} P_m &= \sqrt{P_{mr}^2 + P_{mi}^2} \\ \cos phi &= P_{mr} / P_m \\ \sin phi &= P_{mi} / P_m \\ U_{AC1} &= K_0 \cdot P_m \cdot \mathrm{U}_{DC0} \cdot (\cos phi + \mathrm{j} \cdot \sin phi) \end{aligned} \tag{4.1}$$

where K_0 is a constant that depends on the modulation method and U_{DC0} is the DC nominal voltage. [41]

- ESS, Rin calculation, Battery and Internal Resistance: these elements define the battery storage system, and will be presented in 5.1.3.

4.2.2 VSM model

In the VSM there are various models that need to be analysed. These control schemes are highly inspired by [22] [23].

4.2.2.1 Power Droop Governor

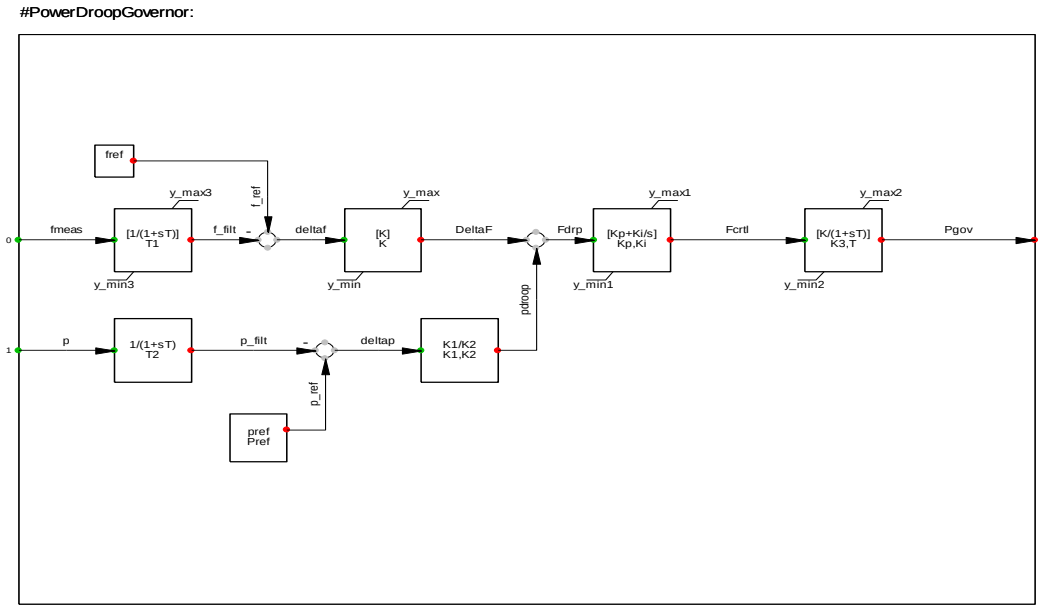

Figure 4.4: Power Droop Governor model in DIgSILENT Powerfactory.

Figure 4.4 shows the power droop governor, which represents the mechanical governor of a synchronous generator. This controller sets the P_{gov}, which stands for the turbine power, through a PI controller based on a frequency gain error and an active power droop. Low Pass Filter (LPF) are applied both on the frequency and active power measurements. Moreover, there is a LPF with gain, which represents the gain and fuel control system.

4.2.2.2 Voltage Regulator

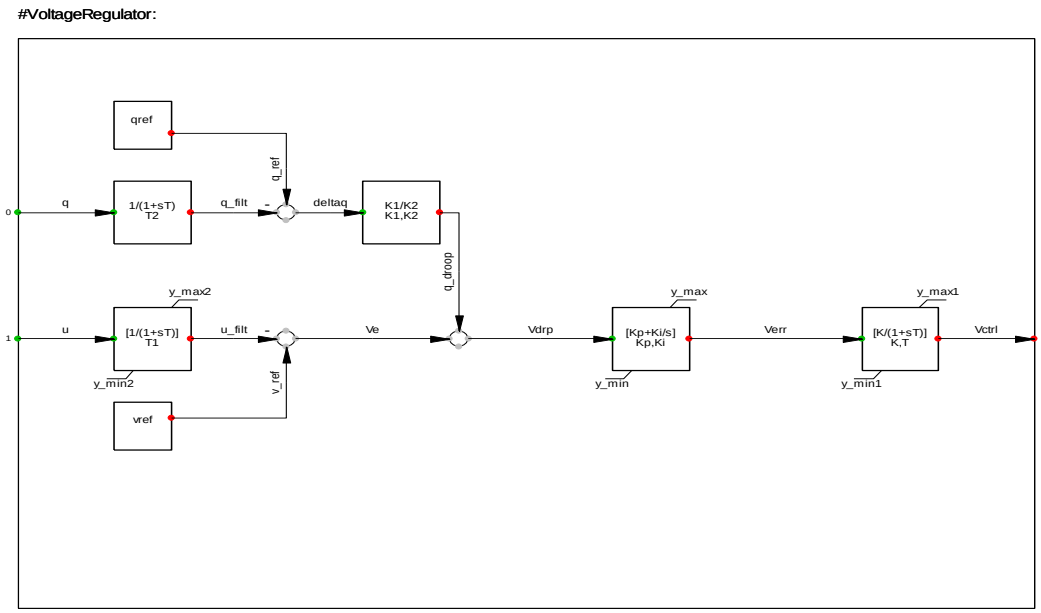

Figure 4.5: Voltage Regulator model in DIgSILENT Powerfactory.

Figure 4.5 shows the voltage regulator, which represents the AVR of a synchronous generator. This controller sets the *Vctrl*, which stands for the excitation voltage, through a PI controller based on a voltage gain error and a reactive power droop. Low Pass Filter (LPF) are applied both on the voltage and reactive power measurements. Moreover, there is a LPF with gain, which represents the gain and field time constant.

4.2.2.3 Current Limiter

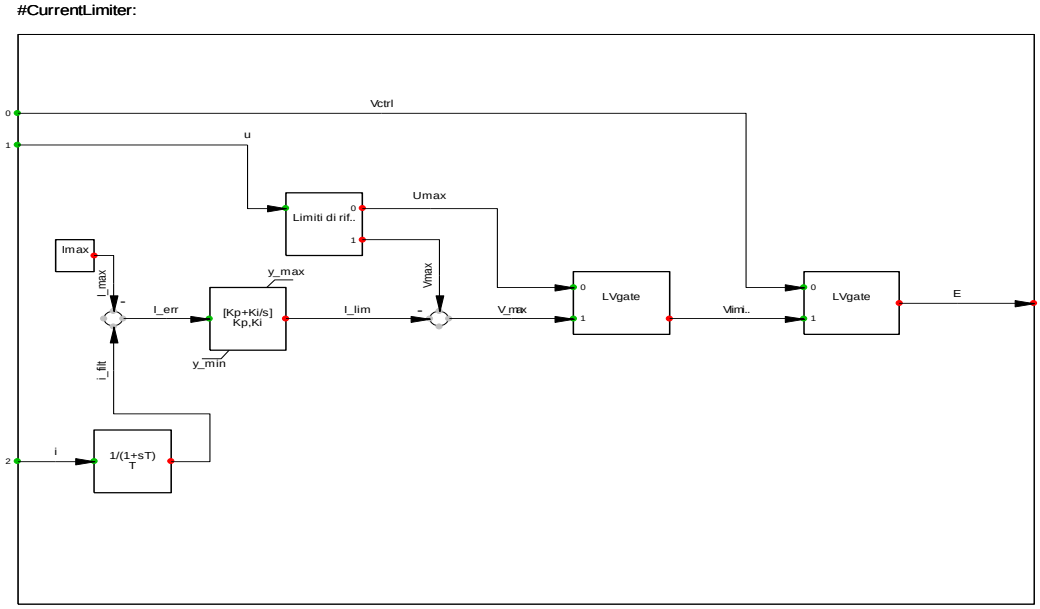

Figure 4.6: Current Limiter in DIgSILENT Powerfactory.

Figure 4.6 shows the current limiter used to prevent the output voltage to exceed 1.25 pu. In normal condition this control block does not act, while under short circuit conditions the output voltage is initially prevented from getting over 1.25 pu, in order to avoid that the current exceed 1.5 pu, then a PI current controller limits to a specified value of 1.25 pu.

4.2.2.4 Rotor Emulation

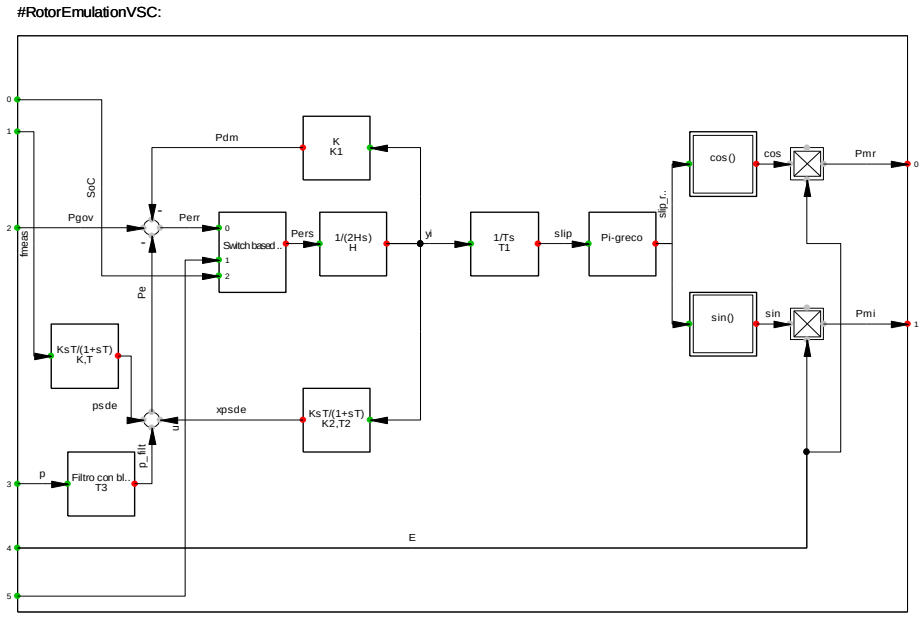

Figure 4.7: Rotor Emulation in DIgSILENT Powerfactory.

Figure 4.7 shows the rotor emulation: this is the actual rotor dynamics simulation that generates synthetic inertia through a $^{1}/_{2Hs}$ block, which is used to emulate the inertia of the rotor. The main inputs of the controller are P_{gov}, ie the output of the power droop governor, and E, ie the output of the voltage regulator in pu, which is passed through the current limiter. Furthermore, there are some feedback signals, that are used to balance the P_{gov} under steady state condition and to damp power oscillation:

- the electrical active power measured at the convertor output *p*, which acts as a feedback;
- *psde*, which is a damping power obtained from the frequency f_{meas} that pass through a LPF with a derivative term;
- *Pdm*, which emulate the mechanical damping of a SG but without real losses;
- *xpsde*, which is the main damping signal applied.

All these signal are subtracted from the P_{gov}, in order to generate a P_{err}: a switch based on the output voltage *u* and the *SoC* controls it and produce P_{ers}, which is used in the inertia block. The output of the inertia block is the virtual rotor frequency in pu, therefore by subtracting the f_{nom}, it is possible to obtain the rotor slip, which define *cosref* and *sinref*. From those and *E*, P_{mr} and P_{mi} are finally set.

4.2.3 Tuning of the VSM

In order to obtain a correct parametrization of the VSM, the following method has been used:

1. The frequency response of the grid without storage, ie the network's response to the loss of generation in the presence of a high penetration of RES, is evaluated on DIgSILENT Powerfactory;
2. A simplified version of the grid is parameterized in MATLAB Simulink, thanks to the Parameter Estimation tool, in order to obtain a response similar to the one in DIgSILENT Powerfactory;
3. The response in active power of a test synchronous generator, sized equal to a VSM and with different levels of inertia, is analyzed in DIgSILENT Powerfactory;
4. A simplified version of the VSM is parameterized in MATLAB Simulink and connected to the network parametrized in point 2, thanks to the Parameter Estimation tool, in order to obtain a response similar to the test synchronous generator;
5. The VSM response (equal in size to the test synchronous generator) is evaluated in DIgSILENT Powerfactory with the values estimated in MATLAB, then, it is compared to the one of the synchronous test generator in DIgSILENT Powerfactory.

In Figure 4.8 the simplified version of the VSM connected to the simplified grid is shown: the grid presents only the primary control and the load transfer function, while the simplified VSM has only the power droop governor and the rotor emulation system. This simplification neglects the voltage regulator and the current limiter because the equivalent model of the grid does not consider the voltage related aspects. Moreover it has not been implemented the VSC and the ESS model, ie the DC side of the VSC of the VSM. In section 6.2.1 will be presented, a complete analysis of the tuning of one VSM, with the method just described.

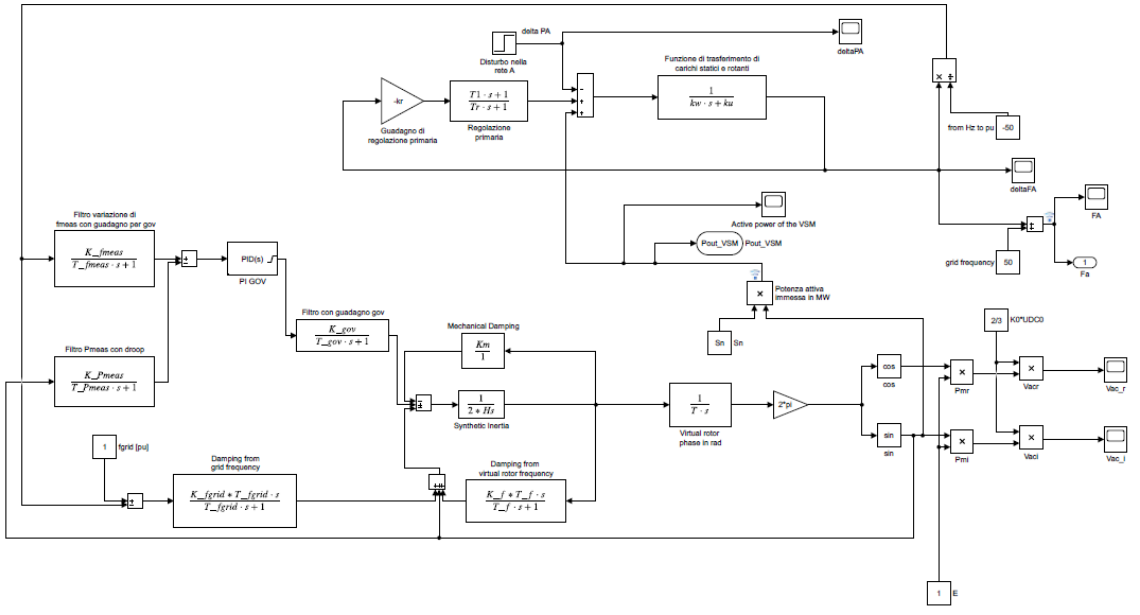

Figure 4.8: Simplified model of the VSM connected to the grid in Matlab Simulink.

5. CASE STUDY

In order to evaluate the inertial response of an electrical network with different levels of renewable penetration and storage systems, a model has been created with the commercial software DIgSILENT Powerfactory.

5.1 MODEL OF THE GRIDS

The network analyzed is a plausible model of the electricity transmission grid of Sicily, which has been made through internal data and GSE reports [42] [43]. In

TEST	Gas	5-10-20	GAST	ESST1A	1	Variable	Variable

Table 5.4 the data of traditional power stations, both thermoelectric and hydroelectric, can be seen. Furthermore, a synchronous generator equivalent to the remaining Italian peninsula, which acts as slack bus, has been inserted. To analyze the phenomenon of the penetration of RES, it has been decided to put a photovoltaic plant and a wind power park, of the DFIG type [44], with the same power for each thermoelectric plants. The ratio between the power generated from the photovoltaic plants and the wind parks has been defined from [42] [43]:

	***P* [*MW*]**	**N° of plants**
SOLAR	1344.0	47072
WIND	1795.2	524

Table 5.1: GSE ratio between solar and wind plants.

$$rapp_{solar} = \frac{P_{solar}}{P_{solar} + P_{wind}} = 42.8\%$$
$$rapp_{wind} = \frac{P_{wind}}{P_{solar} + P_{wind}} = 57.2\% \quad (5.1)$$

Moreover, as it can been seen from the number of plants, the photovoltaic plant has been modelled as PQ nodes while the wind power park as PV nodes. In this way, it is possible to analyze how the frequency response of the network varies, after a generation loss in the Italian peninsula, with different levels of penetration. The loss has been defined as approximately 10% of the demand for active power. The loads has been modelled as industrial loads, according to [45], and can be seen in Table 5.2.

Load	Voltage [kV]	P [MVA]	$cos\varphi$
A	220	1200	0.98
B	220	1200	0.98
C	220	1200	0.98
A	132	1200	0.98
B	132	300	0.98
C	132	300	0.98
D	132	300	0.98
E	132	300	0.98
F	132	300	0.98
G	132	300	0.98
A	20	50	0.95
B	20	50	0.95
C	20	50	0.95

Table 5.2: Data of the loads.

The total power of the grid can be seen in the following table:

	S [MVA]	P [MW]	Q [Mvar]
Traditional generation	5469.705	4992.7345	2384.189135
Loads	6750	6610	1367.6

Table 5.3: Total power of synchronous traditional generation and loads.

In view of a demand of 6610 MW, a generation loss, simulated as a switch load event, of 660 MW (about 10%) has been inserted at the instant $t = 0$. Finally, it has been introduced two type of ESS, with the same battery model but with different type of control system: the SEBIR and the VSM. These storage systems presents different levels of power based on the load demand, from 0.5% up to 3.5%. The DIgSILENT grids model can be seen in:

- Figure 5.1: the 380-132 kV grid, with the external grid representing the Italian peninsula;
- Figure 5.2: the 132-20 kV grid, with the storage bus;
- Figure 5.3: the storage grid, with SEBIR and VSM systems.

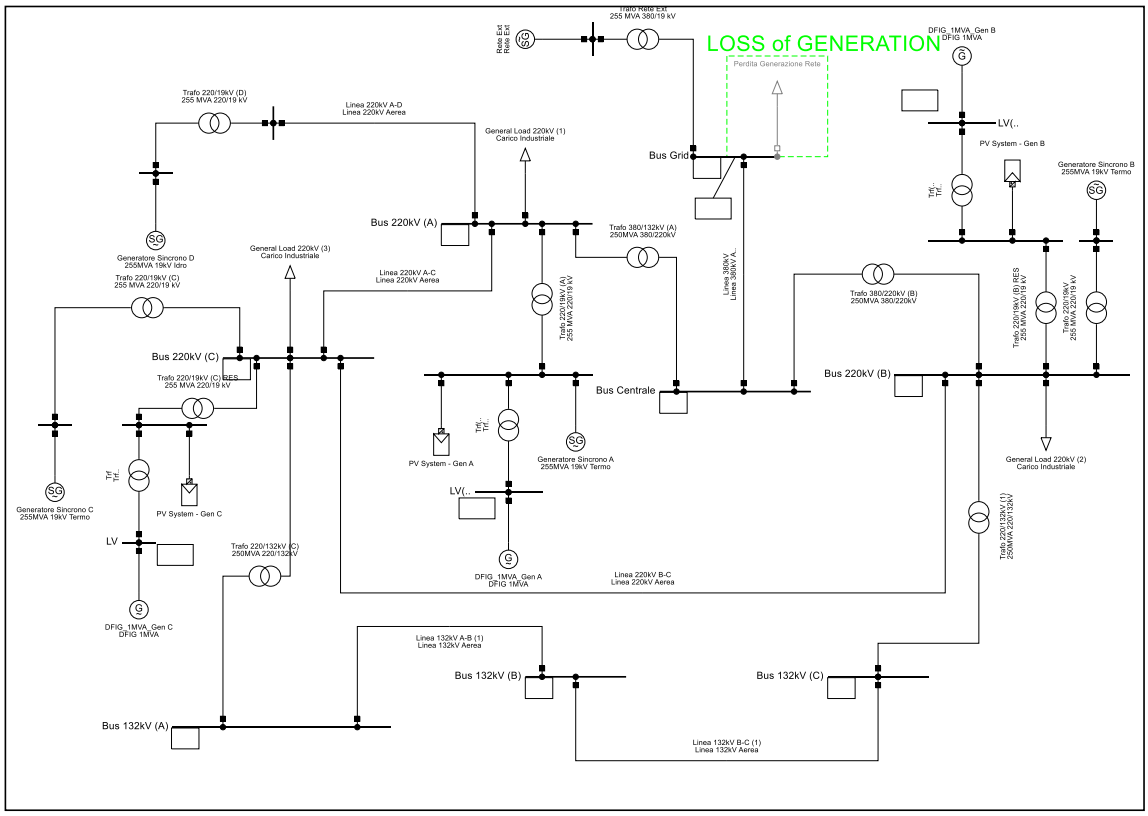

Figure 5.1: 380-132 kV grid.

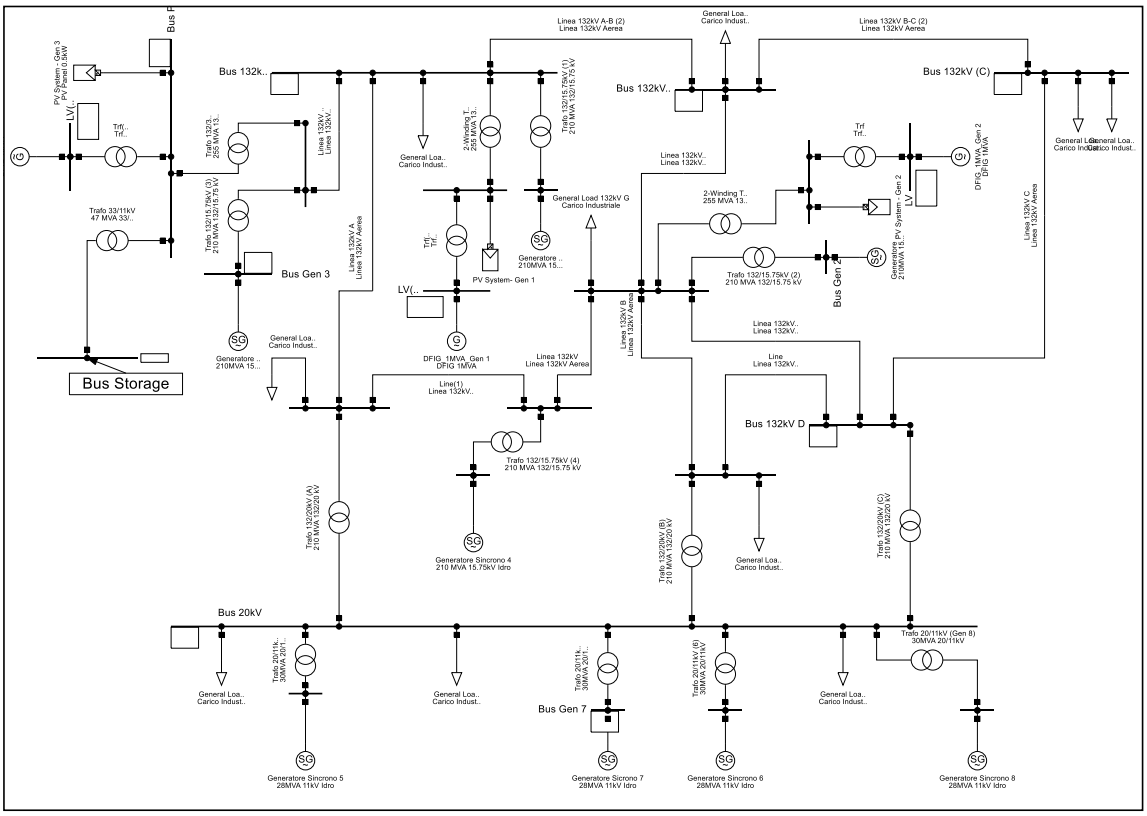

Figure 5.2: 132-20 kV grid.

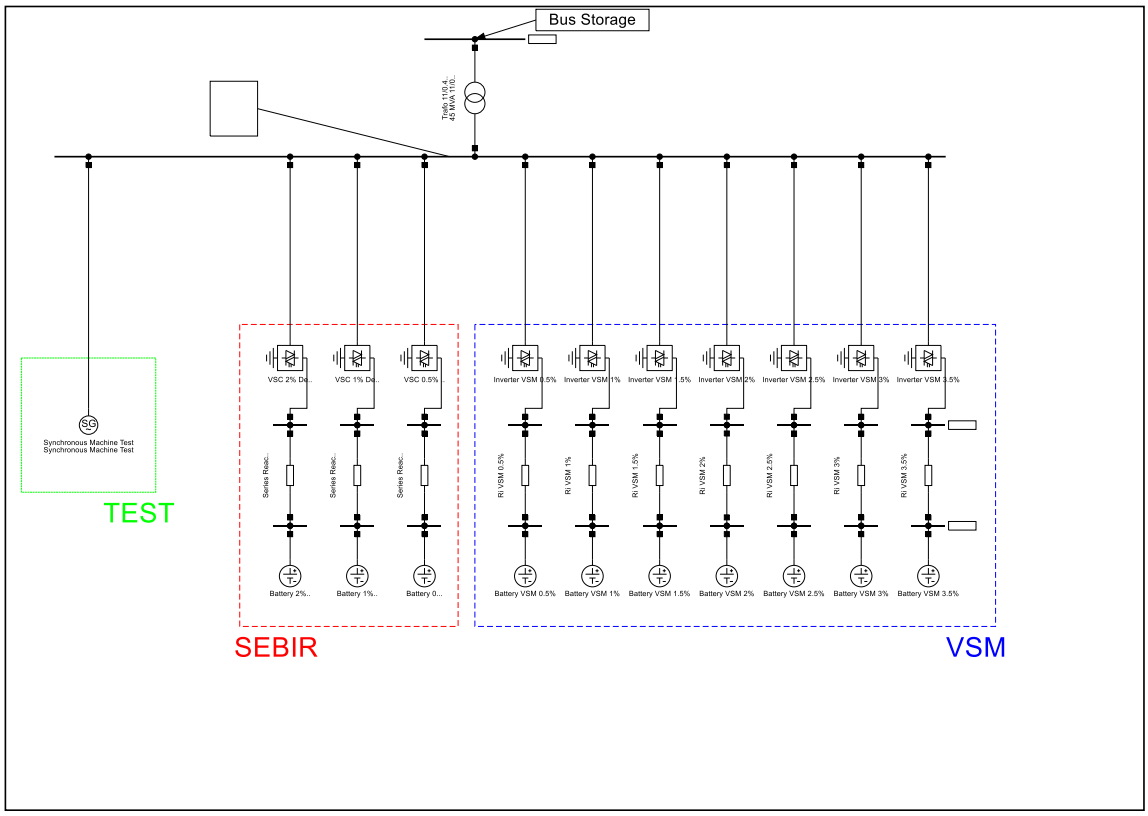

Figure 5.3: Storage grid.

5.1.1 Synchronous generators

The synchronous generators of the grid has been modelled as follow:

Generator	*Type*	*H* [s]	*Governor*	*AVR*	*Droop* [%]	S_{nom} [MVA]	$S_{reserve}$ [MVA]
Rete Ext	-	4	TGOV2	ESST1A	5	14000	-
A	Steam	6	TGOV2	ESST1A	5	765	11.475
B	Steam	6	TGOV2	ESST1A	5	1275	19.125
C	Steam	6	TGOV2	ESST1A	5	1530	22.95
D	Idro	3	IEEEG3	ESST1A	4	765	11.475
1	Steam	6	TGOV2	ESST1A	5	420	6.3
2	Gas	8	GAST	ESST1A	5	210	3.15
3	Gas	8	GAST	ESST1A	5	210	3.15
4	Idro	3	IEEEG3	ESST1A	4	210	3.15
5	Idro	3	IEEEG3	ESST1A	4	28	0.42
6	Idro	3	IEEEG3	ESST1A	4	56	0.84
7	Idro	3	IEEEG3	ESST1A	4	56	0.84
8	Idro	3	IEEEG3	ESST1A	4	28	0.42
TEST	Gas	5-10-20	GAST	ESST1A	1	Variable	Variable

Table 5.4: Data of the synchronous generators.

The values of inertia and frequency droop has been defined following [2] [5]. The power reserve for primary frequency control is 1.5% of the P_n. [5] Finally the $cos\varphi$ has been set to 0.9 according to [46]. It can be noted that in the grid there is a TEST synchronous generator, which is used to design the VSM: it present different levels of inertia, his rated power is equal to the one of the VSM modelled and in normal condition it does not supply power to the grid.

5.1.2 Photovoltaic parks and DFIG wind farms

For the modelling of the photovoltaic parks, it has been used the DIgSILENT PV system, set at a costant power source, because the period of time considered in simulation is approximately 50 s. The DFIG wind farms has been modelled using the DIgSILENT template.

5.1.3 BESS

The ESS has been modelled as: an ideal battery, with an internal resistance, and a VSC, controlled as a SEBIR or a VSM. In order to create a plausible model it has been used cell specification data of Kokam SLPB 100216216H: thanks to the discharge characteristic, it has been found the dependency of the internal resistance from the State of Charge (*SoC*) and the current of discharge I_{dis}, and the open circuit voltage (V_{OC}) in function of the *SoC*. The method used to obtain these relations is the following:

1. The discharge curve has been sampled as in Figure 5.4;

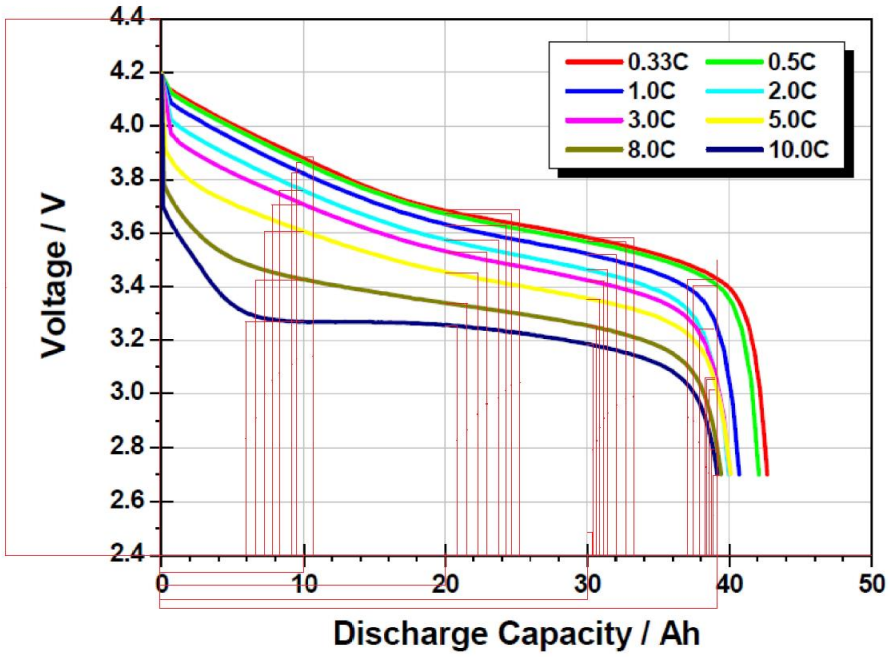

Figure 5.4: Sampled discharge curve.

2. The value, obtained from the sampling, has been plotted as $V = f(I_{dis})$;

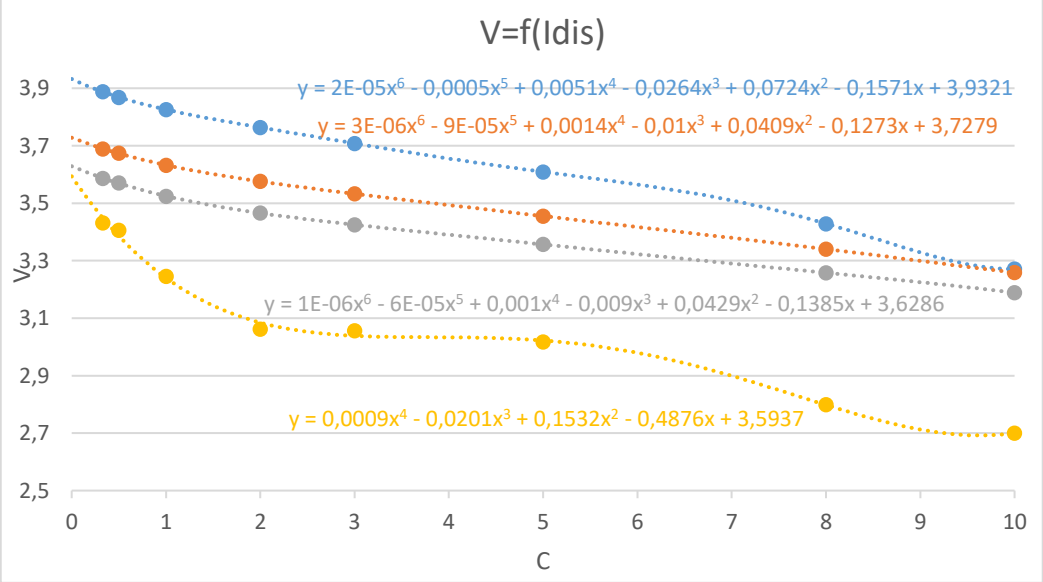

Figure 5.5: Discharge voltage as a function of the discharge current.

3. From Figure 5.5, the relation between the open-circuit voltage V_{oc} and the ampere hour has been found: this equation will be used in the calculation of the *uset* in the ESS model.

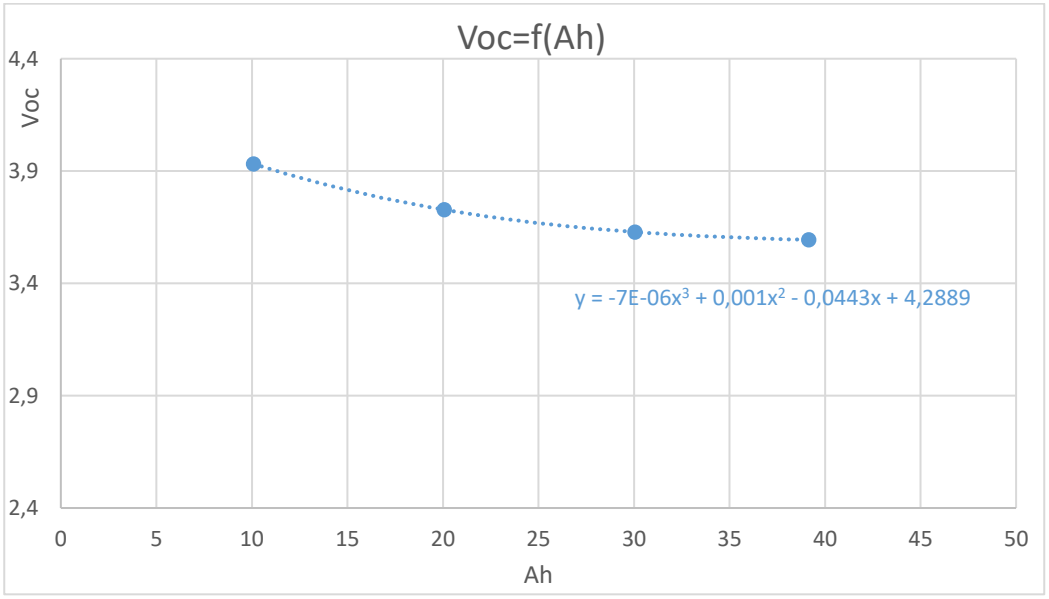

Figure 5.6: Open-circuit voltage as a function of the ampere hour.

4. Appling the relation $V = V_{OC} - R_{int} I_{dis}$, it has been possible to find the relation between the internal resistance and the *SoC* (Figure 5.7) and the relation between the internal resistance and the current of discharge (Figure 5.8);

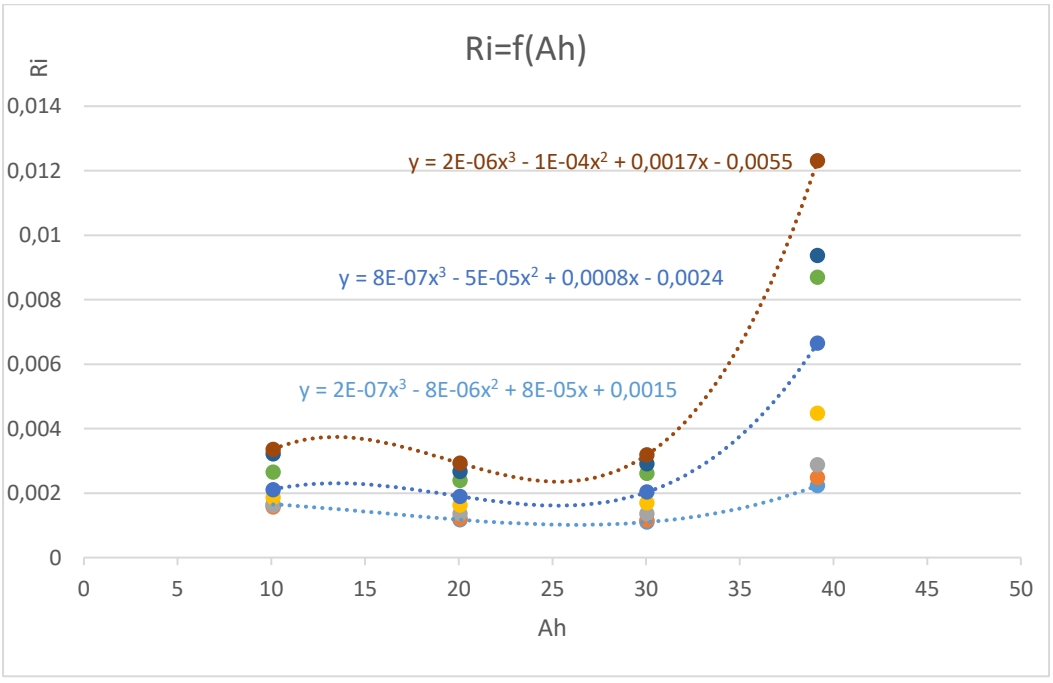

Figure 5.7: Internal resistance as a function of the SoC.

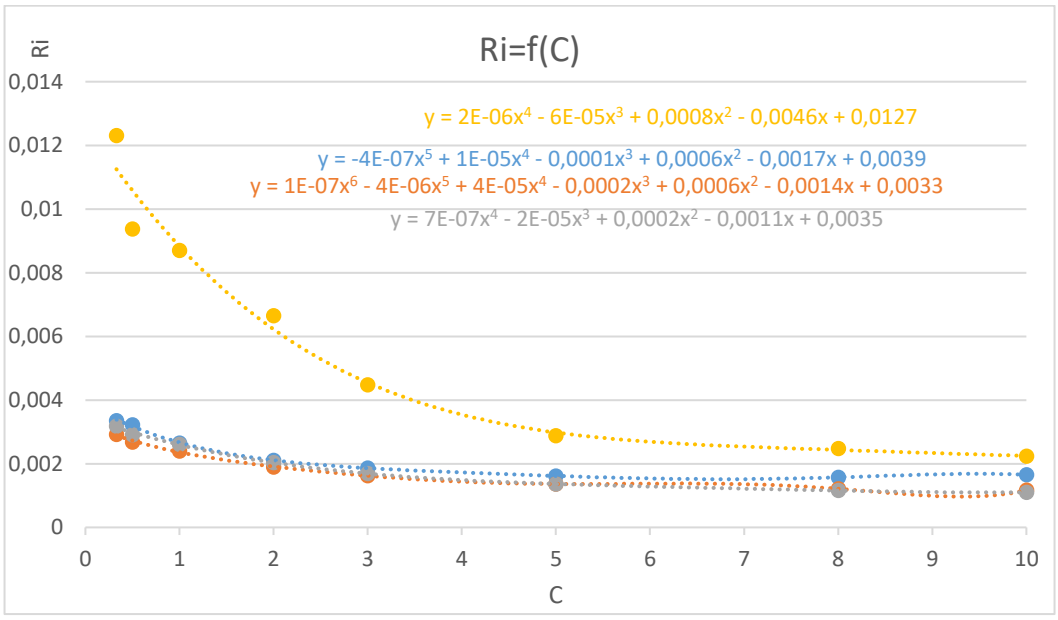

Figure 5.8: Internal resistance as a function of the discharge current.

5. In order to obtain the relation $R_{int} = f(SoC, I_{dis})$, a 3D polynomial interpolation curve has been made in MATLAB. The equation obtained has been implemented in the Rint Calculation of the ESS Frame.

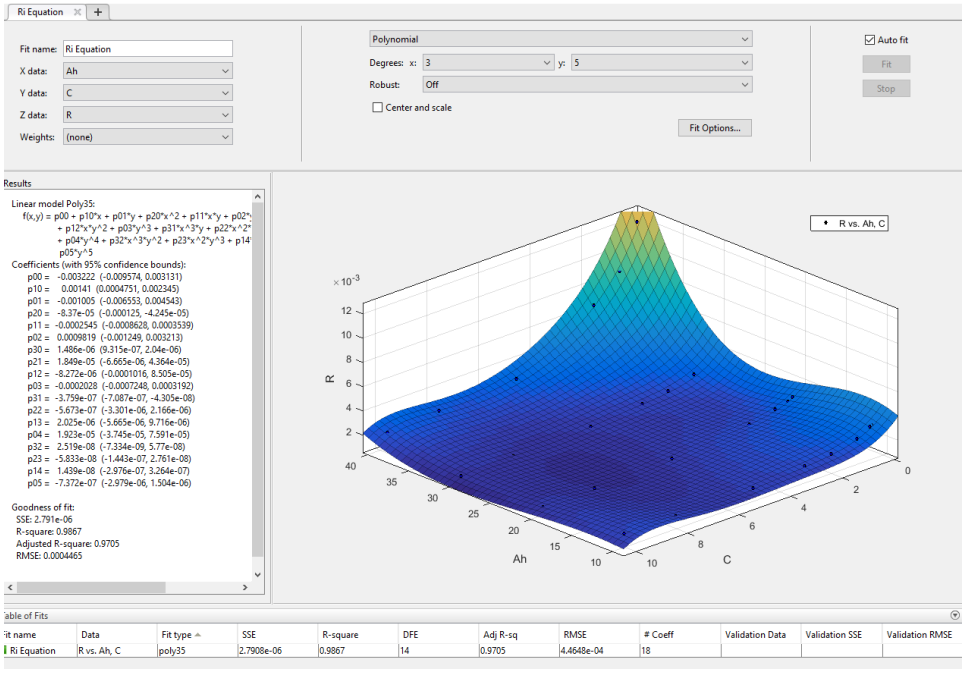

Figure 5.9: Internal resistance as a function of both the SoC and the current of discharge.

After the modelling of the single cell behaviour, it has been done the design of each BESS, based on the rated power of the VSC. As an example, the parameterization of the 135 MVA converter is now presented: considering a DC voltage of 0.6 kV, the nominal DC current is 22.5 kA. Consequently, since the Kokam

SLPB 100216216H has a nominal voltage of 3.7 V and a nominal current of 40 A, this VSC requires 5625 branches, of 163 cells in row, in parallel.

5.1.3.1 ESS Frame

The ESS Frame can be seen both on Figure 4.1 and Figure 4.3, as a part of the SEBIR and VSM frame. It present the following elements:

- ESS: this is the real BESS model, which calculate the *SoC* and the u_{set} from the discharge current i_{DC};
- Rint Calculation: this model calculate the internal resistance from the *SoC* and the i_{DC};
- Battery: this is the real ideal battery, therefore it has u_{set} as an input;
- Internal R: this is the real internal resistance, which has R_{in}, calculated from Rint Calculation, as an input.

5.1.3.2 ESS Model

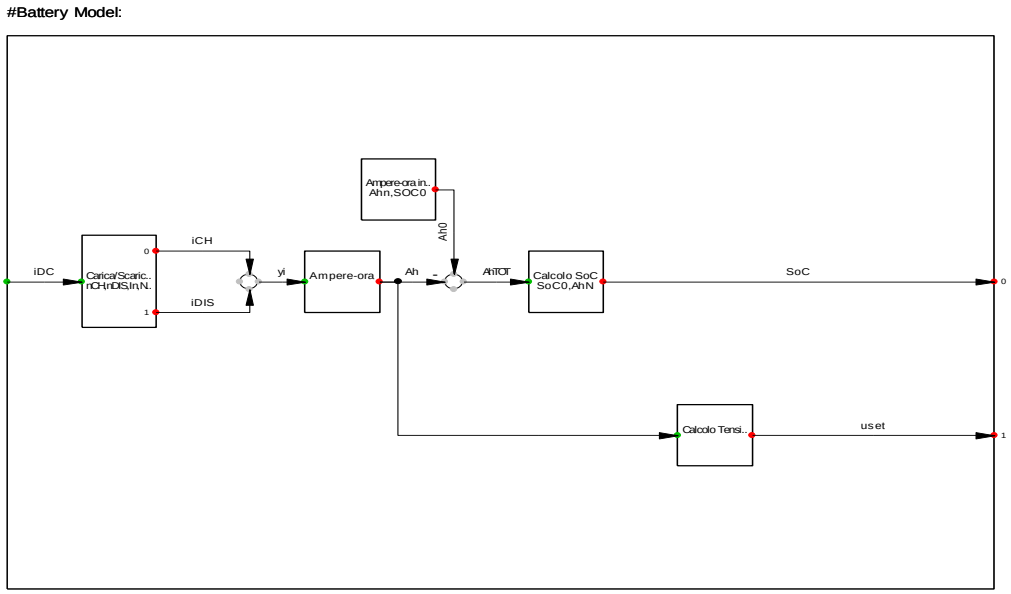

Figure 5.10: BESS model in DIgSILENT Powerfactory.

The ESS model integrates the discharge current, ie the DC current of the VSC, to calculate the ampere hour, which are used to define the *SoC* and the *uset*, ie the open-circuit voltage.

6. SIMULATIONS AND RESULTS

In this chapter, the conducted simulations and their results are described. In order to test the SEBIR and VSM control, the analysis has been done with an high level of penetration of VRG, which are based on a demand of 6610 MW and (5.1):

	Theoretic [%]	***Theoretic [MW]***	***Real [%]***	***Real [MW]***	***Grid Plants***
SOLAR	42.8	1673.2	43.2	1688.8	B,1,3
WIND	57.2	2236.1	56.8	2220.7	A,C,2

Table 6.1: Case study with VRG penetration level sets to 59,142%.

To achieve a complete analysis the VSCs used in the grid present three different levels of rated power, based on the power demand:

VSC	***Sn [MVA]***	***Percentage of active power demand [%]***
A	33.75	0.5%
B	135	2.0%
C	236.25	3.5%

Table 6.2: VSCs rated power.

6.1 TRADITIONAL ELECTRIC POWER GRID

In this first simulation, the behaviour of the grid, with traditional generation only, is presented:

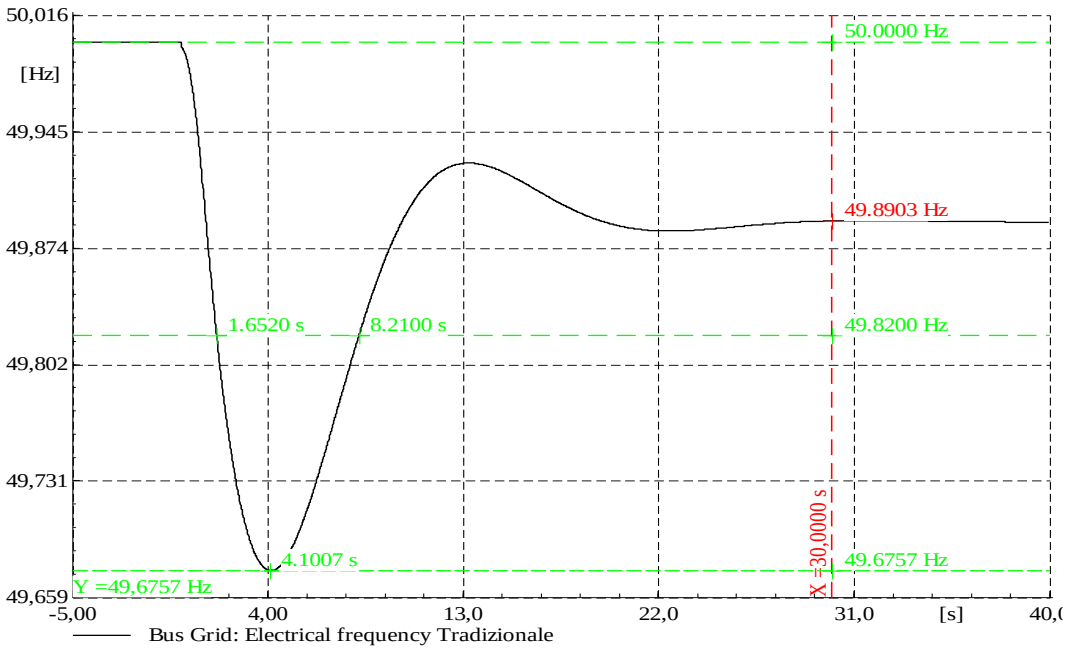

Figure 6.1: Frequency response with traditional generation only.

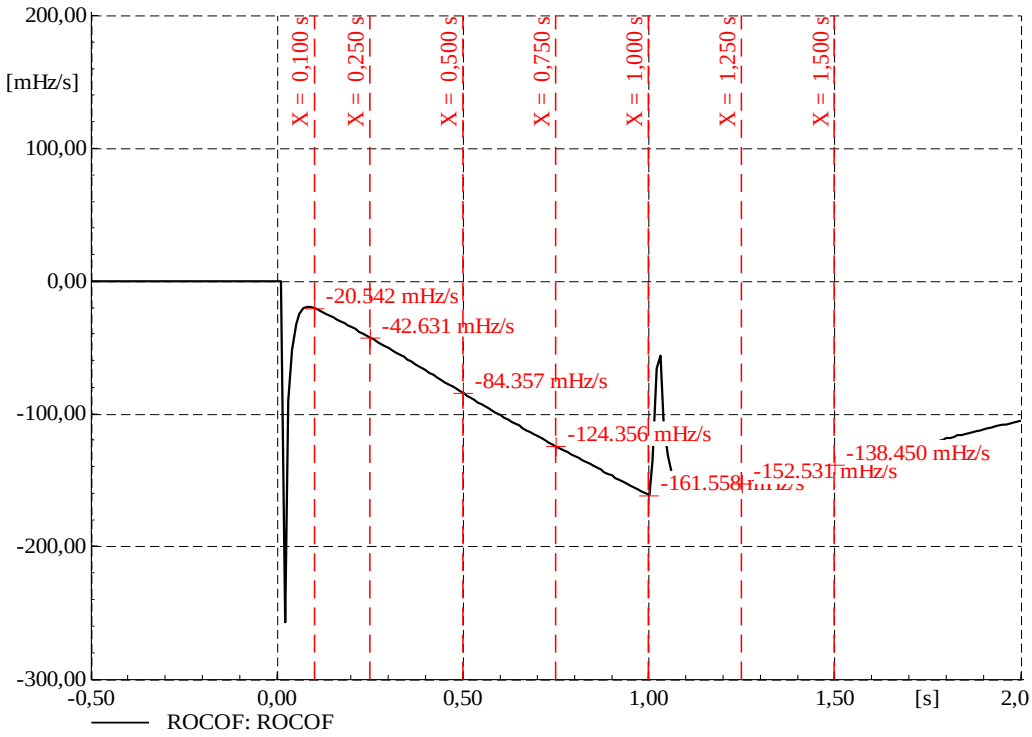

Figure 6.2: ROCOF response with traditional generation only.

6.2 STUDY CASE

First of all, it is necessary to analyse the behaviour of the grid with the penetration of VRG previously defined and, consequently, compare it with the traditional electric power grid.

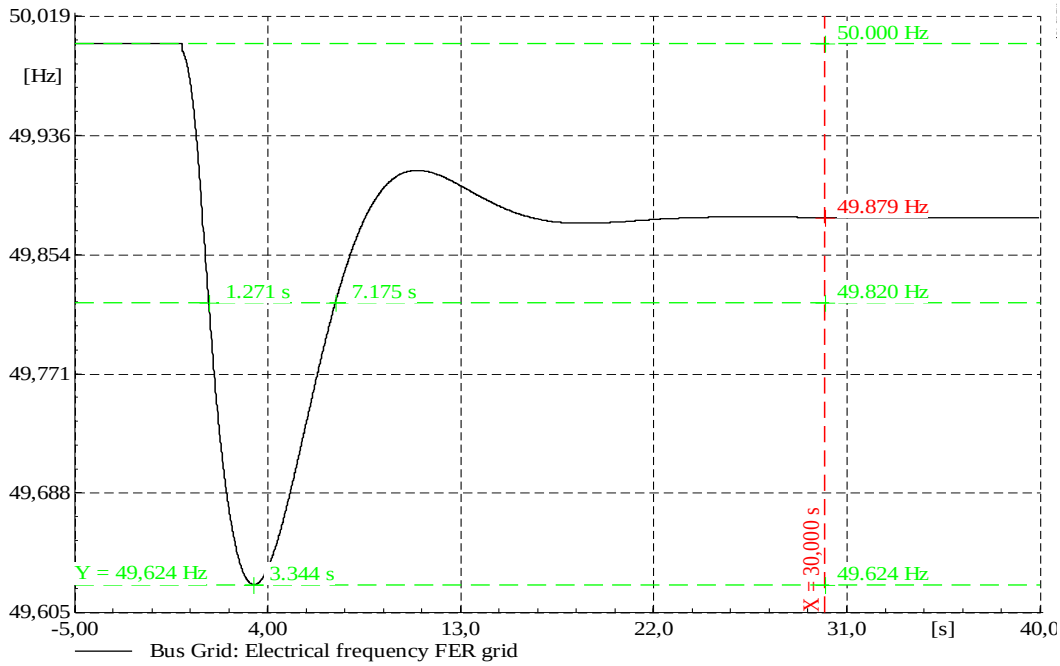

Figure 6.3: Frequency behaviour in the study case.

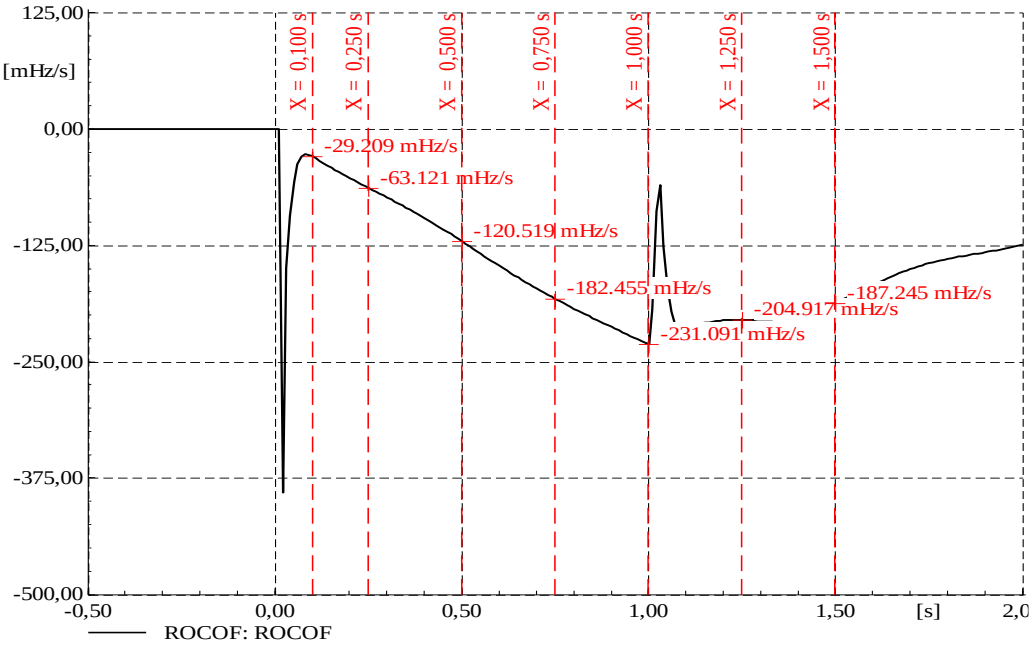

Figure 6.4: ROCOF behaviour in the study case.

As expected, there is an aggravation on the frequency nadir and the ROCOF compared to the grid with traditional generation only.

6.2.1 Parameterization of the VSM

In this section, the tuning of the VSM with the method presented in 4.2.3 is used. In order to avoid a prolix analysis, it will be presented a step by step tuning of only one VSM with the method already presented, while the others cases will be summarized. The VSM chosen for this analysis is the VSM with a VSC of 135 MVA (2% of the power demand), which has been tuned starting from the response of a test synchronous generator with the same rated power, an inertia constant of 5 s, 10 s or 20 s and a frequency droop of 1%. The various steps will now be presented:

1. First of all, the grid built in DIgSILENT has been reduced to an equivalent grid, in MATLAB Simulink, with the same frequency response to a loss of generation. In order to achieve this the model shown in Figure 4.8 has been used: the VSM has been disconnected and the grid frequency response had been modelled with the Parameter Estimation tool of Simulink. The results obtained are presented in Table 6.3: Estimated parameters of the grid in MATLAB. and Figure 6.5:

Grid Parameter	***Estimated Value***
T_1	1.4514 s
T_r	9.1659 s
k_r	5349.1 MW/Hz
k_u	32.781 MW/Hz
k_w	3029.6 MW/Hz

Table 6.3: Estimated parameters of the grid in MATLAB.

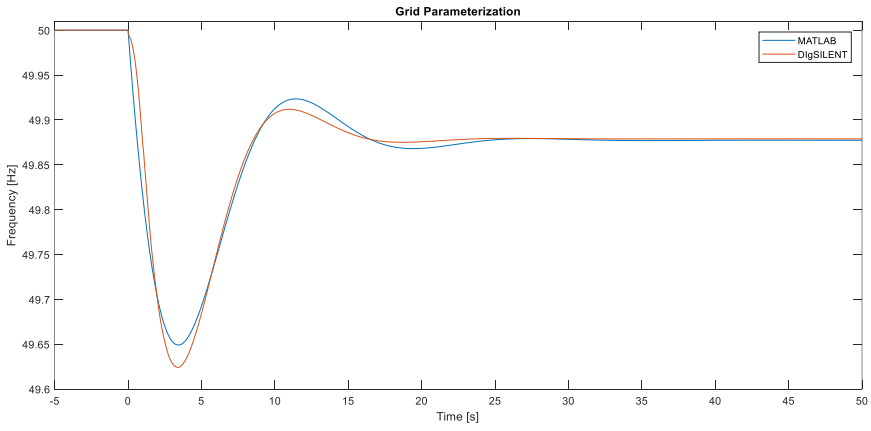

Figure 6.5: Grid parametrization from Parameter Estimation.

2. In the tuning of the VSM, different test synchronous generators, with different levels of inertia, have been used in order to achieve a wider analysis. Every VSM tuned in MATLAB has been modelled starting from the same initial values that can be seen in the script in APPENDIX B. For the VSM tuned in this analysis, the response of the TEST synchronous machine is shown in Figure 6.6:

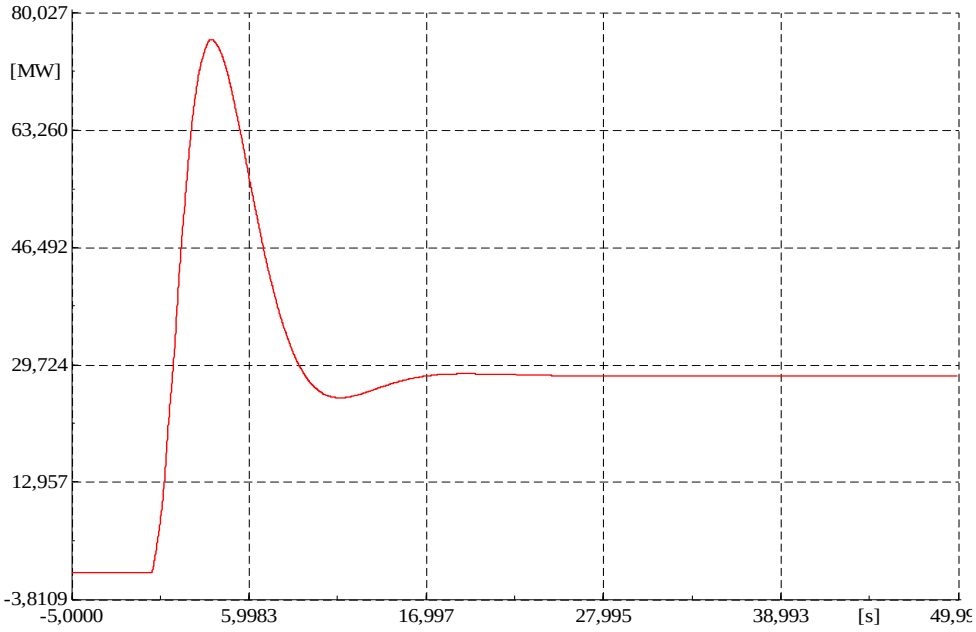

Figure 6.6: Test synchronous generator active power response in DIgSILENT Powerfactory.

Therefore, this response has been imported in MATLAB for the parameter estimation. The results obtained are presented in Table 6.4 and Figure 6.7:

Parameter	***Estimated value***
H	0.97565
K_Pmeas	0.04720
K_f	15.77500
K_fgrid	208.64000
K_fmeas	5.62000
K_gov	17.86000
Ki_gov	0.05010
Km	48.68500
Kp_gov	4.70870
T	0.10939
T_Pmeas	0.81392
T_f	0.79295
T_fgrid	1.32470
T_fmeas	0.86635
T_gov	4.97940

Table 6.4: Parameters estimated for the VSM of 135 MVA and H = 10 s from the initial values.

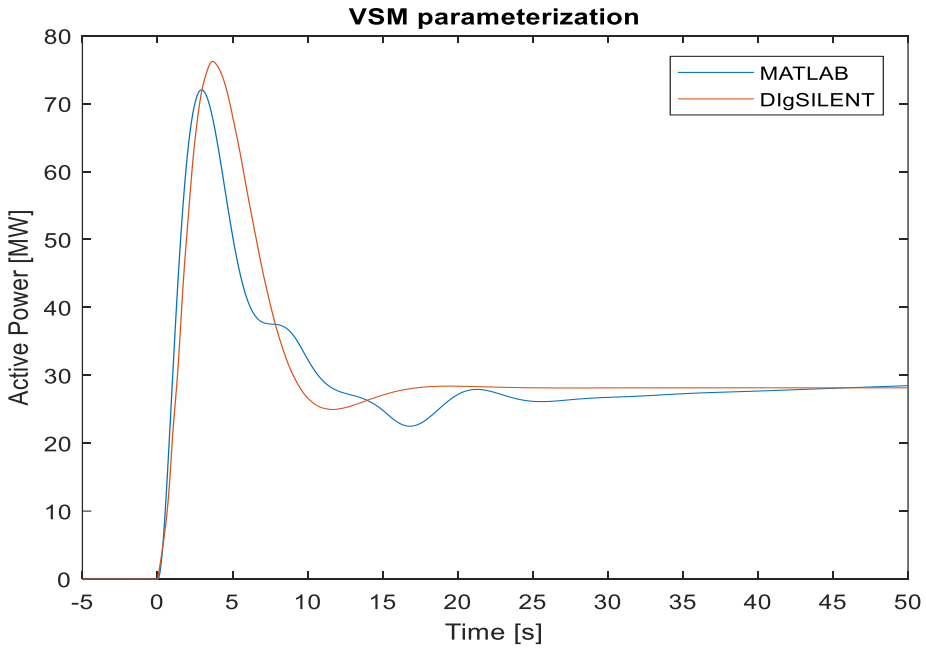

Figure 6.7: VSM parameterization in MATLAB Simulink.

The curve in red is the same as in Figure 6.6, while the one in blue is the response of the VSM tuned through the Parameter Estimation tool.

3. To minimize the error caused by local minimums, the initial values of the parameter estimation has been changed from the ones defined in the script, by the user, to the value estimated for the VSM with different constant of inertia of the test synchronous generator, ie $H = 5\ s, 20s$. The results obtained are the following:

Parameter	*Estimated value from H = 20 s*	*Estimated value from H = 5 s*
H	0.92075	1.6645
K_Pmeas	0.047284	0.05073
K_f	19.174	4.214
K_fgrid	223.82	144.32
K_fmeas	5.9753	5.2938
K_gov	11.311	41.402
Ki_gov	0.048551	0.047336
Km	51.722	63.511
Kp_gov	5.8382	2.4447
T	0.11914	0.076825
T_Pmeas	0.99795	1.4269
T_f	0.073291	4.2499
T_fgrid	1.2065	1.2123
T_fmeas	0.84505	0.87781
T_gov	4.8179	5.816

Table 6.5: Parameters estimated for the VSM of 135 MVA and H = 10 s from the values estimated for H = 5 s, 20 s.

The same procedure done in step 2 and 3 has been made for the VSMs of 135 MVA modelled from the test synchronous machine of the same rated power and with inertia constant of 5 s and 20 s. Therefore, for every VSM, three different sets of parameters have been obtained.

4. In the final phase all the parameters estimated in MATLAB for the different VSM with the same rated power has been implemented in DIgSILENT Powerfactory, in order to analyse the response of the tuned VSMs. Then, thanks to MATLAB, the error, committed in every parameterization, has been calculated as the average deviation of each point of the VSM power response curve generated in DIgSILENT Powerfactory with respect to the one of the test synchronous generator.

H of the TEST generator [s]	*VSM starting conditions*	*Average deviation*
5	Initial	5.2822
5	From 10 s	5.0475
5	From 20 s	5.7712
10	Initial	5.4997
10	From 5 s	2.8528
10	From 20 s	5.7672
20	Initial	9.1334
20	From 5 s	4.9049
20	From 10 s	5.3186

Table 6.6: Average deviation of the VSM power response in DIgSILENT Powerfactory.

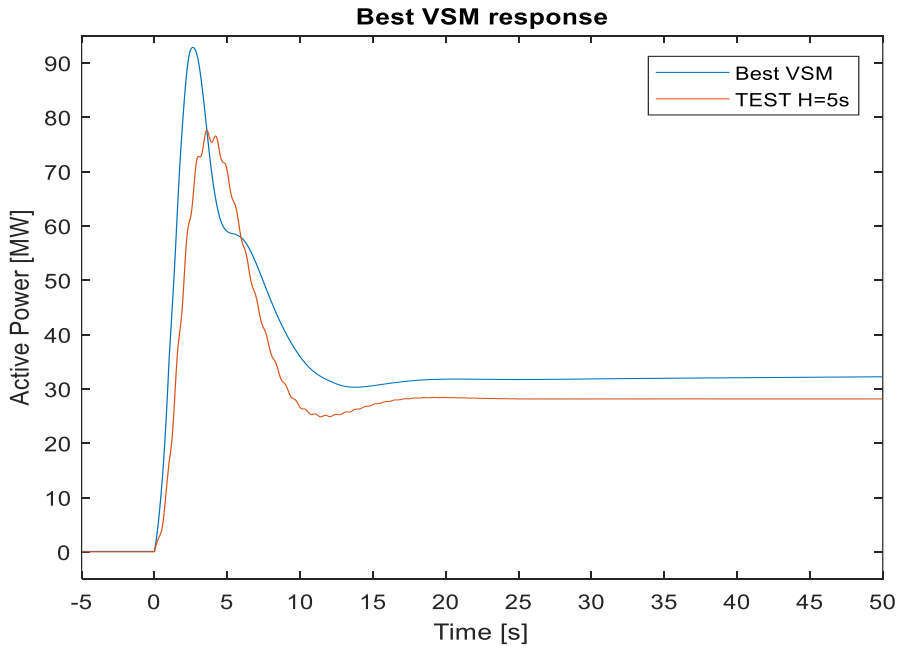

Figure 6.8: VSM tuned from test machine with H = 5 s, with the smallest average deviation.

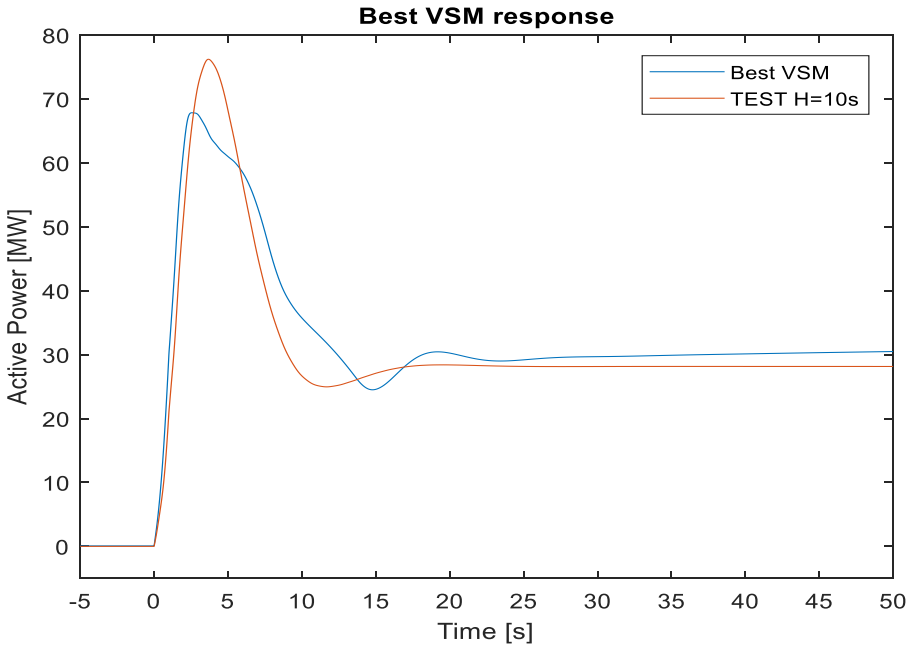

Figure 6.9: VSM tuned from test machine with H = 10 s, with the smallest average deviation.

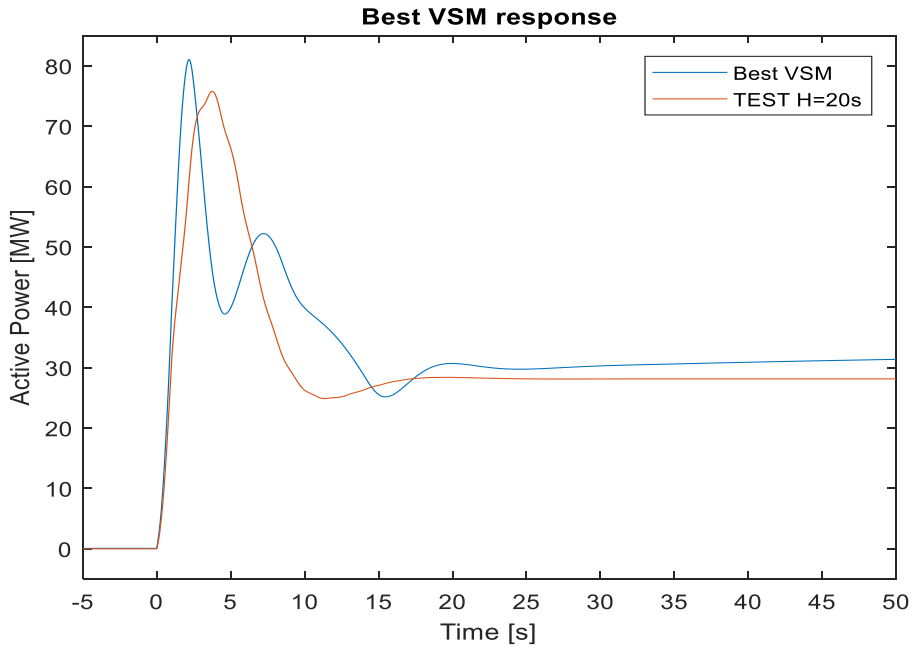

Figure 6.10: VSM tuned from test machine with H = 20 s, with the smallest average deviation.

As can be noted Table 6.6, the best VSM is the one tuned from the TEST synchronous generator with $H = 10\ s$ and initial condition of the VSM modelled from the TEST synchronous generator with $H = 5\ s$ (with initial condition defined by the user).

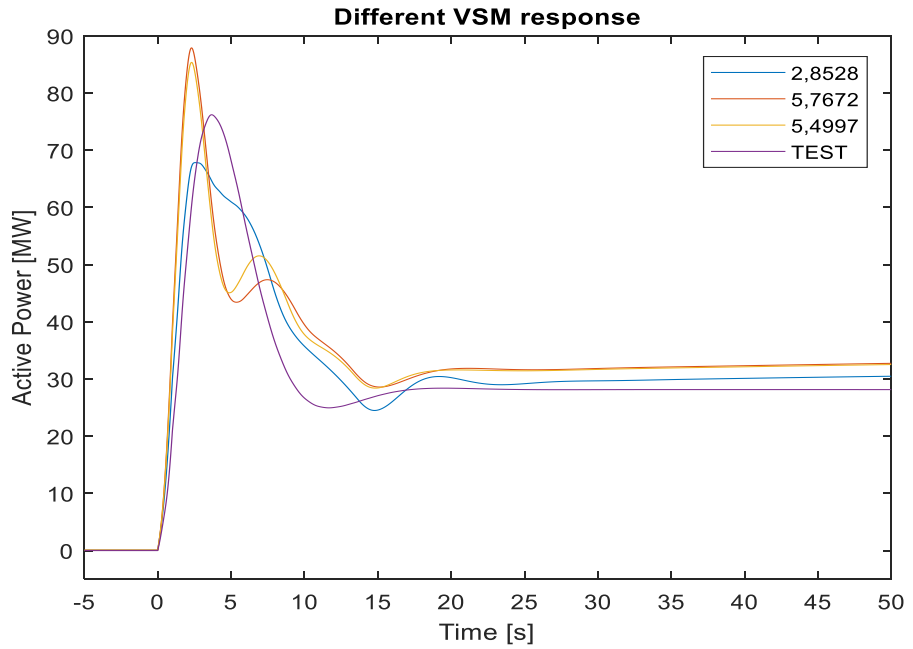

Figure 6.11: Different VSM response for sets of parameters estimated from different initial conditions.

In Figure 6.11 the different power response of the VSM with different initial condition, based on the test synchronous generator with 135 MVA, are shown: the legend represent the average error with the test machine. Therefore, the curve in blue is the best parameterization of the VSM.

Note that Figure 6.8Figure 6.9-Figure 6.10-Figure 6.11 are the active power response in DIgSILENT Powerfactory, imported in MATLAB for the error calculation.

In conclusion, for the others VSMs with different rated power, ie 33.75 MVA and 236.25 MVA, it has been done a simplified version of the tuning that exclude the step 3. In order to maintain the same common thread, for the comparison between the VSM and the SEBIR both these VSM have been modelled from the TEST synchronous generator with H = 10 s. In the following figures is shown, the active power response of the different rated VSM, which will be used in section 6.2.2:

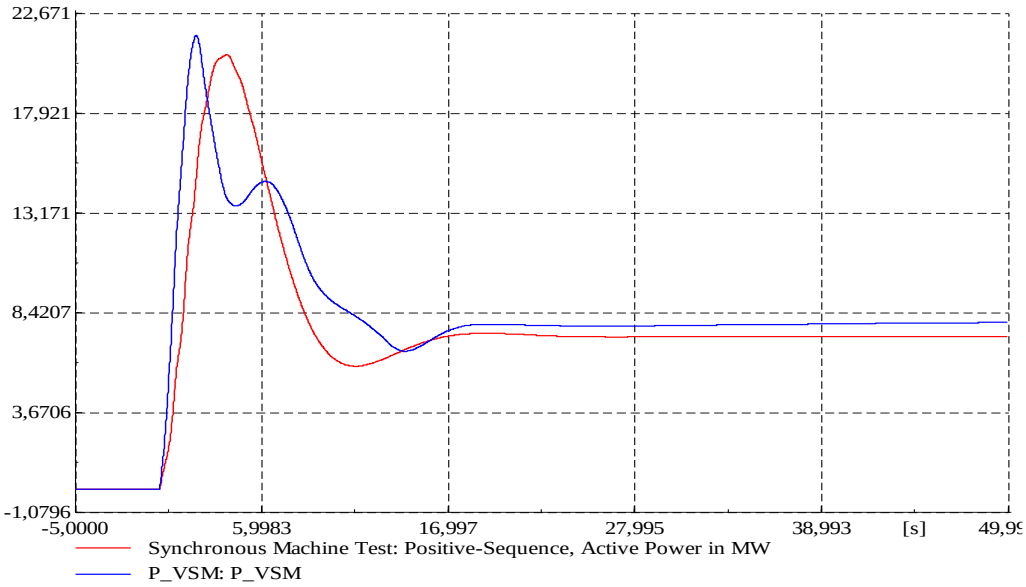

Figure 6.12: Comparison of the active power response of the VSM and TEST machine with 33.75 MVA rated power.

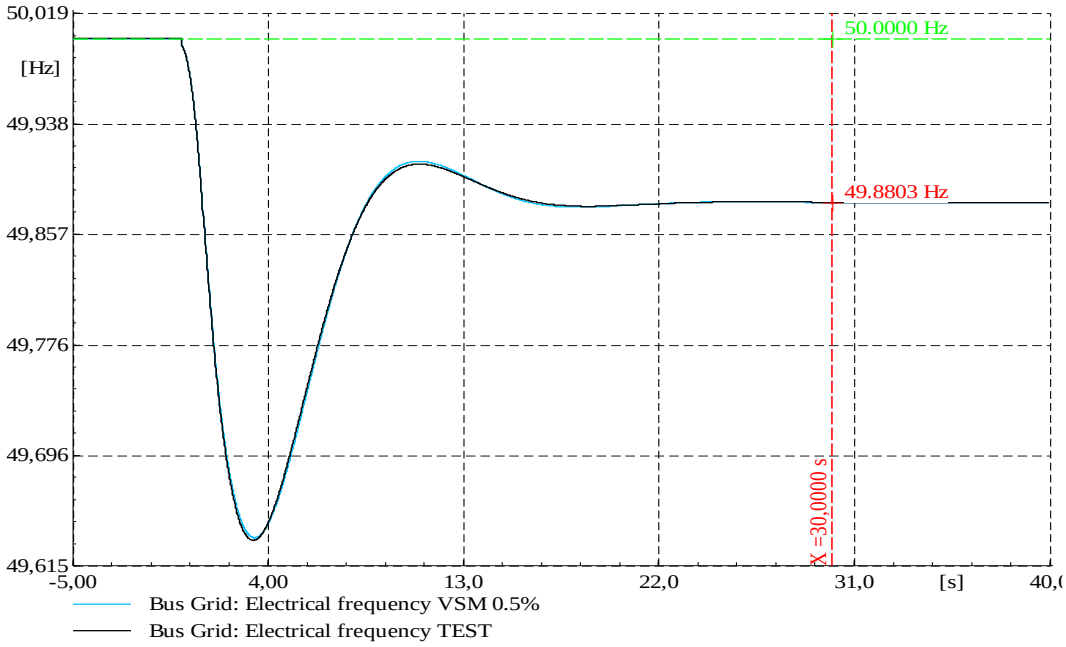

Figure 6.13: Comparison in the frequency response of the grid with VSM or TEST machine with 33.75 MVA rated power.

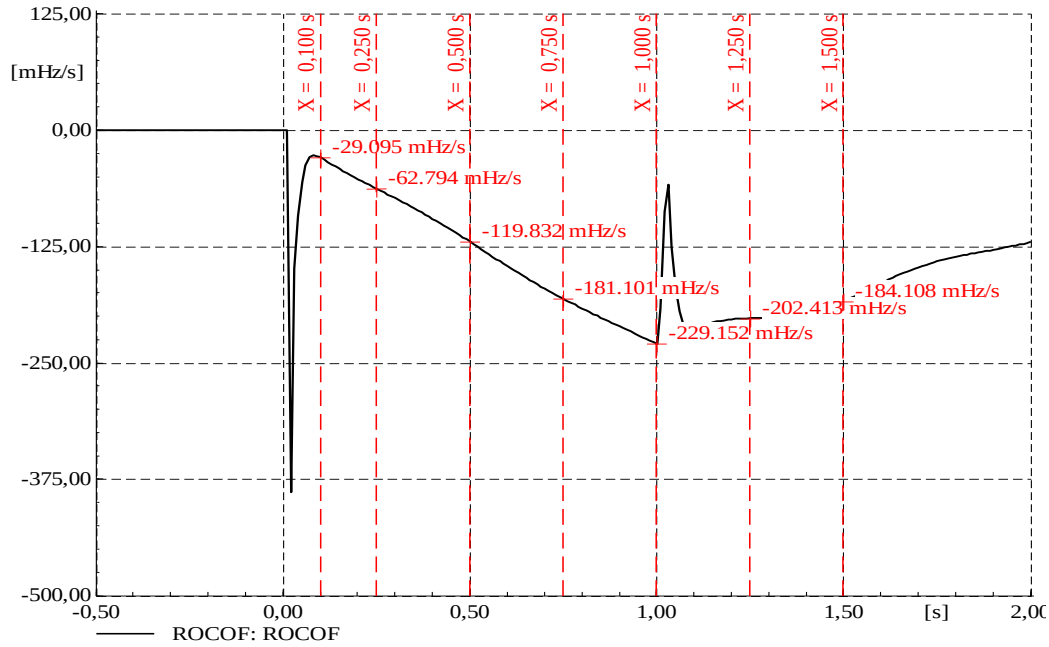

Figure 6.14: ROCOF response with TEST synchronous generator 33.75 MVA.

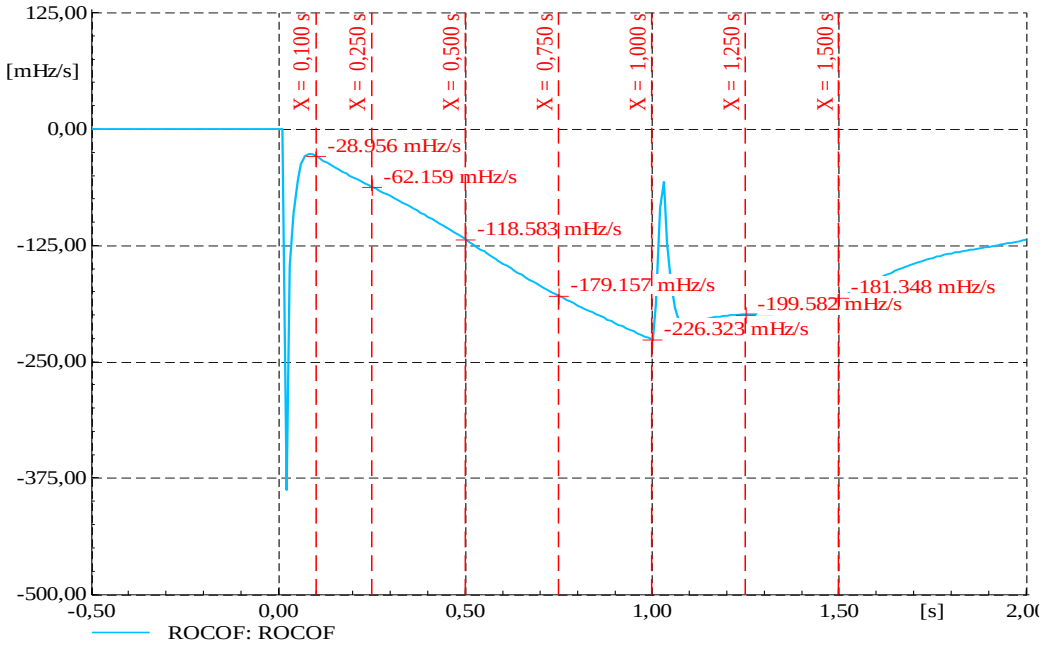

Figure 6.15: ROCOF response with VSM 33.75 MVA.

	RoCoF at 100 ms [mHz/s]	*RoCoF at 250 ms [mHz/s]*	*RoCoF at 500 ms [mHz/s]*	*RoCoF at 750 ms [mHz/s]*	*RoCoF at 1000 ms [mHz/s]*	*RoCoF at 1250 ms [mHz/s]*	*RoCoF at 1500 ms [mHz/s]*
TEST	29.095	62.794	119.832	181.101	229.152	202.413	184.108
VSM	28.956	62.159	118.583	179.157	226.323	199.582	181.348

Table 6.7: ROCOF comparison between test machine and VSM 33.75 MVA.

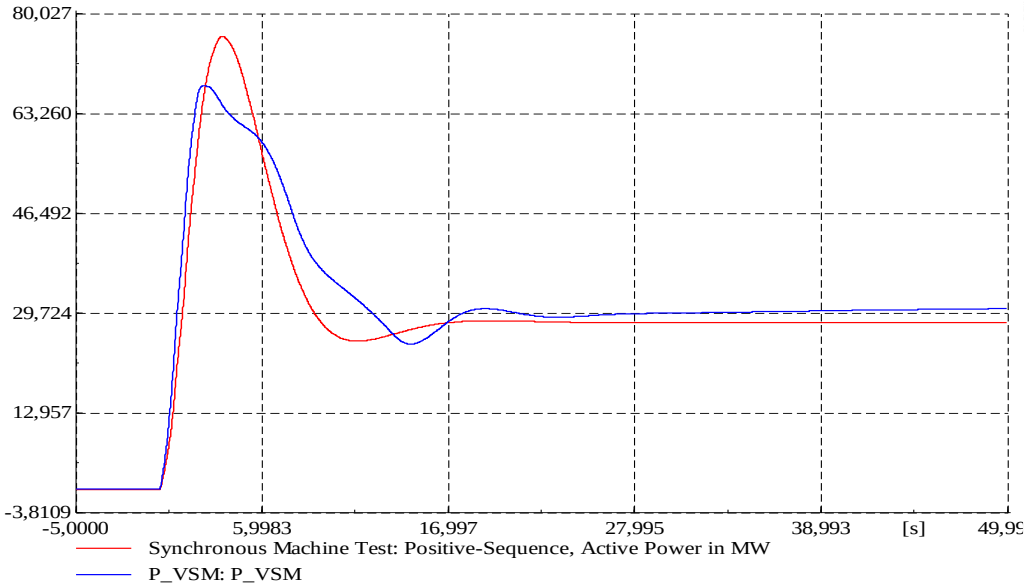

Figure 6.16: Comparison of the active power response of the VSM and TEST machine with 135 MVA rated power.

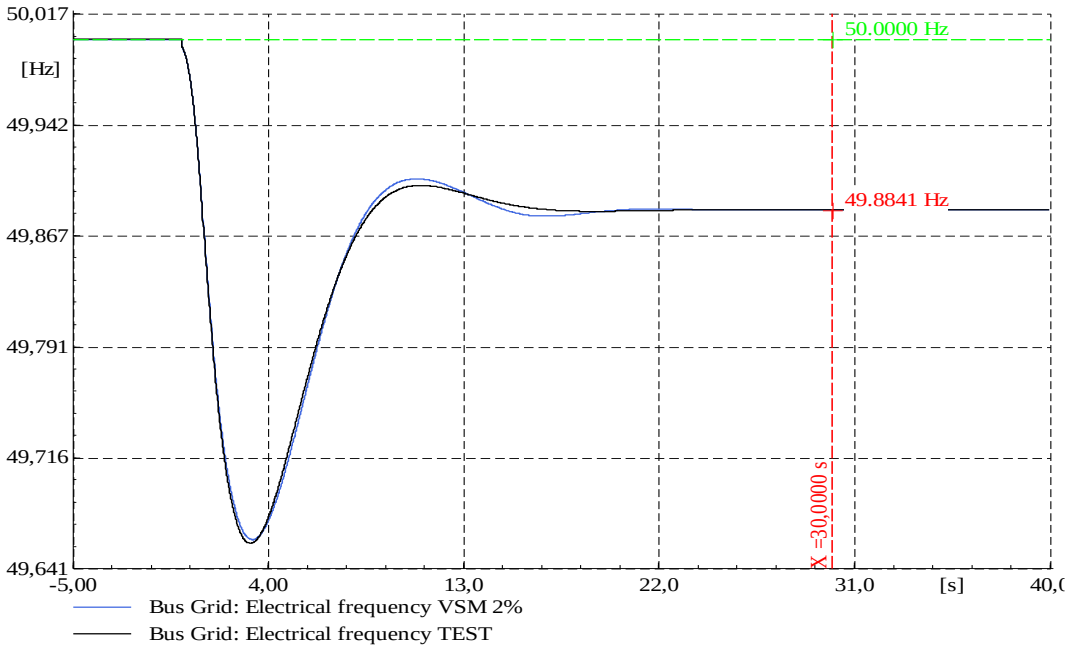

Figure 6.17: Comparison in the frequency response of the grid with VSM or TEST machine with 135 MVA rated power.

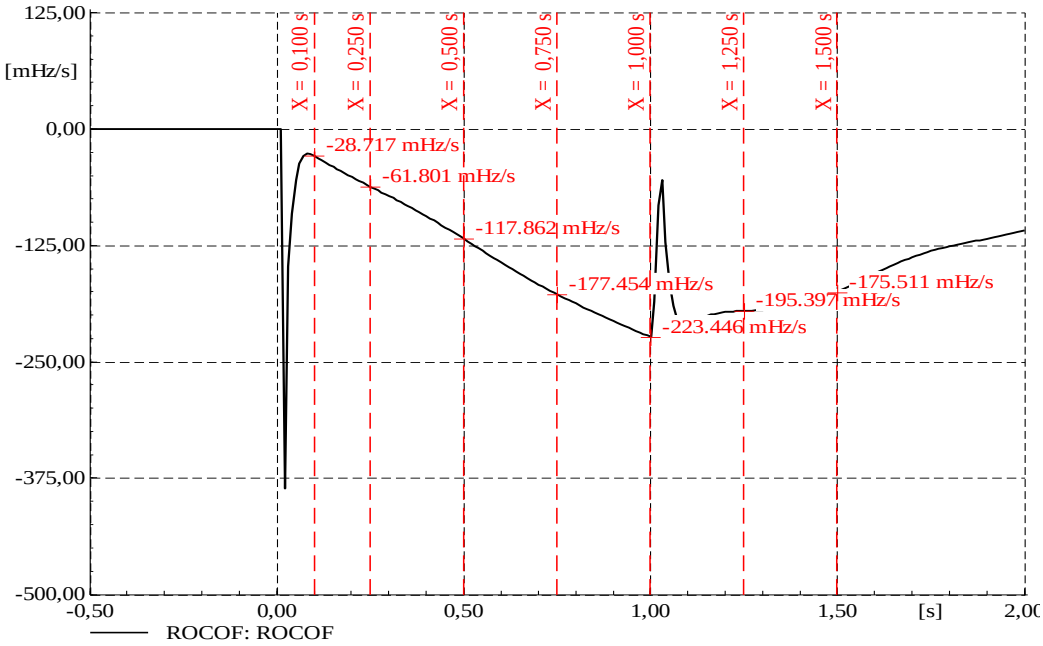

Figure 6.18. ROCOF response with TEST synchronous generator 135 MVA.

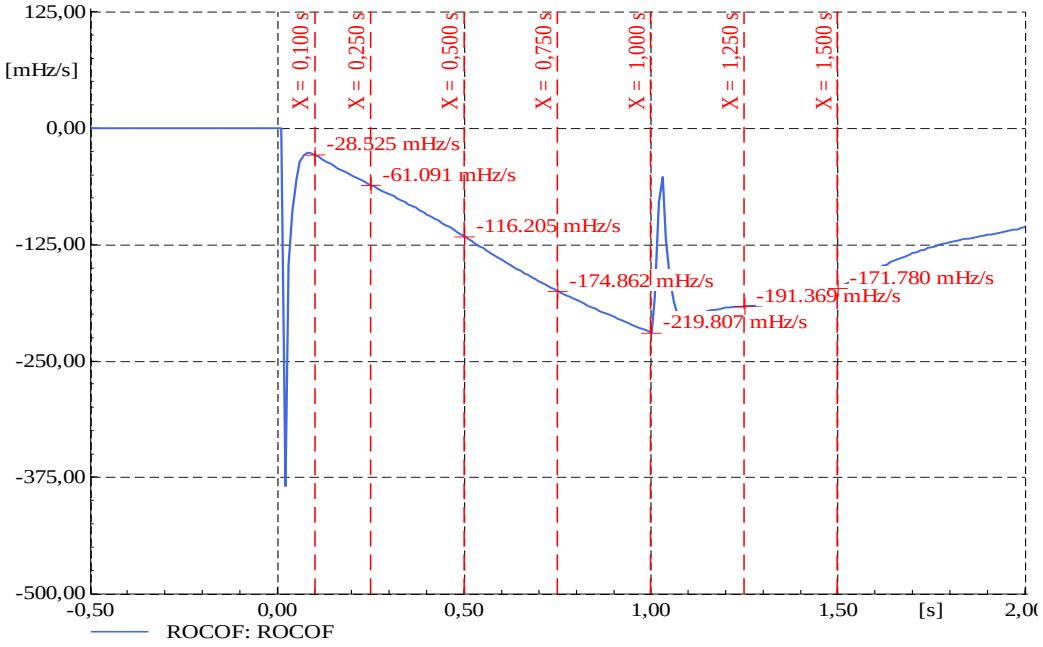

Figure 6.19: ROCOF response with VSM 135 MVA.

	RoCoF at 100 ms [mHz/s]	*RoCoF at 250 ms [mHz/s]*	*RoCoF at 500 ms [mHz/s]*	*RoCoF at 750 ms [mHz/s]*	*RoCoF at 1000 ms [mHz/s]*	*RoCoF at 1250 ms [mHz/s]*	*RoCoF at 1500 ms [mHz/s]*
TEST	28.717	61.801	117.862	177.454	223.446	195.397	175.511
VSM	28.525	61.091	116.205	174.862	219.807	191.369	171.780

Table 6.8: ROCOF comparison between test machine and VSM 135 MVA.

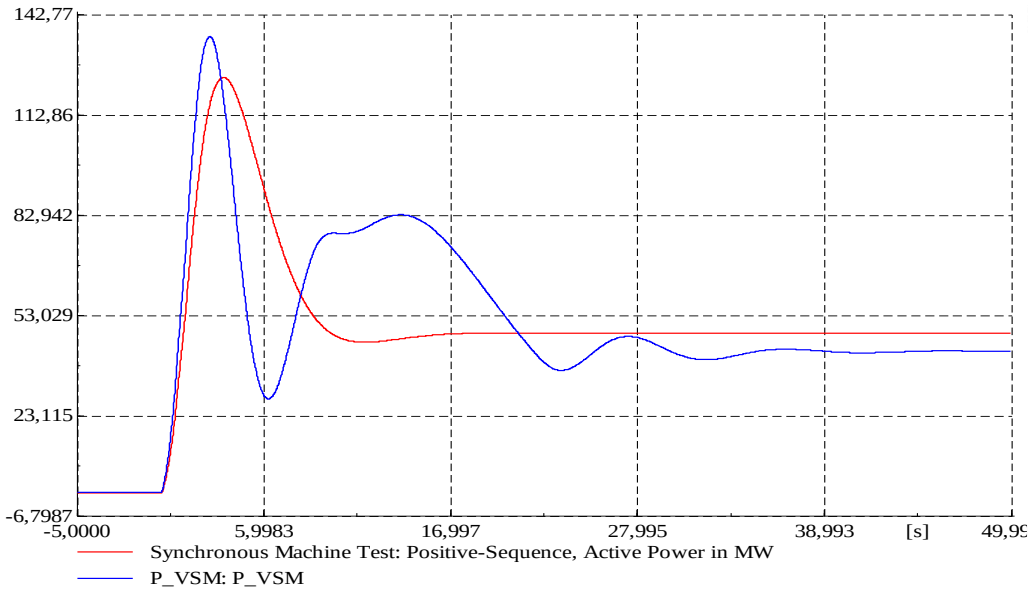

Figure 6.20: Comparison of the active power response of the VSM and TEST machine with 236.25 MVA rated power.

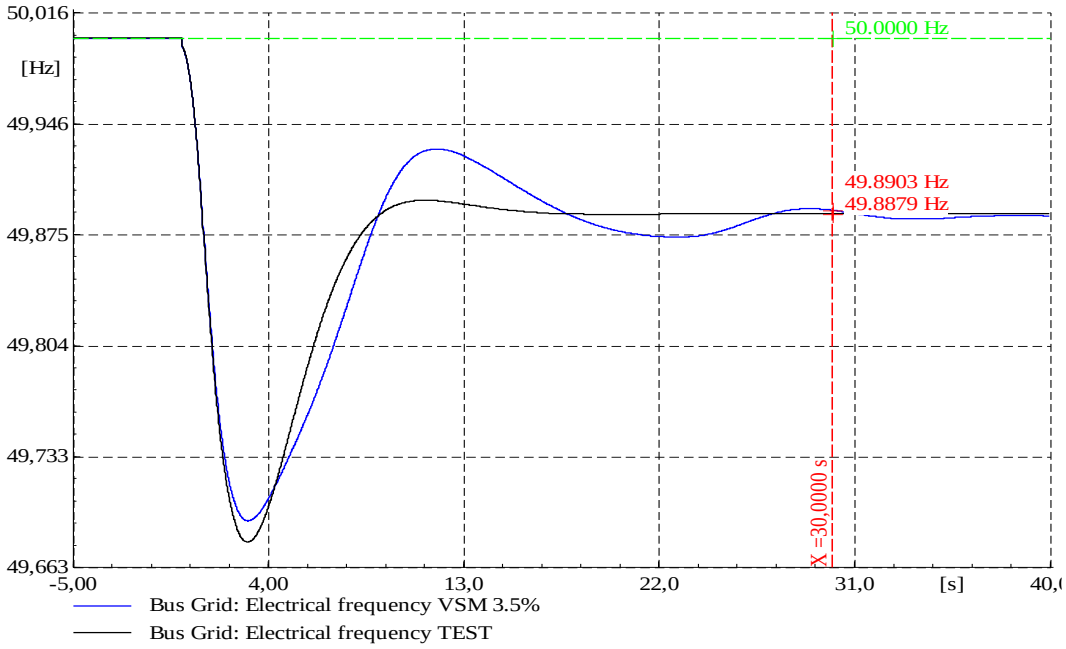

Figure 6.21: Comparison in the frequency response of the grid with VSM or TEST machine with 236.25 MVA rated power.

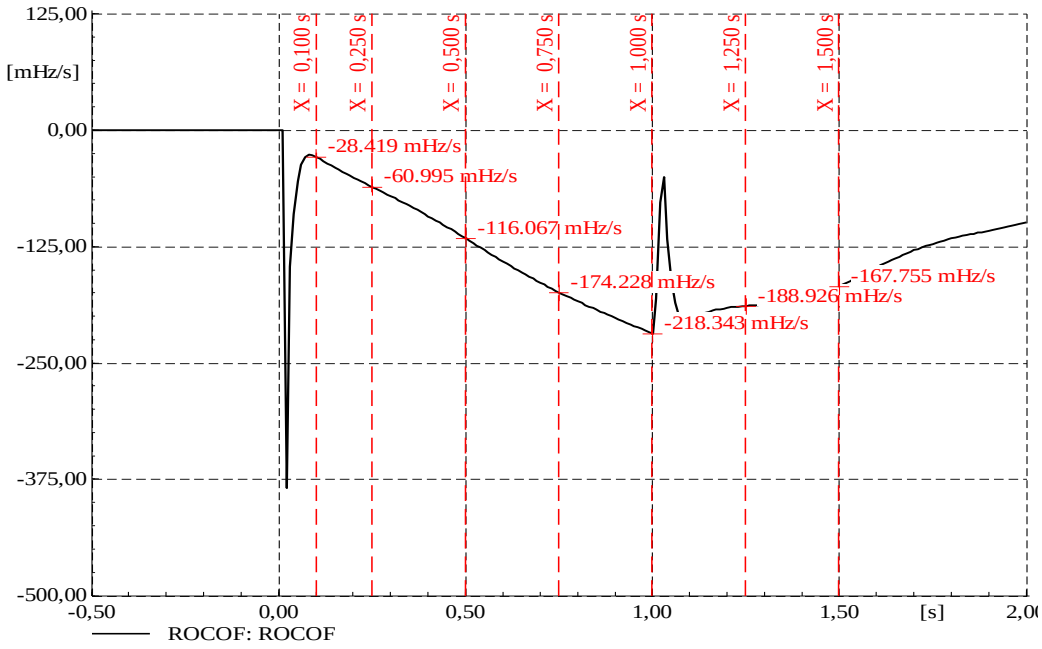

Figure 6.22: ROCOF response with TEST synchronous generator 236.25 MVA.

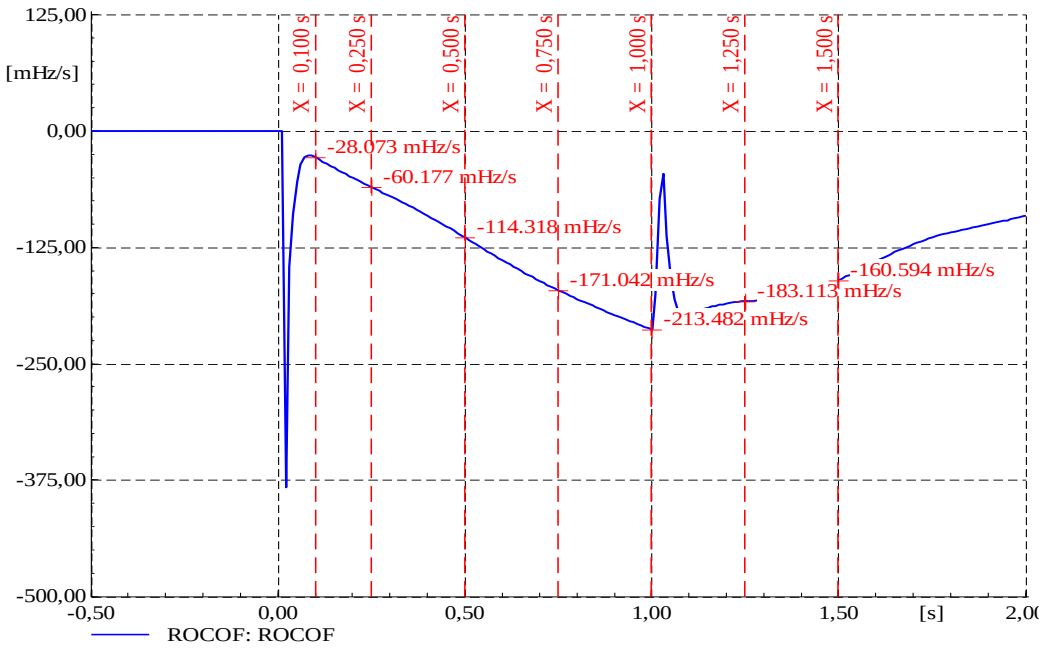

Figure 6.23: ROCOF response with VSM 236.25 MVA.

	RoCoF at 100 ms [mHz/s]	*RoCoF at 250 ms [mHz/s]*	*RoCoF at 500 ms [mHz/s]*	*RoCoF at 750 ms [mHz/s]*	*RoCoF at 1000 ms [mHz/s]*	*RoCoF at 1250 ms [mHz/s]*	*RoCoF at 1500 ms [mHz/s]*
TEST	28.419	60.995	116.067	174.228	218.343	188.296	167.775
VSM	28.073	60.177	114.318	171.042	213.482	183.113	160.594

Table 6.9: ROCOF comparison between test machine and VSM 236.25 MVA.

It is important to point out that the VSM at 2% has a better response thanks to step 3, while the others present a higher error in the active power response, compared with the one of the test synchronous.

6.2.2 Comparison between SEBIR and VSM

To compare the different types of control systems, three levels of power of the VSC has been chosen based on the grid active power demand. In other words, in these simulations it has been analysed the response of two VSCs with the same rated power, but with different control system: one has a SEBIR control system while the other one is a VSM. In the following figures, the comparison of the frequency response between the different rated VSM and SEBIR are illustrated. Moreover, the power response of the VSCs with SEBIR is shown while the one of the VSM-converters has already been presented in section 6.2.1.

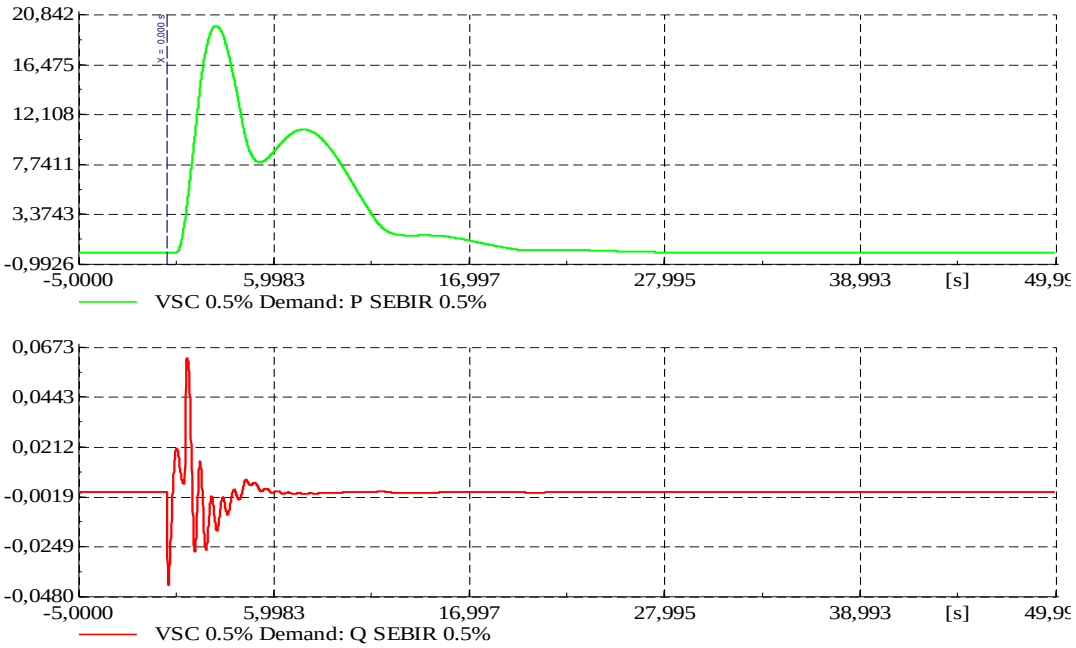

Figure 6.24: Active and reactive power response of the SEBIR 0.5%.

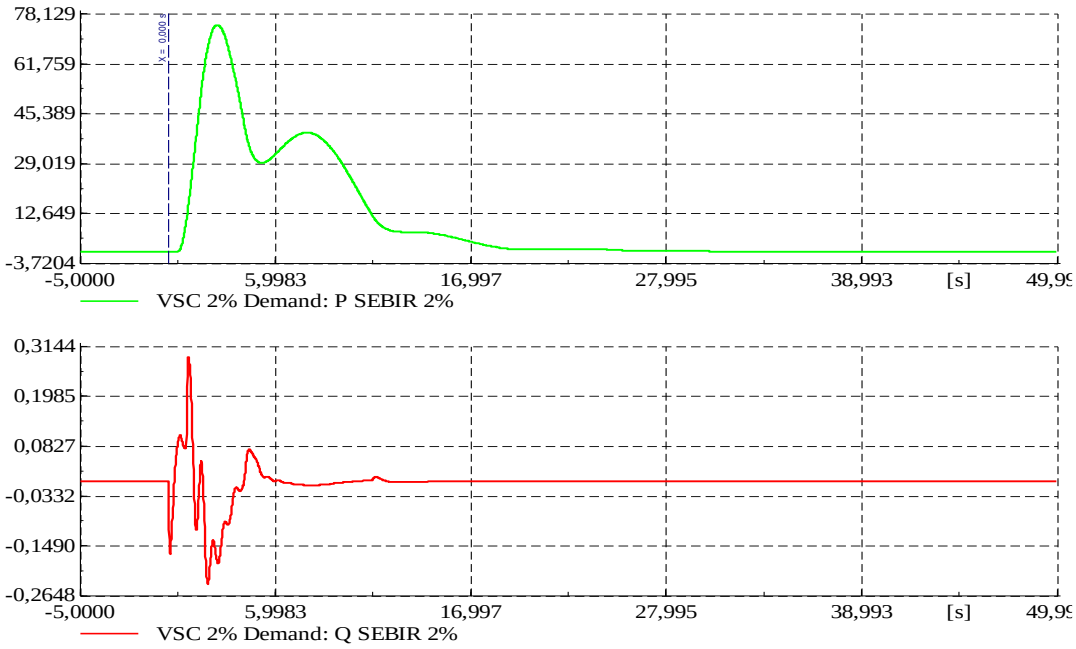

Figure 6.25: Active and reactive power response of the SEBIR 2.0%.

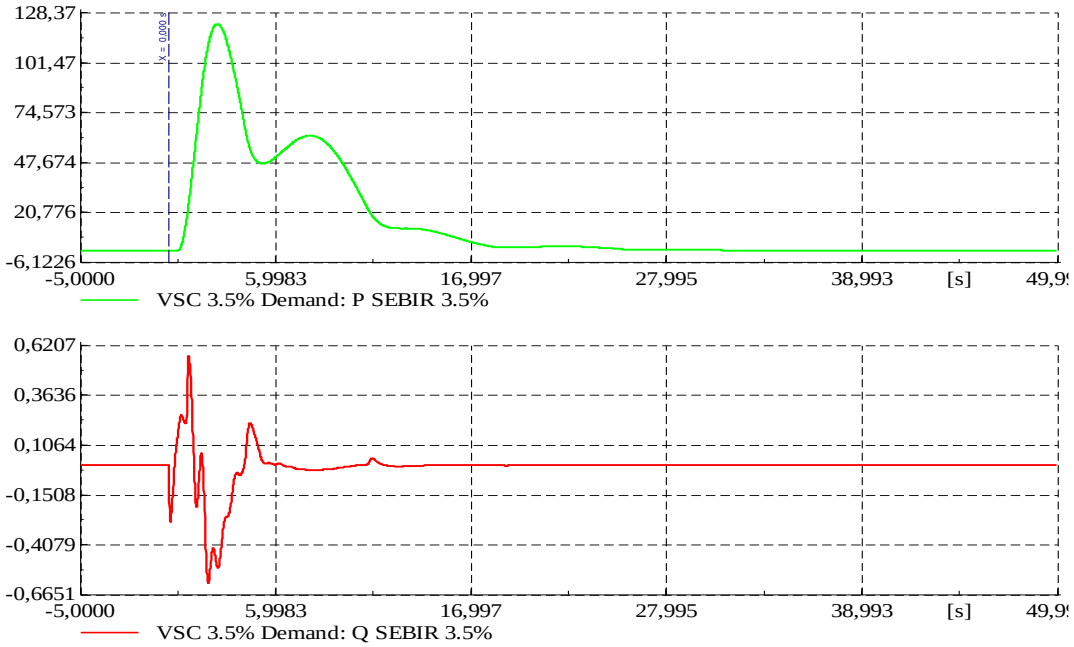

Figure 6.26: Active and reactive power response of the SEBIR 3.5%.

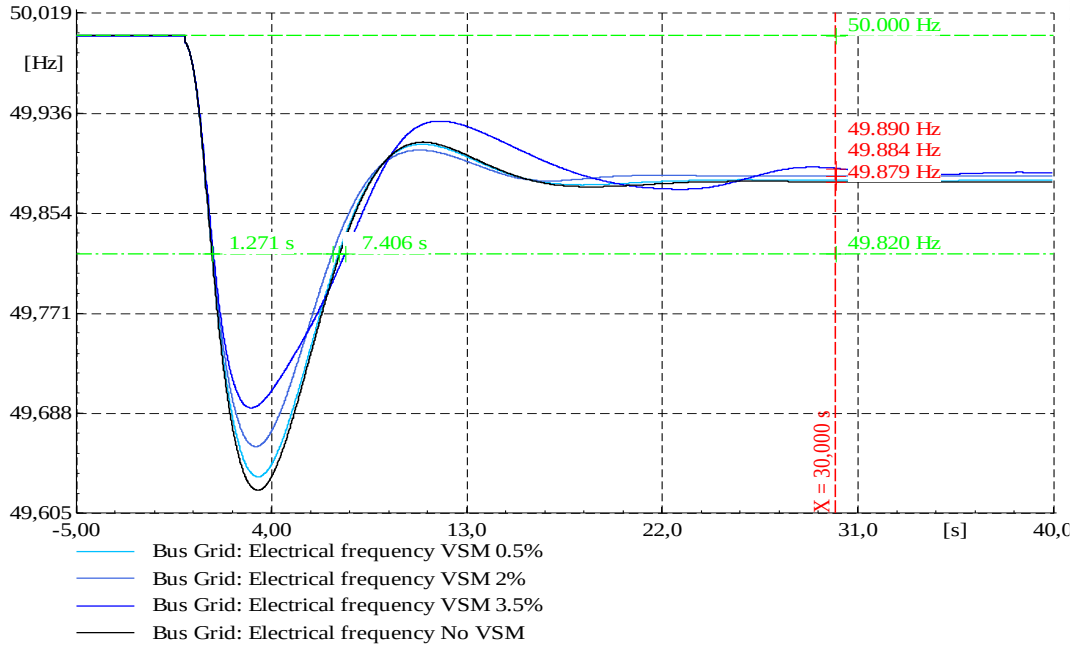

Figure 6.27: Frequency response with different levels of VSM.

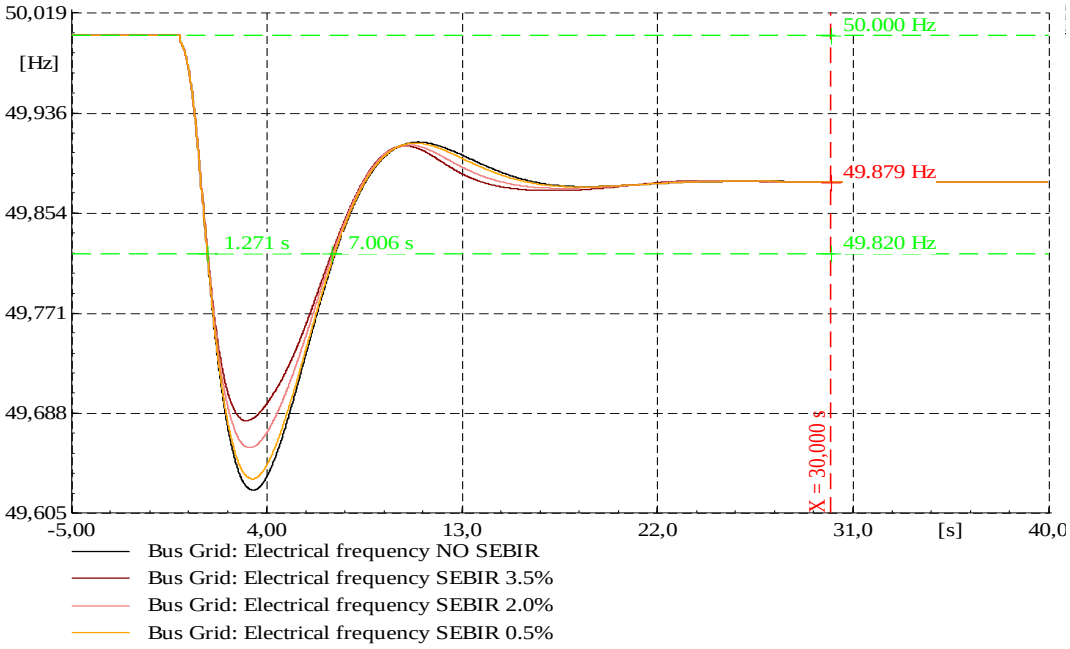

Figure 6.28: Frequency response with different levels of SEBIR.

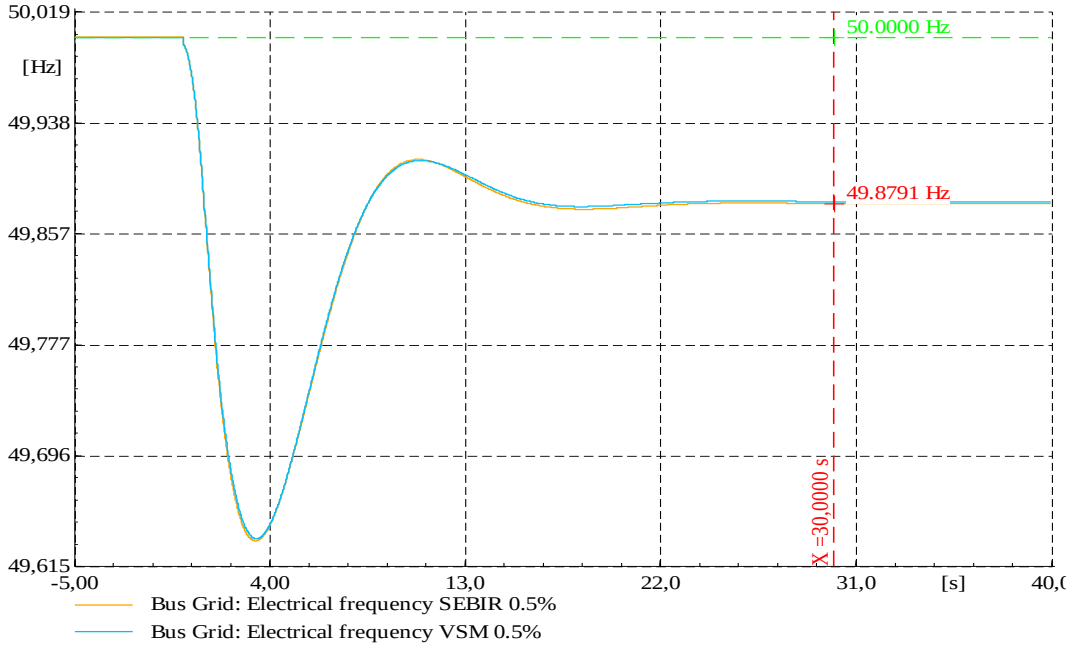

Figure 6.29: Comparison in the frequency response between SEBIR and VSM 0.5%.

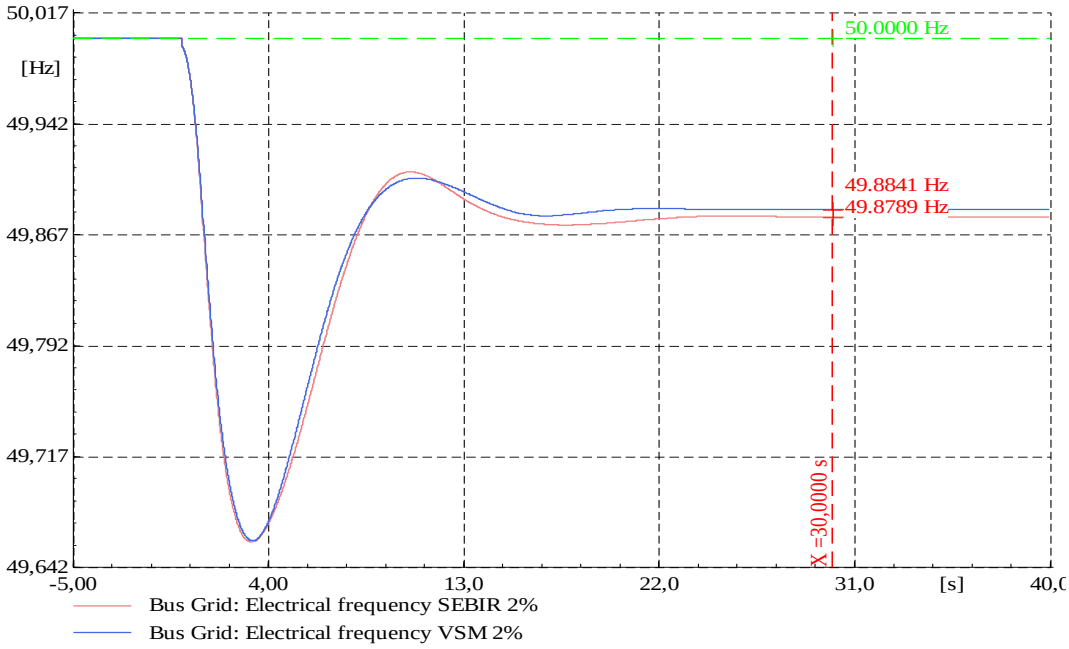

Figure 6.30: Comparison in the frequency response between SEBIR and VSM 2%.

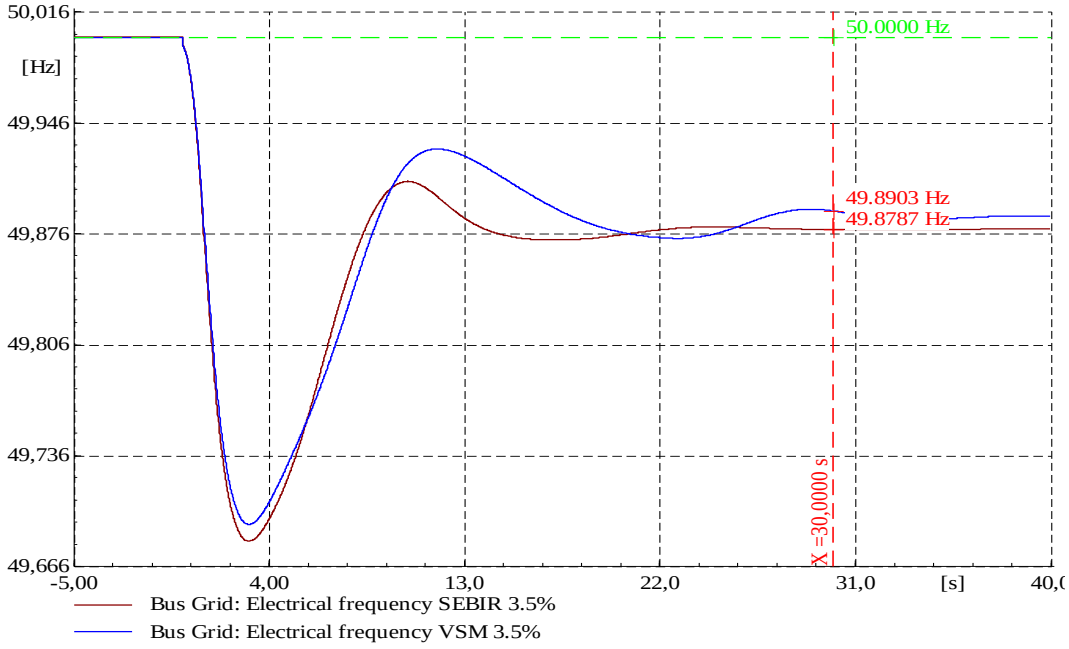

Figure 6.31: Comparison in the frequency response between SEBIR and VSM 3.5%.

From the previous figures, in which VSM and SEBIR are compared, it can be noted that:

- Both VSM and SEBIR, with the increase of the rated power, have a beneficial effect on the frequency response;

- VSM has a greater impact however it entails higher frequency oscillation, which are worse with the increase of the rated power;
- VSM and SEBIR allow to reach a higher frequency at stability, which is higher for VSM. However, VSM requires more time to have a stable frequency level, which is greater than 30 s with an increased rated power.

In the following tables and figures it will be presented a detailed analysis of: frequency nadir, time passed since the fault to reach the frequency nadir, time passed since the fault to return into acceptable frequency limits (defined in [7]), the frequency after 30s from the disturbance and the ROCOF in various instants.

VRG [%]	*S_n of SEBIR [%]*	*S_n of VSM [%]*	*Frequency Nadir (F.N.) [Hz]*	*t [s] to reach F.N.*	*Δt [s] to return into acceptable frequency limits*	*f [Hz] after 30 s from the disturbance*
0	0	0	49.6757	4.1007	8.2100	49.8903
59.142	0	0	49.6242	3.3444	7.1750	49.8791
59.142	0	0.5	49.6353	3.3664	7.1118	49.8803
59.142	0	2	49.6604	3.2595	6.8245	49.8841
59.142	0	3.5	49.6925	2.9992	7.4061	49.8903
59.142	0.5	0	49.6337	3.2838	7.1422	49.8791
59.142	2	0	49.6595	3.1774	7.0603	49.8789
59.142	3.5	0	49.6819	2.9804	7.0058	49.8787

Table 6.10: Analysis of the frequency response.

VRG [%]	*S_n of SEBIR [%]*	*S_n of VSM [%]*	*RoCoF at 100 ms [mHz/s]*	*RoCoF at 250 ms [mHz/s]*	*RoCoF at 500 ms [mHz/s]*	*RoCoF at 750 ms [mHz/s]*	*RoCoF at 1000 ms [mHz/s]*	*RoCoF at 1250 ms [mHz/s]*	*RoCoF at 1500 ms [mHz/s]*
0	0	0	20.542	42.631	84.358	124.357	161.559	152.532	138.451
59.142	0	0	29.209	63.121	120.519	182.455	231.091	204.917	187.245
59.142	0	0.5	28.956	62.159	118.583	179.157	226.323	199.582	181.348
59.142	0	2	28.525	61.091	116.205	174.862	219.807	191.369	171.780
59.142	0	3.5	28.073	60.177	114.318	171.042	213.482	183.113	160.594
59.142	0.5	0	29.231	63.132	120.531	182.016	229.917	202.789	183.955
59.142	2	0	29.326	63.149	120.484	180.803	226.687	196.846	174.894
59.142	3.5	0	29.478	63.160	120.454	179.728	223.821	191.520	166.754

Table 6.11: Analysis of the ROCOF response.

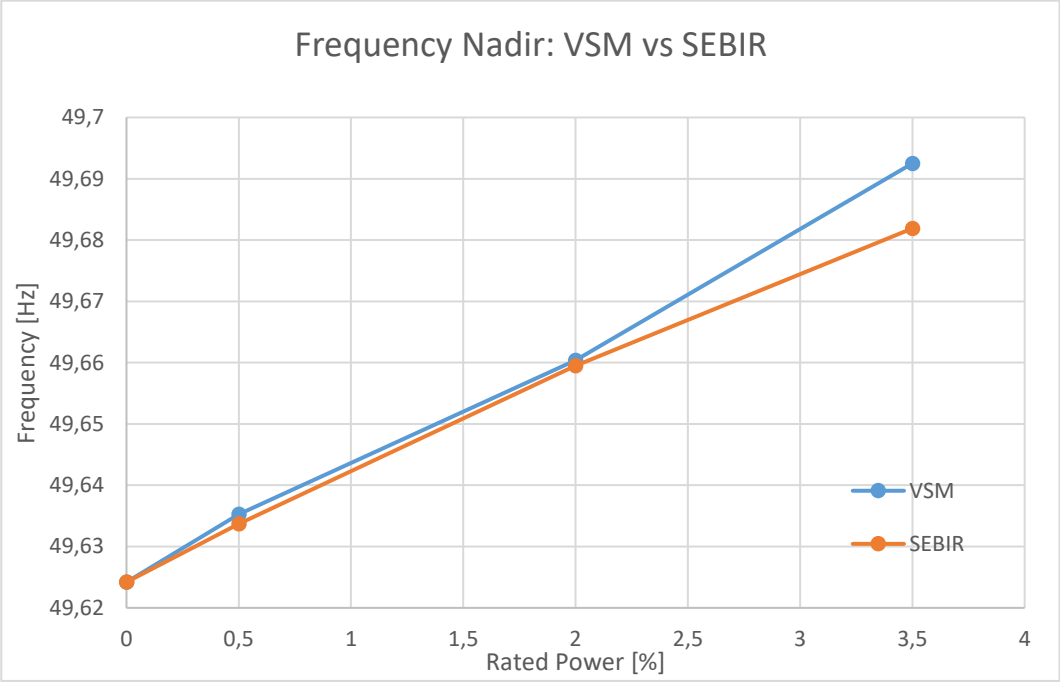

Figure 6.32: Frequency nadir with the increase of VSM/SEBIR rated power.

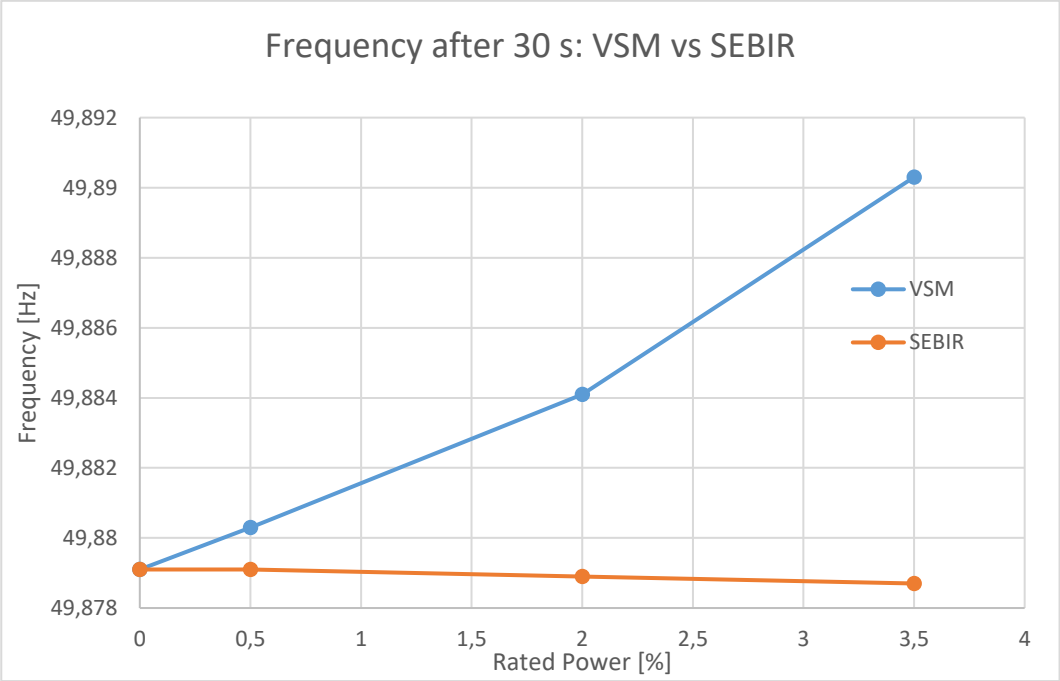

Figure 6.33: Frequency after 30 s with the increase of VSM/SEBIR rated power.

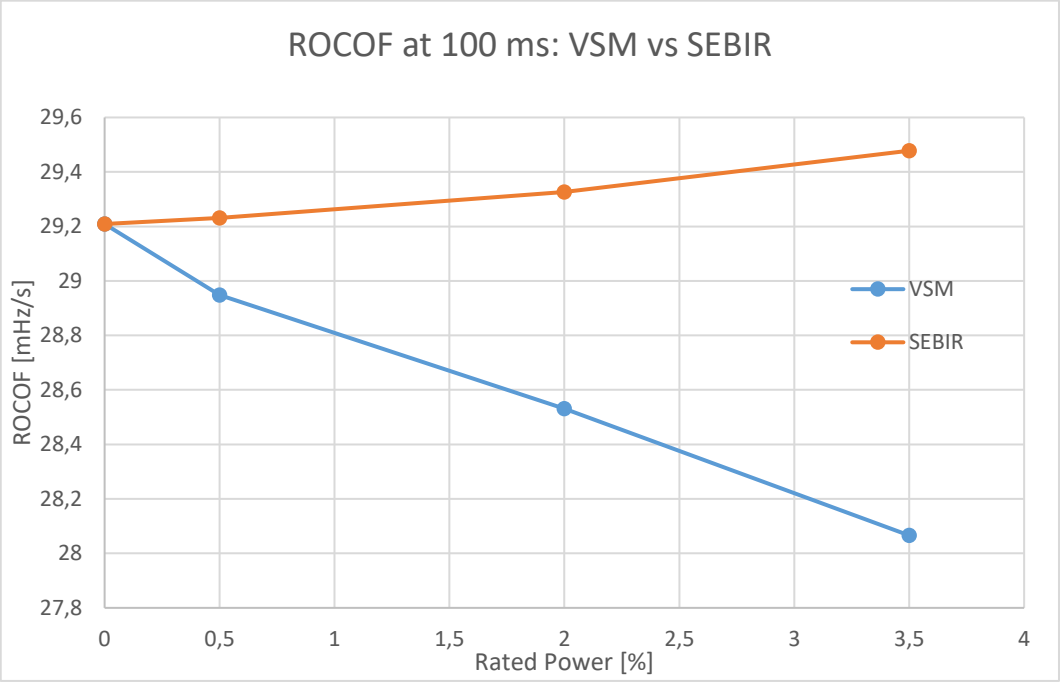

Figure 6.34: ROCOF at 100 ms with the increase of VSM/SEBIR rated power.

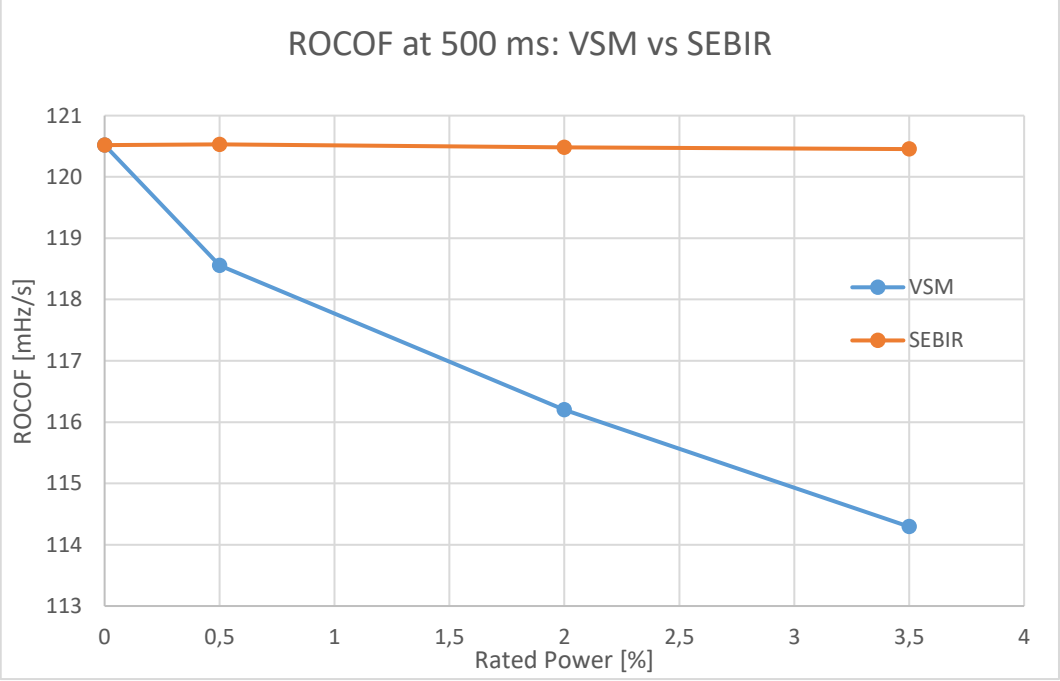

Figure 6.35: ROCOF at 500 ms with the increase of VSM/SEBIR rated power.

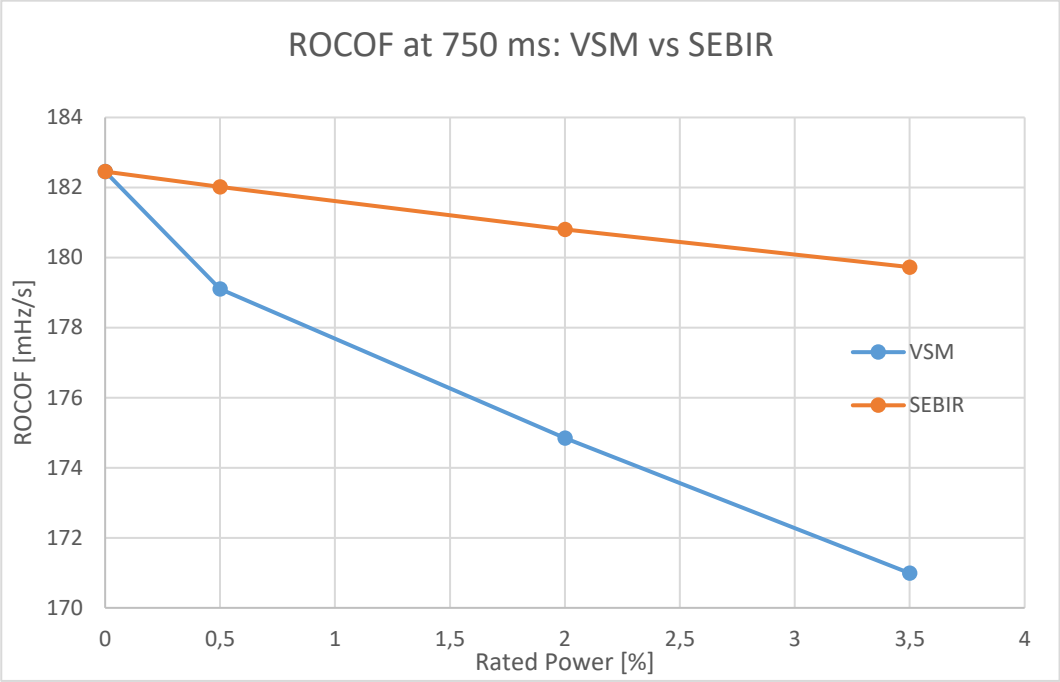

Figure 6.36: ROCOF at 750 ms with the increase of VSM/SEBIR rated power.

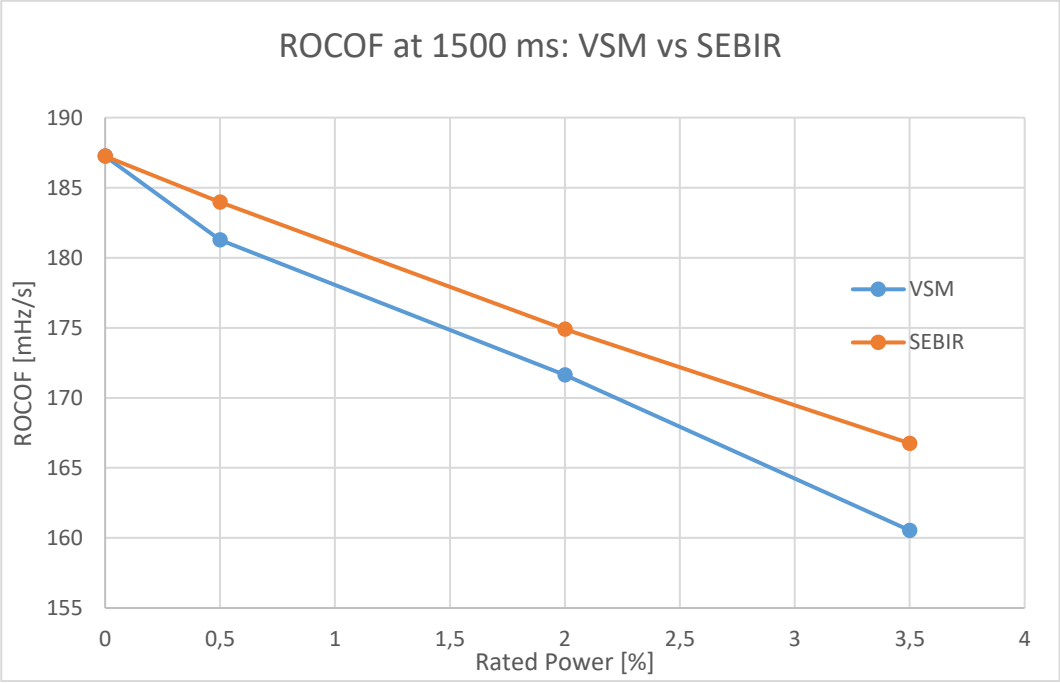

Figure 6.37: ROCOF at 1500 ms with the increase of VSM/SEBIR rated power.

From the data just presented, it can be observed that:

- Both models are able to improve the frequency nadir, however VSM has a slightly better response;
- VSM improves the ROCOF from the very first instant. Moreover it has a higher impact on the ROCOF compared to SEBIR;
- VSM generates a primary reserve that increase the frequency value after 30 s, while SEBIR does not improve it;
- SEBIR creates problem in the initial ROCOF: in facts, it worsens the ROCOF in the first 500 ms, then it starts getting better. This phenomena could be caused by the reactive power oscillations;

6.2.3 Analysis of the battery model response

As previously stated both SEBIR and VSM VSCs, with the same rated power, are equipped with the same storage system. In this section, the behaviour of the BESS will be presented, and SEBIR and VSM battery model response will be compared; in order to avoid a prolix analysis only the BESS of the VSC rated at 2% will be shown.

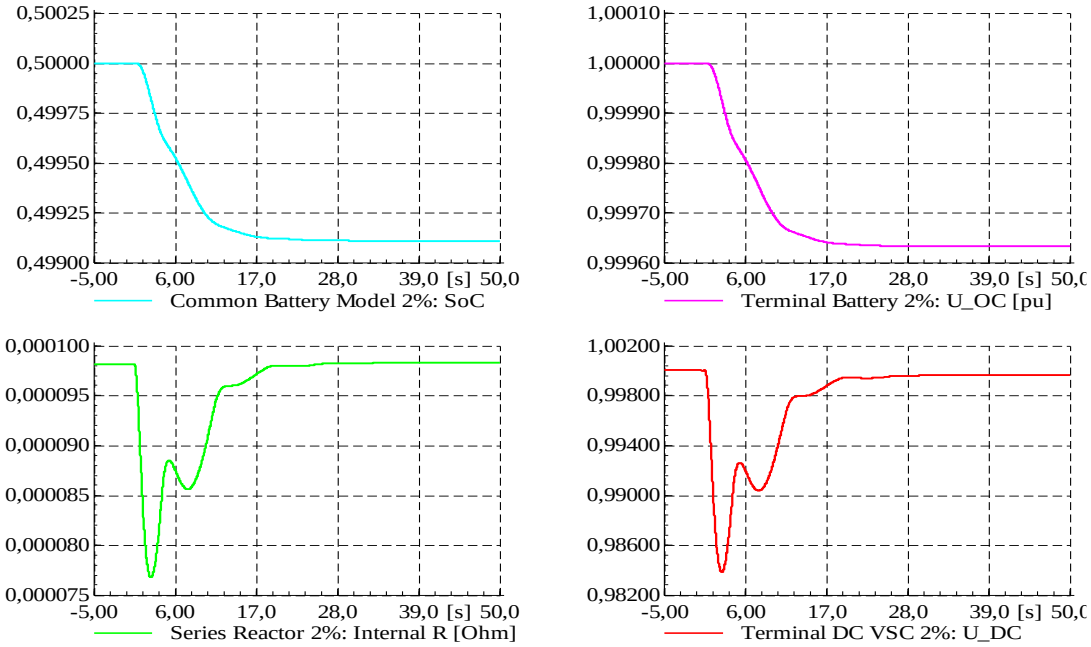

Figure 6.38: BESS-SEBIR behaviour.

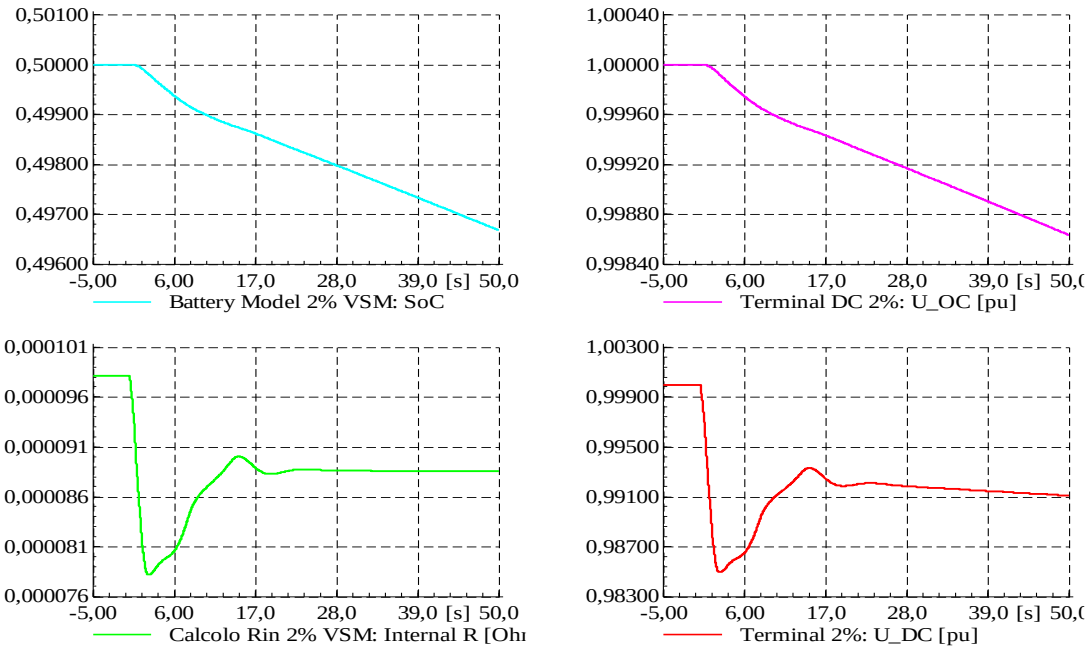

Figure 6.39: BESS-VSM behaviour.

In the previous figures, the BESS response of both SEBIR and VSM is illustrated:

- Cyan: the SoC of the battery, which has been set to 50% for both model;
- Fuchsia: the open circuit voltage of the battery, ie the tension of an ideal battery;
- Green: the internal resistance;
- Red: the DC voltage, ie the voltage of the BESS seen by the VSC.

As can be noted from the curves trend, the SoC practically does not vary, consequently also the open circuit voltage does not change and only the DC current influences the internal resistance. This phenomenon reflects to the DC voltage, which has the same trend of the internal resistance. Moreover, it can be observed that the BESS behaviour, in terms of SoC and open-circuit voltage, is the same for both SEBIR and VSM, therefore the control system of the VSC does not seem to reflect on the BESS response. On the other hand, the internal resistance, due to a small variation in the SoC, is highly influenced by the current of discharge. Finally, it is important to state that the disturbance, and the subsequent reaction of the control systems, seem to require little energy for both SEBIR and VSM. The energy used in both cases can be calculated from the power response, that can be seen in Figure 6.25 and Figure 6.16 respectively, thanks to *trapz* function in MATLAB.

	Energy in 5 s [kWh]	Energy in 10 s [kWh]	Energy in 15 s [kWh]	Energy in 20 s [kWh]	Energy in 30 s [kWh]	Energy in 40 s [kWh]	Energy in 50 s [kWh]
SEBIR	57,9	105,6	120,2	124,1	125,5	125,7	125,7
VSM	70,5	138,2	179,3	218,8	300,6	383,7	467,8

Table 6.12: Energy by SEBIR and VSM.

	Average power in first 5 s [MW]	Average power in first 10 s [MW]	Average power in first 15 s [MW]	Average power in first 20 s [MW]	Average power in first 30 s [MW]	Average power in first 40 s [MW]	Average power in first 50 s [MW]
SEBIR	41.67	38.03	28.85	22.33	15.06	11.31	9.05
VSM	50.74	49.76	43.04	39.39	36.07	34.53	33.68

Table 6.13: Power by SEBIR and VSM.

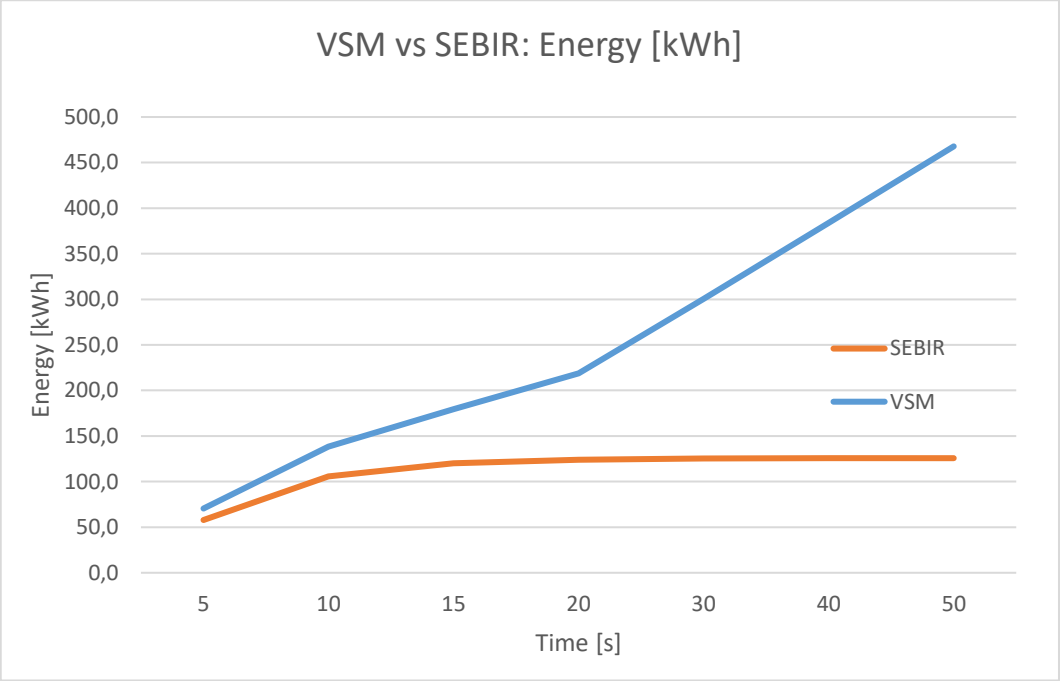

Figure 6.40: Energy trend in the first 50 s for BESS of VSM and SEBIR.

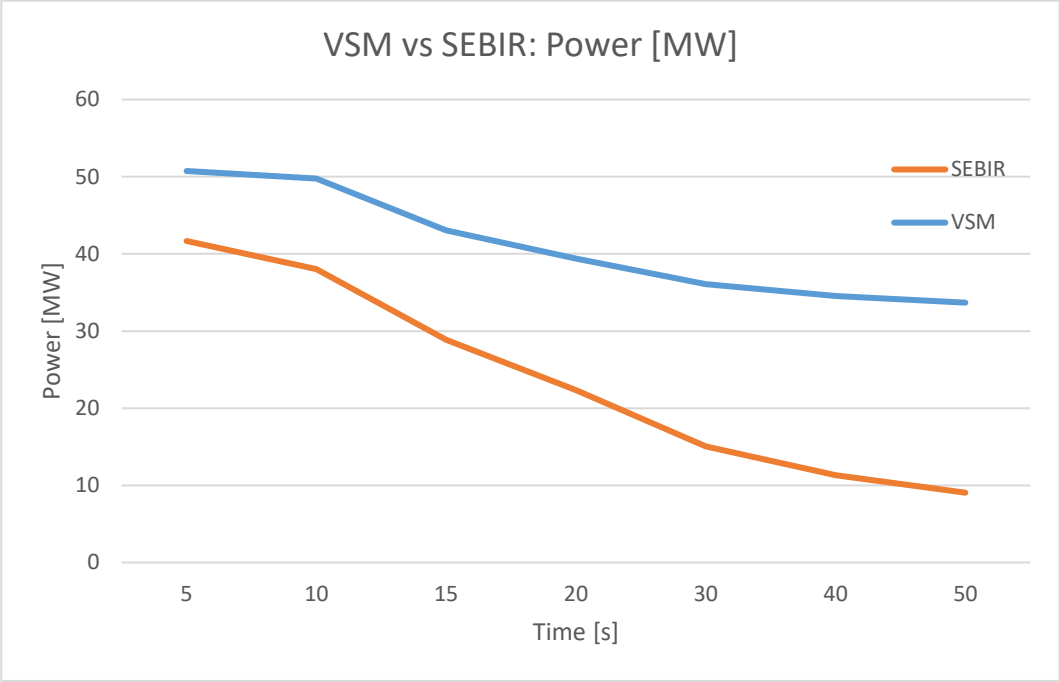

Figure 6.41: Power trend in the first 50 s for BESS of VSM and SEBIR.

Figure 6.40 shows the variation of the energy required from VSM (blue) and SEBIR (orange) after the disturbance, while Figure 6.41 illustrates the power trend. It can be observed that VSM needs higher energy than SEBIR, however in both cases the inertial response seems to require little energy, as a consequence, others ESSs, with lower energy density than battery, such as supercapacitor and HVDC-capacitor, in the future could be used with both SEBIR and VSM.

CONCLUSIONS

In this master's thesis, the influence of synthetic inertia on the grid stability has been analyzed. The intent has been to present alternative solutions, therefore SEBIR and VSM control systems have been modelled for a BESS. In order to study a plausible future case, a detailed grid with high penetration of variable renewable generation has been implemented in the software environment DIgSILENT Powerfactory, which has been chosen in order to conduct the dynamical simulations. Moreover, the VSM control scheme has been parameterized to obtain a response similar to the one of a test synchronous generator with the same rated power of the VSM. In order to do this, a simplified version of the grid with the VSM has been modelled in MATLAB Simulink, then, the VSM has been configured, through the Parameter Estimation tool. The main question of this thesis was how SEBIR and VSM react in case of power imbalances consequently frequency response of the system, with different rated power of these technologies, has been tested. The simulations results show different behaviours: while both the control systems improve the frequency nadir, only VSM is able to reduce the initial ROCOF, ie in the first 500 ms. Furthermore, it seems that SEBIR slightly worsens the ROCOF in the first 500 ms, probably due to high reactive power oscillations. However, SEBIR is more stable with the increase of the rated power on the contrary VSM generates more frequency oscillations. In future works, both SEBIR and VSM could be used with others ESS, such as supercapacitors, or in HVDC systems. In fact, it has been calculated that the energy required for SEBIR and VSM is pretty low, therefore ESS with small energy density could be used for the inertial response, ie in the first few seconds after the disturbance. Moreover, SEBIR and VSM could work in parallel with PV and wind turbine, in order to, not only to compensate power imbalances, but also regulate these variable energy sources: in this way, a more stable frequency could be obtained also in normal grid condition. Furthermore, it is important to note that major research works have to be done in order to test SEBIR and VSM under short-circuit condition and evaluate their response in abnormal situations. Finally, SEBIR and VSM could be tested in an islanded grid to analyse their behaviour in a situation with practically 100% penetration of VRG.

APPENDIX A

It is fundamental to remark the difference between current source converters and voltage source converters, and to distinguish this concept from the current-sourced converters and voltage-sourced converters one: most modern converters using self-commutated devices (IGBTs, IGCTs, MMC HVDC, etc.) are described as VSC (Voltage-Sourced Converters). This is a name given to them historically, to differentiate them from converters based on thyristor technology, which are Line Commutated Converter (LCC) devices and known as “Current-Sourced Converters”. The term “VSC” refers to the fact that the DC bus sits at a nominally constant voltage, and so at any instant the converter bridge can apply a controlled proportion of that voltage to the AC system, via the filter impedance. However, most grid-connected converters using VSC technology do not behave as voltage sources. Inside the control software there are a pair of set-points for active (P) and reactive (Q) power, which are translated into I_d and I_q axis current references. The inner control loop within the converter software is a current-control loop whose primary goal is to source/sink balanced, positive-sequence sinusoidal currents matching the I_d - I_q references, and thereby the P-Q set-points. [18]

APPENDIX B

The MATLAB script used to define the initial condition of the parameters of the simplified grid is illustrated below:

```
% Questo programma esegue l'analisi della dinamica di una VSM
interconnessa
% ad una rete di trasmissione

%   clear all;
%   close all;
%   clc;
% Impostazione dei dati:
% Sistema A                    Grandezza
% Dati della rete di prima ipotesi
  PN    = 8000;               % Potenza nominale del sistema [MW]
  Ta    = 10;                 % Tempo di avviamento della rete [s]
  fN    = 50;                 % Frequenza nominale di regime [Hz]
  Pu    = 6600;               % Potenza assorbita dal carico prima del
disturbo [MW]
  alpha    = 1.75;            % Dipendenza del carico da f [ ]
  stat = 5/100;               % Grado di statismo del regolatore
  Tr    = 15;                 % Tempo di regolazione primaria [s]
  T1    = 5;                  % Tempo accelerometrica = 2H [s]
  tA     = 30;                % Tempi di integrazione del regolatore di
rete [s]
  kB    = 0.125;              % Fattore del guadagno in regolazione
secondaria [ ]

% VSM valori di stima iniziali        Grandezza
  H = 1;                              % Synthetic inertia []
  K_fmeas    = 5;                     % Guadagno variazione di
frequenza misurata [ ]
  T_fmeas    = 1;                     % Costante di tempo variazione di
frequenza misurata  [s]
  K_Pmeas    = 0.05;                  % Droop potenza attiva in
percentuale [ ]
  T_Pmeas    = 1;                     % Costante di tempo variazione di
potenza attiva misurata [s]
  Kp_gov    = 2.5;                    % Guadagno componente
proporzionale governor [ ]
  Ki_gov    = 0.05;                   % Guadagno componente integrativa
governor [ ]
  K_gov    = 30;                      % Potenza nominale del sistema
[MW]
  T_gov    = 5;                       % Costante di tempo governor [s]
  Km = 30;                            % Mechanical damping [ ]
  K_f = 25;                           % Guadagno damping da frequenza
virtuale [ ]
  T_f = 1;                            % Costante di tempo filtro
frequenza virtuale [s]
```

```
  K_fgrid = 250;                      % Guadagno damping da frequenza
rete [ ]
  T_fgrid = 1;                        % Costante di tempo damping da
frequenza rete [s]
  T = 0.1;                            % Costante di tempo per virtual
rotor phase [s]

% Taglia VSM
  Sn = 135;             % Potenza base dalla VSM [MVA]
                        % La potenza è basata sulla percentuale di
carico
                        % I livelli di potenza possibili sono 33.75,
135,
                        % 236,25

% Impostazione della condizione di disurbo introdotta nel sistema
% interconnesso
  ndist    = 1;       % Numero di condizioni di disurbo in analisi
  distA    = 660;     % Entità del disurbo nel sistema A
  ritardoA = 0;       % Ritardo del disturbo nel sistema A rispetto
all'istante t=0


% Elaborazione delle costanti per la modellazione della rete
% con Simulink
  kw = PN*Ta/fN;           % Sistema A: [MW/Hz]

  kr = PN/(fN*stat);       % Sistema A: Energia regolante del
generatore [MW/Hz]

  ku = Pu*alpha/(fN);      % Sistema A: Energia regolante del
generatore [MW/Hz]

% parametri stimati della rete al passaggio 1
    T1 = 1.4514;
    Tr = 9.1659;
    kr = 5349.1;
    ku = 32.781;
    kw = 3029.6;

%grafico analisi frequenza
  tanalisi=40;
  Hvett=[1];

 for z = 1:1
     deltaPA = distA(1);
     tritA   = ritardoA(1);
     tsimul  = tritA+tanalisi;
     H=Hvett(z);
     sim('rete_VSM');
     tempo = Pot_att(:,1);
     hf=figure(1);
     set(hf,'Color',[1 1 1]);
     hold on;
```

```
    y1 = Pot_att(:,2);
    p(1)=plot(tempo,y1);
end
```

BIBLIOGRAPHY

[1] IEEE/CIGRE Joint Task Force on Stability Terms and Definitions, “Definition and Classification of Power System Stability,” 2004, pp. 1387-1400.

[2] P. Kundur, Power System Stability and Control, McGraw-Hill, 1994.

[3] G. Andersson, “Dynamics and Control of Electric Power Systems,” 2012.

[4] ENTSO-E, “Frequency Stability Evaluation Criteria for the Synchronous Zone of Continental Europe,” 2016.

[5] TERNA, “PARTECIPAZIONE ALLA REGOLAZIONE DI FREQUENZA E FREQUENZA-POTENZA,” 2008.

[6] P. H. Jensen, “Frequency stability improvement of low inertia systems using synchronous condensers,” *IEEE Journal*, 2016.

[7] ENTSO-E, "Operational Handbook - Policy 1," 2004.

[8] A. U. T. S. B. Goran Andersson, “Impact of low rotational inertia on power system stability and operation,” Cape Town, South Africa, 2014.

[9] D. V. H. Pieter Tielens, "The relevance of inertia in power systems," *Elsevier*, vol. Renewable and Suitanable Energy Reviews, pp. 999-1008, 2015.

[10] V. S. M. L.-B.-Z. Ye Wang, “Impact of high penetration of variable renewable generation on frequency dynamics in the continental Europe interconnected system,” *IET Renewable Power Generation*, vol. 10, pp. 10-16, 2016.

[11] D. V. H. Steven De Boeck, “Under frequency load shedding schemes in systems with high PV penetration: Impact and improvements,” PowerTech, IEEE Eindhoven, 2015.

[12] ENTSO-E, "Technical background for the Low Frequency Demand Disconnection requirements," 2014.

[13] T. K. Y. L. S. K. K. N. C. Y. Chan, “An impact study of ROCOF relays for islanding detection,” in *10th International Conference on Advances in Power System Control, Operation & Management (APSCOM 2015)*, 2015.

[14] H. Z. W. X. Ali Kasem Alaboudy, "Performance of Frequency Relays with Multiple Synchronous Based DG Units," in *IEEE International Symposium on Industrial Electronics*, Hangzhou, China, 2012.

[15] N. M. K. E. Robert Eriksson, “Synthetic inertia versus fast frequency response: a definition,” *IET Renewable Power Generation,* 2017.

[16] T. P. V. V. A. J. R. J. M. a. N. M. Thomas Ackermann, “A Future Without Inertia Is Closer Than You Think,” *IEEE power & energy magazine,* 2017.

[17] A. D. A. J. R. C. B. R. I. H. U. J. Z. M. Yu, "Effects of Swing Equation-Based Inertial Response (SEBIR) Control on Penetration Limits of Non-Synchronous Generation in the GB Power System," *IET Renewable Power Generation,* 2015.

[18] ENTSO-E, “High Penetration of Power Electronic Interfaced Power Sources (HPoPEIPS),” 2017.

[19] A. J. R. A. D. C. D. B. R. I. J. Z. H. U. Mengran Yu, “Instantaneous penetration level limits of nonsynchronous devices in the British power system,” *IET Renewable Power Generation,* 2016.

[20] R. H. Hans-Peter Beck, “Virtual Synchronous Machine,” 2007.

[21] C. A. B. K. Xiaodong Liang, “Virtual Synchronous Machine Method in Renewable Energy Integration,” in *IEEE PES Asia Pacific Power and Energy Conference* , Xian, China, 2016.

[22] A. J. R. A. D. C. D. B. R. I. J. Z. H. U. Mengran Yu, "Effects of VSM Convertor Control on Penetration Limits of Non-Synchronous Generation in the GB Power System," 2016.

[23] A. J. R. A. D. C. D. B. R. I. J. Z. H. U. Mengran Yu, “A VSM (Virtual Synchronous Machine) Convertor Control Model Suitable for RMS Studies for Resolving System Operator/Owner Challenges,” 2017.

[24] G. W. Qing-Chang Zhong, “Synchronverters: Inverters That Mimic Synchronous Generators,” *IEEE TRANSACTIONS ON INDUSTRIAL ELECTRONICS,* vol. 58, no. 4, 2011.

[25] C. Pelczar, Mobile Virtual Synchronous Machine for Vehicle-to-Grid Applications, 2012.

[26] J. A. S. Salvatore D’Arco, "Virtual Synchronous Machines – Classification of Implementations and Analysis of Equivalence to Droop Controllers for Microgrids".

[27] “Use of an Inertia-less Virtual Synchronous Machine within Future Power Networks with High Penetrations of Converters”.

[28] ENTSO-E, “Need for synthetic inertia (SI) for freqeuncy regulation,” 2017.

[29] A. J. R. A. D. C. D. B. R. I. J. Z. H. U. Mengran Yu, “Use of an Inertia-less Virtual Synchronous Machine within Future Power Networks with High Penetrations of Converters”.

[30] D. A. P. S. Luis Marroyo, “Virtual synchronous generators classfication and common trend,” *IEEE Journal*, 2016.

[31] H. S. M. Mohammad Dreidy, "Inertia response and frequency control techniques for renewable energy sources: A review," *Elsevier*, vol. Renewable and Sustainable Energy Reviews, no. 69, pp. 144-155, 2017.

[32] M. S. G. L. P. S. Tobias Hess, “Case study on primary frequency control with wind-turbines and photovoltaic plants,” in *Power Systems Computation Conference*, Wroclaw, Poland, 2014.

[33] G. D. G. M. Bruno François, “Dynamic Frequency Control Support by Energy Storage to Reduce the Impact of Wind and Solar Generation on Isolated Power System’s Inertia,” *IEEE* , vol. Transactions on Sustainable Energy, no. 3, pp. 931-939, 2012.

[34] G. Y. A. H. N. P. H. J. Ha Thi Nguyen, “Frequency stability improvement of low inertia systems using synchronous condensers,” in *IEEE International Conference on Smart Grid Communications (SmartGridComm)*, Sydney, NSW, Australia, 2016.

[35] S. Y. S. Z. F. Z. P. Yang Liu, “Comparison of synchronous condenser and STATCOM for inertial response support,” in *IEEE Energy Conversion Congress and Exposition (ECCE)*, Pittsburgh, PA, USA, 2014.

[36] C. P. S. S. R. M. P. R. A. Ervin Spahic, “Multilevel STATCOM with power intensive energy storage for dynamic grid stability - frequency and voltage support,” in *IEEE Electrical Power and Energy Conference (EPEC)*, London, ON, Canada, 2015.

[37] B. B. Z. A. P. J. L. F. V. H. Hasanvand, “Voltage support and damping of low frequency oscillations in a large scale power system using STATCOM,” in *IEEE Energy Conference (ENERGYCON)*, Leuven, Belgium, 2016.

[38] J.-P. H. N. J. L. Ä. H.-P. N. Hongyang Zhang, “Frequency response improvement with synchronous condenser and power electronics converters,” in *IEEE Future Energy*

Electronics Conference and ECCE Asia (IFEEC 2017 - ECCE Asia), Kaohsiung, Taiwan, 2017.

[39] S. J. F. J. B. M. F. E. A. S. Elansari, “Frequency control capability of VSC-HVDC transmission system,” in *11th IET International Conference on AC and DC Power Transmission*, Birmingham, UK, 2015.

[40] R. P. M. B. John Fradley, “VSC-HVDC for frequency support (a review),” in *13th IET International Conference on AC and DC Power Transmission (ACDC 2017)*, Manchester, UK, 2017.

[41] DIgSILENT PowerFactory, DIgSILENT PowerFactory User Manual, 2017.

[42] GSE, "Rapporto Statistico 2016: Solare Fotovoltaico," 2016.

[43] GSE, "Rapporto Statistico 2016: Energia da Fonti Rinnovabili in Italia," 2016.

[44] D. C. A. G. A. P. E. Ciapessoni, "Renewable power integration in Sicily: Frequency stability issues and possible countermeasures," in *Bulk Power System Dynamics and Control - IX Optimization, Security and Control of the Emerging Power Grid (IREP), 2013 IREP Symposium*, Rethymno, Greece, 2013.

[45] Working Group C4.605, "Technical Brochure 566: Modelling and Aggregation of Loads in Flexible Power Networks," Cigrè, 2014.

[46] TERNA, "Codice di trasmissione dispacciamento, sviluppo e sicurezza della rete," 2004.